Siting, Sizing, and Energy Management System for Future Manned Lunar Microgrids

Saha, Diptish

DOI (link to publication from Publisher):
10.54337/aau550446302

Publication date:
2023

Document Version
Publisher's PDF, also known as Version of record

SITING, SIZING, AND ENERGY MANAGEMENT SYSTEM FOR FUTURE MANNED LUNAR MICROGRIDS

BY
DIPTISH SAHA

DISSERTATION SUBMITTED 2023

AALBORG UNIVERSITY
DENMARK

Siting, Sizing, and Energy Management System for Future Manned Lunar Microgrids

Ph.D. Dissertation

Diptish Saha

Aalborg University
AAU Energy
Pontoppidanstræde 111
DK-9220 Aalborg

Dissertation submitted: May 2023

PhD supervisor: Professor Josep M. Guerrero
Aalborg University

PhD committee: Associate Professor Erik Schaltz
Aalborg University, Denmark

Professor Adriano Camps
Universitat Politècnica de Catalunya (UPC), Spain

Professor Ausias Garrigos Sirvent
Universidad Miguel Hernández (UMH), Spain

PhD Series: Faculty of Engineering and Science, Aalborg University

Department: AAU Energy

ISSN (online): 2446-1636
ISBN (online): 978-87-7573-698-0

Published by:
Aalborg University Press
Kroghstræde 3
DK – 9220 Aalborg Ø
Phone: +45 99407140
aauf@forlag.aau.dk
forlag.aau.dk

Printed in Denmark by Stibo Complete, 2023

Abstract

In recent years, several space organizations have been actively working on developing plans to establish human settlements on the Moon.

The human base on the Moon needs a reliable and resilient electrical power system to operate life support systems (LSSs) for the crew members, scientific equipment for lunar exploration, and communication systems within the base and ground station.

Several technologies in the fields of power generation, distribution, and energy storage systems (ESS), together with in-situ resource utilization (ISRU) are investigated in this PhD project, together with novel control and power management architectures to conceive the future lunar power system called space microgrids (MG). Optimal sizing, operational planning, and siting a cost-effective location among several highly illuminated sites near the Shackleton crater are also investigated and discussed. The possibility of forming a lunar multi-microgrid (MMG) system is also investigated to share and utilize the resources of several MGs and improve the reliability and resiliency of the system.

In this project, a hybrid PV-ESS MG is considered as a case study for the lunar base. Installing PV arrays on top of towers enhances the illumination condition and increases the power generation of the PV system. A novel methodology is presented to determine the PV power generation profile considering the Sun illumination time-series profile at PV arrays. Furthermore, the power demand profile of the candidate site is determined, taking into account the power consumption of several power-consuming units in the base and the Sun illumination time-series profile. An optimization framework is proposed to determine the optimal area of the PV array and capacity of the battery at a location to minimize the mass of the PV array and the battery and the total cost per day of the battery. The optimization problem is solved for an optimization horizon of 1 year without considering the decline in the battery capacity and for 5 years considering the decline in the battery capacity. The total PV-battery MG system mass at the sites is also analyzed when the power-consuming units are segregated into three MGs, namely, habitat, laboratory, and ISRU MGs, to increase the reliability and resource sharing in the system. Furthermore, a new mass-per-unit-load (MPUL) criterion is proposed to determine the site that can satisfy the highest total power demand with the least overall

PV-battery system mass.

The project further analyzes the interaction of several subsystems for oxygen and water management in the base, considering the daily activities of the crew members. The interaction among several subsystems in the base affects the operation rate and mode of several power-consuming units. Furthermore, an optimization framework is proposed to determine the optimal power demand profile of ISRU, ensuring that the oxygen and water tanks of the ISRU and habitat remain at the appropriate levels taking into consideration the oxygen and water consumption profiles of the habitat, the interaction of ISRU, habitat, and wastewater subsystems and the Sun illumination time-series profile at the candidate location for an optimization horizon of 1 month. The power demand profile of the habitat is also determined based on the daily activities of the crew members. The overall power demand profile of the ISRU and the habitat are considered for the optimal operation management of two MGs, namely, ISRU and habitat, with each MG possessing its own PV array and battery system. The optimal operation management of the PV-battery-based MG is proposed, which determines the optimal PV power generation and battery charging/discharging profiles, maintaining an appropriate level of the battery stored energy and minimizing the PV array and battery mass, and the total surplus PV power generation. Furthermore, 15 candidate sites featuring high illumination are compared in terms of the required PV array area and battery capacity and their mass, average illumination, and longest continuous darkness period. Finally, the conclusions of this Ph.D. project are presented along with the potential directions for future research works.

Resumé

I de senere år har flere rumorganisationer arbejdet aktivt på at udvikle planer for at etablere menneskelige bosættelser på Månen.

Den menneskelige base på Månen har brug for et pålideligt og modstandsdygtigt elektrisk kraftsystem til at betjene livsunderstøttende systemer (LSSs) for besætningsmedlemmerne, videnskabeligt udstyr til måneudforskning og kommunikationssystemer i base- og jordstationen.

Adskillige teknologier inden for energiproduktion, distribution og energilagringssystemer (ESS) sammen med in-situ ressourceudnyttelse (ISRU) undersøges i dette ph.d.-projekt sammen med nye kontrol- og strømstyringsarkitekturer for at udtænke fremtidens månekraft system kaldet space microgrids (MG). Optimal dimensionering, operationel planlægning og placering af en omkostningseffektiv placering blandt flere stærkt oplyste steder nær Shackleton-krateret er også undersøgt og diskuteret. Muligheden for at danne et Lunar Multi-microgrid (MMG) system er også undersøgt for at dele og udnytte ressourcerne fra flere MG'er og forbedre systemets pålidelighed og modstandsdygtighed.

I dette projekt betragtes en hybrid PV-ESS MG som et casestudie for månebasen. Installation af PV-arrays oven på tårne forbedrer belysningstilstanden og øger PV-systemets strømproduktion. En ny metode præsenteres for at bestemme PV-strømgenereringsprofilen under hensyntagen til solbelysningens tidsserieprofil ved PV-arrays. Ydermere bestemmes strømbehovsprofilen for kandidatstedet under hensyntagen til strømforbruget for flere strømforbrugende enheder i basen og solbelysningens tidsserieprofil. Der foreslås en optimeringsramme for at bestemme det optimale område af PV-panelet og batteriets kapacitet på et sted for at minimere massen af PV-panelet og batteriet og den samlede pris pr. dag for batteriet. Optimeringsproblemet løses for en optimeringshorisont på 1 år uden hensyntagen til faldet i batterikapaciteten og i 5 år under hensyntagen til faldet i batterikapaciteten. Den samlede PV-batteri MG-systemmasse på stederne analyseres også, når de strømforbrugende enheder adskilles i tre MG'er, nemlig habitat, laboratorium og ISRU MG'er, for at øge pålideligheden og ressourcedelingen i systemet. Endvidere foreslås et nyt masse-per-enhed-belastning (MPUL)-kriterium for at bestemme det sted, der kan tilfredsstille det højeste samlede effektbehov med den

mindste samlede PV-batterisystemmasse.

Projektet analyserer yderligere samspillet mellem adskillige delsystemer til ilt- og vandhåndtering i basen under hensyntagen til besætningsmedlemmernes daglige aktiviteter. Interaktionen mellem flere undersystemer i basen påvirker driftshastigheden og tilstanden for flere strømforbrugende enheder. Endvidere foreslås en optimeringsramme for at bestemme den optimale strømbehovsprofil for ISRU, der sikrer, at ilt- og vandtankene i ISRU'en og habitatet forbliver på de passende niveauer under hensyntagen til habitatets ilt- og vandforbrugsprofiler, samspillet mellem ISRU, habitat- og spildevandsundersystemer og solbelysningens tidsserieprofil på kandidatstedet for en optimeringshorisont på 1 måned. Levestedets strømbehovsprofil bestemmes også ud fra besætningsmedlemmernes daglige aktiviteter. Den overordnede effektbehovsprofil for ISRU'en og habitatet tages i betragtning for den optimale driftsstyring af to MG'er, nemlig ISRU og habitat, hvor hver MG besidder sit eget PV-array og batterisystem. Den optimale driftsstyring af den PV-batteribaserede MG foreslås, som bestemmer den optimale PV-strømgenerering og batteriopladnings-/afladningsprofiler, opretholdelse af et passende niveau af den lagrede batterienergi og minimering af PV-panelet og batterimassen og den samlede overskydende PV-strømproduktion. Desuden sammenlignes 15 kandidatsteder med høj belysning med hensyn til det nødvendige PV-array-areal og batterikapacitet og deres masse, gennemsnitlige belysning og længste kontinuerlige mørkeperiode. Endelig vil konklusionerne af denne ph.d. Projektet præsenteres sammen med de potentielle retninger for fremtidige forskningsarbejder.

Contents

Abstract iii

Resumé v

Thesis Details xi

Preface xiii

I Extended Summary 1

Acronyms 3

List of symbols 7

Chapter 1: Introduction 13
1.1 Motivation . . . 13
1.2 Background . . . 14
1.2.1 Illumination conditions . . . 15
1.2.2 Topography and temperature . . . 16
1.2.3 Electrical power system . . . 18
1.2.3.1 Power generation technologies . . . 18
1.2.3.1.1 Nuclear fission-based reactor . . . 18
1.2.3.1.2 Lunar regolith electrostatic charge . . . 19
1.2.3.1.3 Solar photovoltaic . . . 19
1.2.3.2 Power consuming units . . . 20
1.2.3.3 Energy storage systems . . . 21
1.2.3.4 Power distribution technologies . . . 23
1.2.3.5 Power systems design and operation . . . 24
1.2.3.5.1 Multi-microgrid topologies . . . 25
1.2.3.5.2 Control framework . . . 26

1.3 Research questions and hypothesis 27
1.4 Outline of the thesis 30

Chapter 2: Optimal sizing and siting of PV-battery-based lunar MGs 33
2.1 Introduction 33
2.2 PV power generation 35
2.3 Power demand profile 36
2.4 Optimal sizing of PV and battery systems 38
2.4.1 Battery constraints 39
2.4.2 Battery degradation 39
2.4.3 Power balance constraint 41
2.4.4 Proposed optimal sizing algorithm 41
2.4.5 Simulation results and discussion 42
2.4.5.1 Single MG system design 43
2.4.5.2 MMG system design 47
2.5 Site selection 49
2.6 Conclusion 50

Chapter 3: Energy management system for lunar MG 53
3.1 Introduction 53
3.2 Interacting subsystems for oxygen and water management 55
3.3 ISRU optimal power demand profile 58
3.3.1 Maintaining artificial atmosphere in habitat 58
3.3.2 Water management system in habitat 60
3.3.3 Proposed power demand profile optimization algorithm 64
3.3.4 Simulation results and discussion 68
3.4 Optimal sizing and operation management of PV-battery based MGs . . 71
3.4.1 ISRU power consumption profile 71
3.4.2 Habitat power demand profile 72
3.4.3 Proposed optimal sizing and operation management algorithm . 74
3.4.4 Simulation results and discussion 77
3.4.4.1 ISRU operation management 77
3.4.4.2 Habitat operation management 81
3.5 Site selection 82
3.6 Conclusion 84

Chapter 4: Closing remarks 87
4.1 Overall conclusion 87
4.2 Contribution 89
4.3 Future work 90

Chapter 5: References 93

References 93

II Papers **99**

Chapter A: Space Microgrids for Future Manned Lunar Bases: A Review **101**

Chapter B: Multiple Microgrids: A Review of Architectures and Operation and Control Strategies **103**

Chapter C: Optimal Sizing and Siting of PV and Battery based Space Microgrids near the Moon's Shackleton Crater **105**

Chapter D: Lunar Habitat Wastewater Subsystem Power and Water Management **107**

Chapter E: Power and Energy Management System of a Lunar Microgrid - Part I: Optimal Power Demand of ISRU **109**

Chapter F: Power and Energy Management System of a Lunar Microgrid - Part II: Optimal Sizing and Operation of ISRU **111**

Chapter G: Optimal PV and Battery Sizing for a Space Microgrid Near the Lunar South Pole Considering ISRU, Habitat and Water Subsystem Power Demand **113**

Thesis Details

Thesis Title:	Power and Energy Management System for Future Manned Lunar Microgrids
Ph.D. Student:	Diptish Saha
Supervisors:	Prof. Josep M. Guerrero, Aalborg University Prof. Juan C. Vasquez, Aalborg University Prof. Najmeh Bazmohammadi, Aalborg University

The main body of this thesis consist of the following papers.

[A] Diptish Saha, Najmeh Bazmohammadi, José Maurilio Raya-Armenta, Angelina D. Bintoudi, Abderezak Lashab, Juan C. Vasquez, Josep M. Guerrero, "Space Microgrids for Future Manned Lunar Bases: A Review," *IEEE Open Access Journal of Power and Energy*, vol. 8, pp. 570-583, 2021.

[B] Diptish Saha, Najmeh Bazmohammadi, Juan C. Vasquez, Josep M. Guerrero, "Multiple Microgrids: A Review of Architectures and Operation and Control Strategies," *Energies*, vol. 16, no. 2, p. 600, Jan. 2023.

[C] Diptish Saha, Najmeh Bazmohammadi, José Maurilio Raya-Armenta, Angelina D. Bintoudi, Abderezak Lashab, Juan C. Vasquez, Josep M. Guerrero, "Optimal Sizing and Siting of PV and Battery based Space Microgrids near the Moon's Shackleton Crater," *IEEE Access*, vol. 11, no. 2, pp. 8701-8717, Jan. 2023.

[D] Diptish Saha, Najmeh Bazmohammadi, Abderezak Lashab, Juan C. Vasquez, Josep M. Guerrero, "Lunar Habitat Wastewater Subsystem Power and Water Management," *2023 International Conference on Power, Instrumentation, Energy and Control (PIECON)*, pp. 1-6, Feb. 2023.

[E] Diptish Saha, Najmeh Bazmohammadi, Abderezak Lashab, Juan C. Vasquez, Josep M. Guerrero, "Power and Energy Management System of a Lunar Microgrid - Part I: Optimal Power Demand of ISRU," *IEEE Transactions on Aerospace and Electronic Systems*, vol. XX, no. X, pp. XXXX, 2023. *(Under review)*

[F] Diptish Saha, Najmeh Bazmohammadi, Abderezak Lashab, Juan C. Vasquez, Josep M. Guerrero, "Power and Energy Management System of a Lunar Microgrid - Part II: Optimal Sizing and Operation of ISRU," *IEEE Transactions on Aerospace and Electronic Systems*, vol. XX, no. X, pp. XXXX, 2023. *(Under review)*

[G] Diptish Saha, Najmeh Bazmohammadi, Juan C. Vasquez, Josep M. Guerrero, "Optimal PV and Battery Sizing for a Space Microgrid Near the Lunar South Pole Considering ISRU, Habitat and Water Subsystem Power Demand," *52nd International Conference on Environmental Systems (ICES)*, pp.XXXX, 2023. *(Accepted)*

Preface

Humans have always shown a keen interest in exploring space and life beyond Earth. In recent days, humans have been looking forward to expanding their civilization beyond Earth to other celestial bodies. However, several critical technological advances must be made to support the lives of humans in an environment without a habitable atmosphere. The thesis is developed in this aspect to contribute towards advancing human civilization by providing and maintaining a habitable environment on the Moon. The thesis is submitted for fulfilling the criteria for obtaining a Doctor of Philosophy in Energy Engineering at AAU Energy, Aalborg University.

This dissertation is a compilation of various research papers resulting from the research activities conducted by the author, along with collaboration with other researchers throughout their doctoral studies. The first part of the thesis presents the undertaken research activities, while the second part of the thesis presents the publications obtained from them.

I would like to thank my supervisors, Prof. Josep M. Guerrero and Prof. Juan C. Vasquez, for giving me the opportunity to contribute to the Center of Research on Microgrids (CROM). The relentless support and guidance have helped and encouraged me to persevere and accomplish several tasks during the project. I am highly grateful and indebted to Prof. Najmeh Bazmohammadi for her constant support, for sharing valuable ideas, for making herself accessible at all times and for working with a sense of ownership during times of need. I would like to express my gratitude to Dr. Abderezak Lashab for productive conversations and for exchanging fruitful ideas and suggestions.

I am thankful to Prof. Francesc Godia Casablancas for allowing me to contribute to the MELiSSA Pilot Plant (MPP) at Universitat Autònoma de Barcelona, Spain. During my study abroad period at MPP, I acquired a wealth of knowledge about various other aspects of the project. I sincerely thank Otto Mønsteds Fond, Denmark for their assistance and for enabling me to embark on my journey at MPP.

I attribute my success to my parents who always believed in me. Their support, motivation and direction have been instrumental in all of my accomplishments in life.

Last but not least, I would like to express my appreciation to CROM group members and all staff at AAU Energy and IT support for their assistance throughout my academic

quest and stay at Aalborg University.

Diptish Saha
Aalborg University
May 31, 2023

Part I

Extended Summary

Acronyms

APC autonomous power controller.

AWP alternative water processor.

CNSA China National Space Administration.

DEM digital elevation model.

DOD depth of discharge.

DW drinking.

ECLSS environment control and life support system.

EMS energy management system.

EPS electrical power system.

ESA European Space Agency.

ESS energy storage system.

EV electric vehicle.

EVA extra-vehicular activity.

FC fuel cell.

FR food rehydration.

HCS hierarchical control structure.

ISRU in-situ resource utilisation.

ISS International Space Station.

JAXA Japan Aerospace Exploration Agency.

KRUSTY Kilopower Reactor Using Stirling TechnologY.

LEPS lunar electrical power system.

Li-ion lithium-ion.

LOLA Lunar Orbiter Laser Altimeter.

LRO Lunar Reconnaissance Orbiter.

LSS life support system.

MG microgrid.

MJ multi-junction.

MMG multi-microgrid.

MPP MELiSSA pilot plant.

MPUL mass-per-unit-load.

NASA National Aeronautics and Space Administration.

Ni-H_2 nickel-hydrogen.

PCC point of common coupling.

PEM proton exchange membrane.

PH personal hygiene.

PPF photosynthetic photon flux.

PV photovoltaic.

RF radio frequency.

RFC regenerative fuel cell.

SH shower.

SO solid oxide.

SoC state-of-charge.

TJ triple-junction.

UF urinal flush.

UMM upright metamorphic.

UPA urine processor assembly.

WPA water processor assembly.

WRS water recovery system.

List of symbols

Battery

η_c Battery charging efficiency [%]

η_d Battery discharging efficiency [%]

λ_i Depth-of-discharge of the i^{th} battery cycle [%]

$\overline{\rho}$ Average SoC of the battery

$\overline{T}_c$ Average cell temperature

ρ_i Average SoC of the i^{th} battery cycle [%]

ρ_{ref} Reference battery SoC level

B^{max} Battery maximum charge coefficient [%]

B_{cycles} Number of battery cycles

B_{dod} Battery depth of discharge [%]

$B_{totcycles}$ Total number of battery cycles

$E(0)$ Initial amount of energy stored in the battery $[Wh]$

$E(T)$ Final amount of energy stored in the battery $[Wh]$

$E(t)$ Battery energy at a given time instant t $[Wh]$

$E(t+1)$ Battery energy at the next time instant t $[Wh]$

E^{max} Maximum battery allowable energy $[Wh]$

E^{min} Minimum battery allowable energy $[Wh]$

E_{cap} Battery capacity $[Wh]$

E_{cap}^{new} New battery capacity after degradation $[Wh]$

f_d Battery capacity fading

FC Battery first time cost [/kWh]

k_T Coefficients for battery temperature stress

k_t Coefficient for battery calendar time stress

$k_{\lambda 1/\lambda 2/\lambda 3}$ Coefficients for battery depth-of-discharge

k_ρ Coefficients for battery SoC

l Battery lifetime $[years]$

L_{cal} Battery calendar aging

L_{cyc} Battery cyclic aging

M_B Battery mass $[kg]$

MC Battery maintenance cost [/kWh]

N Number of battery cycles

n_i Number denoting i^{th} battery cycle type

P_B^t Battery charging/discharging power at each hour t $[W]$

P_c^t Battery charging power $[W]$

$P_c^{t,max}$ Maximum battery charging power $[W]$

P_d^t Battery discharging power $[W]$

$P_d^{t,max}$ Maximum battery discharging power $[W]$

r Battery financing interest rate [%]

S_b Battery specific energy $[Wh/kg]$

S_λ Battery stress due to depth-of-discharge

S_ρ Battery stress due to SoC

S_T Battery stress due to cell temperature

S_t Battery stress due to time period

$T_{c,i}$ Average cell temperature of the i^{th} battery cycle $[K]$

T_{ref} Reference battery temperature $[K]$

PV power

α Sun elevation angle $[rad]$

β PV array inclination angle $[rad]$

χ_d Dust coverage [%]

η_{sc} PV cell efficiency [%]

ϕ lunar latitude $[rad]$

ψ Lunar declination angle $[rad]$

σ_a PV array areal density $[kg/m^2]$

σ_s PV array structure specific mass $[kg/m^2]$

A_a PV array area $[m^2]$

d_n Day number $\in [1 \dots 365]$ $[day]$

d_{nt} Total number of days in a year $[day]$

f_{sc} PV cell fill factor [%]

I_s Solar intensity $[W/m^2]$

M_{PV} PV mass $[kg]$

P_{PV}^t Hourly PV power generation$[W]$

t_d Total number of hours in a lunar day $[h]$

t_i Instantaneous lunar daytime $[h]$

Power demand

P_L^t Power consumption at each hour t $[W]$

P_u^a Active-state power $[W]$

P_u^s Survival-state power $[W]$

P_L^{total} Total power demand served $[W]$

U Set of all power consuming devices

u Power consuming device number

Energy management system

$\delta_{P_{PV}}^{shed}$ Fraction of total PV power shed [%]

$C_{FW/UF/WW/WRS}$ Amount of freshwater/urine wastewater/wastewater/water recovery system freshwater collected $[kg]$

CM Total number of crew members

M_{O_2} Molar mass of oxygen molecule (O_2) $[g/mol]$

n Number of moles $[mol]$

$n_{O_2}^{in/out}$ Oxygen infused/consumed in the habitat by all crew members, measured in number of moles $[mol/min]$

$O_2^{in_{(max)}/out}$ Rate of oxygen infusion (maximum)/consumption in the habitat by all crew members $[g/min]$

$O_{2_{ISRU-hab}}^{(max)}$ Rate of oxygen transfer (maximum) from ISRU to habitat oxygen tank $[g/h]$

p Pressure $[Pa]$

P_{ISRU}^{t} Total power consumption of ISRU $[W]$

$P_{V_{ir}}^{t}$ Power consumption of ISRU for maintaining the desired levels of oxygen and water in the respective ISRU tanks $[W]$

$pV_{O_2}^{(err/ref/min/max)}$ Amount of oxygen pV (error/reference/minimum/maximum) in the habitat $[Pa.m^3]$

R Gas constant $[m^3 PaK^{-1}mol^{-1}]$

T Temperature $[K]$

T_H Optimization horizon $[h]$

$T_{FW}^{(err/ref/min/max)}$ Amount of freshwater (error/ reference/minimum/maximum) in the freshwater tank $[kg]$

$T_{hab_{H_2O}}^{(err/ref/min/max)}$ Amount of water (error/reference/minimum/maximum) in the habitat water tank $[kg]$

$T_{hab_{O_2}}^{(err/ref/min/max)}$ Amount of oxygen (error/reference/minimum/maximum) in the habitat oxygen tank $[g]$

$T_{ISRU_{H_2O}}^{(ref/min/max)}$ Amount of water (reference/minimum/maximum) in the ISRU water tank $[kg]$

$T_{ISRU_{O_2}}^{(ref/min/max)}$ Amount of oxygen (reference/minimum/maximum) in the ISRU oxygen tank $[kg]$

$T_{UF}^{(err/ref/min/max)}$ Amount of urine wastewater (error/reference/minimum/maximum) in the urine wastewater tank $[kg]$

T_{WRS}^{ph} Ability of the water recovery system to treat wastewater $[kg/h]$

$T_{WW}^{(err/ref/min/max)}$ Amount of wastewater (reference/minimum/maximum) in the wastewater tank $[kg]$

$TOT_{H_2O_{out}}$ Total amount of water that is transferred to the habitat water tank from ISRU water tank and freshwater tank $[kg]$

V Volume $[m^3]$

V_{ir} Amount of ilmenite added to the reactor volume per hour $[1/h]$

$W_{FW_{out}}^{max}$ Maximum capacity at which water can be transferred from the freshwater tank to the habitat water tank $[kg/h]$

$W_{ISRU_{H_2O_{out}}}^{max}$ Maximum capacity at which water can be transferred from ISRU water tank to the habitat water tank $[kg/h]$

WW_{total} Total amount of wastewater collected $[kg]$

Chapter 1: Introduction

1.1 Motivation

Multiple space organizations such as National Aeronautics and Space Administration (NASA), European Space Agency (ESA), Japan Aerospace Exploration Agency (JAXA), China National Space Administration (CNSA), and SpaceX are intending to create a human base on the Moon from 2025 [1–6]. Other organizations, such as BlueOrigin, have also interest in setting up solar-powered industries on the Moon [7]. Establishing a human base on the Moon requires a habitat for the crew members, laboratories to perform several scientific experiments and lunar exploration, facilities to utilize local resources such as lunar regolith for producing life-supporting elements such as water and oxygen, and electric vehicles and rovers to transport equipment and visit lunar sites of interest.

Several factors, such as the surrounding terrain, topography and temperature, potential points of interest, availability of water, and electrical energy, affect the choice of the base location. Several space missions using orbiters have already taken place and are even continuing their operation to gather more information about these factors. Such a critical space mission to expand human civilization and make humans interplanetary species is to be carried out in several phases [8] as listed in Table 1.1. Presently several robotic missions are being deployed or accomplished, denoting the implementation of "Phase 0". In 2025, the *Artemis-III* mission [2] by NASA will deploy humans on the

Table 1.1: Phases of human deployment on the Moon

Phase	Operation	Human presence	Stay period
0	Robotic site preparation	Minimum or not present	No stay
1	Human deployment initiation	3 to 4 personnel	4 to 6 months
2	Expansion	10 personnel (approx.)	1 year
3	Self-sufficiency	10 to 100 personnel	Extended periods
4	Science and commercialization	More than 100 personnel	Unlimited duration

lunar surface to have a stay of one week on the Moon, and thereafter, gradually increasing the mission duration in "Phase 1". In subsequent years, several other space agencies have similar plans to deploy humans on the lunar surface, increasing the human presence on the Moon with more crew members and longer mission duration in "Phase 2". Once the lunar base is capable of operating without any external support, an extended period of stay is planned in "Phase 3". In "Phase 4", a completely self-governing, safe, and reliable operating system is desired to enable continuous human habitation on the Moon [8].

The base must consist of an efficient electrical power system (EPS) to maintain the habitable atmosphere for the crew members, establish reliable communication with the ground station at Earth, produce water and oxygen for crew members, run scientific equipment to perform experiments and charge electric vehicles and autonomous rovers, among others. The lunar electrical power system (LEPS) is an aggregation of several components for power generation, transmission, distribution, and energy storage to supply a number of interdependent power-consuming units. Therefore a LEPS can be defined as *space microgrids (MGs) on the Moon*. Thus, developing an efficient power control and energy management system (EMS) for coordinating the operation of the space MGs is critical. The control and EMS of space MG on the Moon should support not only the vital life support system (LSS) of the crew members but also ensure optimal, safe, reliable operation and timely execution of the space mission, ensuring the reliability required in the hostile space environment.

1.2 Background

There are several factors that are necessary to consider for building a lunar base, such as solar irradiance profile, topography, temperature, power system technologies, and operation and management [9]. The solar irradiance, length of dark periods and its frequency, and eclipses affect not only the possibility of harnessing solar energy but also the thermal conditions of the base regarding technical operation and crew survivability in adverse environmental circumstances. The surrounding topography of the base or region of interest affects the solar energy reception, extra-vehicular activity (EVA), charging/discharging of electric vehicle (EV) and rovers, and communication, among others. The temperature range of the location affects the designing operating range of several technical components of the base and their energy consumption. The power demand of the base depends on the number of crew members, supporting their LSS, duration, distance and frequency of EVA, nature of experiments and interests and so on. The required power can be supplied from several power generation technologies such as solar, nuclear and electrostatic charge, and energy storage systems (ESSs) are to be utilized during power fluctuation or unavailability [9–11]. Moreover, the power is to be transmitted from the point of generation to consumption, and several technologies such as cables, lasers, and radio frequency (RF) can be utilized. Thereafter, suitable

Table 1.2: Some highly illuminated sites near the lunar polar regions [12–14]

North Pole			South Pole		
Longitude	**Latitude**	**Mean illumination (%)**	**Longitude**	**Latitude**	**Mean illumination (%)**
326.44	89.65	72.60	222.84	−89.45	76.00
110.38	89.85	78.10	203.97	−89.78	81.00
126.80	89.37	84.60	245.94	−89.31	75.60
130.56	89.35	84.01	204.27	−89.78	86.71
127.94	89.36	83.87	123.64	−88.81	85.50
128.94	89.36	82.02	197.05	−89.69	85.24
242.24	88.06	86.08	198.43	−89.69	84.44
232.04	87.31	81.55	205.14	−89.79	82.37
7.22	87.20	82.16	123.95	−88.80	82.37
8.11	87.00	79.53	37.07	−85.30	85.95
7.78	87.05	77.87	37.57	−85.55	82.34
8.07	86.99	76.51	243.22	−85.73	79.54
7.02	87.12	76.94	356.80	−85.96	80.61

operation and EMS techniques are to required to ensure the safety and reliability of the base considering the timely execution of the space mission. Each of these factors is discussed in detail in the following sub-sections.

1.2.1 Illumination conditions

Various space missions for exploring the Moon, like *Lunar Reconnaissance Orbiter (LRO)*, *Clementine* and *Kaguya* by organizations like NASA and JAXA provided knowledge about the state and quality of illumination on the Moon. Highly illuminated locations near the rim of "*Shackleton crater*" [15] at the south pole and "*Peary crater*" at the north pole [10] were identified by *Kaguya* and *Clementine* mission, respectively. The average irradiance from the Sun in a year near the Shackleton crater is 86% and the duration of the most extended eclipse is 11.5 Earth days [15]. Several sites in close proximity to Shackleton crater also witness uninterrupted illumination for approximately half a year, whereas experiencing repeated cycles of daytime-nighttime for the rest of the year with a continued eclipse period of $71 - 120$ h [9, 16, 17]. The authors of [12–14] have identified locations with significant illumination in the close proximity of lunar north and south poles as listed in Table 1.2. Conversely, the non-polar regions have alternate continuous daytime and nighttime for a stretch of approximately 15 days. During a continuous nighttime of approximately 15 days, the ESS are utilized to supply the power demand, increasing the size of the ESS. Therefore, polar regions are favourable for establishing a human base.

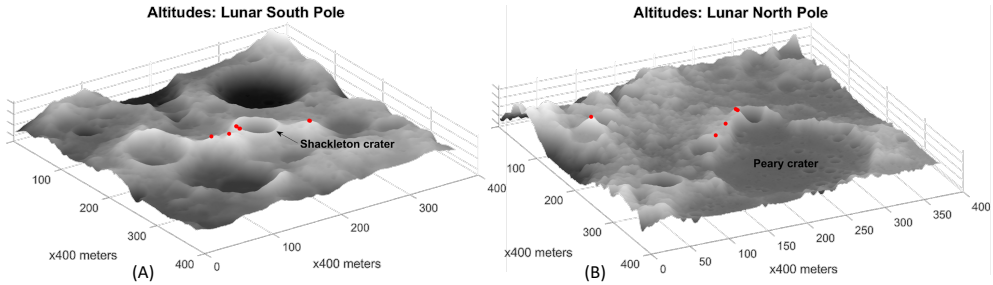

Fig. 1.1: Lunar polar topography stereographic projection from latitude $\mp 87.5°$ to $\mp 90°$. (A) South polar region. (B) North polar region. Some highly average illumination locations provided in Table 1.2 are denoted in red dots. [12–14, 20].

1.2.2 Topography and temperature

Although polar regions have a high average illumination, they do not receive continuous solar illumination due to the topography of the polar regions. The digital elevation models (DEMs) obtained from the NASA Lunar Orbiter Laser Altimeter (LOLA) orbiter shows that there are landscapes with high altitudes around the polar regions. The high terrains hinder the Sun illumination due to the low Sun elevation angle at the polar regions resulting in the formation of long shadows in the range of kilometers [9, 16, 18]. The lengthy shadows sometimes cover a portion or entirety of the site [9]. Therefore, estimating the movement of the Sun near the polar regions and the critical relief elevations[1] is required to determine the illumination of the Sun at a certain site [9]. The methodology to estimate the illumination profile of the Sun considering the terrain near the lunar polar regions is explained by the authors in [19]. Some of the highly illuminated locations and the topography near the polar regions are shown in Fig. 1.1. A highly illuminated location encourages utilizing the energy from the Sun using photovoltaic (PV) arrays, reducing the dependence on ESS.

Besides, it is observed that solar illumination can also be increased by mounting the PV arrays on high towers as shown in Fig. 1.2 [9]. In the literature, it was reported that mounting PV arrays on 100 m high towers at certain locations in the close proximity of the north polar region could reduce the required capacity of the ESS by up to 4%. At this location, mounting PV arrays on a tower with a height of 1500 m could entirely remove the requirement of ESSs. It was reported that there is a possibility to shorten the intervals in which the ESS should be operational by 0.2 h/m through an increase in the height of the tower to 300 m [16]. However, designing, transporting and deploying such high towers might be unrealistic and impractical. A list of several sites with high amount of illumination in the close proximity of Shackleton crater and their average

[1] The angle of an elevation, in a specific longitude, that is the highest relative to an observer at the base site.

Table 1.3: High average illumination sites in the close proximity of Shackleton crater with towers of height 10 m [21]

Site #	Latitude	Longitude	Mean illumination (%)
1	−89.4511	222.6627	91.84
2	−89.4333	222.6415	85.09
3	−89.4390	222.8084	91.68
4	−89.7797	203.6490	86.90
5	−89.7731	203.2861	84.34
6	−85.2963	37.1013	78.84
7	−88.8084	123.7604	84.94
8	−89.6866	197.1382	86.18
9	−89.4407	222.4191	91.76
10	−85.2897	37.0207	82.44
11	−88.6704	291.7803	86.12
12	−89.6884	197.7447	80.18
13	−89.7624	202.8645	82.39
14	−89.4734	222.5634	87.87
15	−89.4502	222.7638	92.23

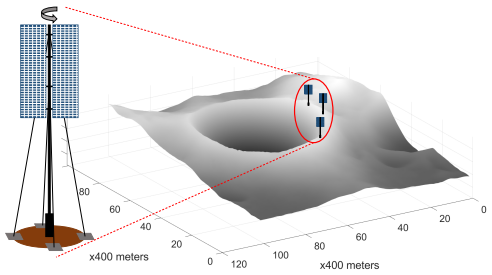

Fig. 1.2: PV arrays on top of towers near the rim of craters [9]

illumination [21] is given in Table 1.3. To calculate illumination at each site, towers of height 10 m are assumed and the polar region's topography is taken into account.

Together with high illumination in the polar regions, the safety of the site from meteorite activities is also to be ensured. Based on the scarce data collected from several spacecraft and radars, the chances of meteoroid impact are higher in the low latitudes $(0° - 30°)$ than high latitude $(60° - 90°)$ by 10% [22–24]. Complete protection from meteoroids can never be ensured. However, the resiliency can be improved by shielding and burying installations or considering redundant structures and distributing them across different locations [22, 25]. Therefore, sites in the polar regions have both high illumination and low meteorite flux.

The surface temperature near the equatorial region varies approximately from $112°C$ to $-173°C$ through the daytime to nighttime [10]. At the polar regions, the maximum surface temperature is approximately $-120°C$ due to low Sun elevation angles. The LRO orbiter by NASA has collected the surface temperature data discussed by the authors of [10]. The maximum surface temperature near the south pole Shackleton crater region is close to approximately $-193.15°C$ to $-163.15°C$ [9, 26, 27]. The range of surface temperature affects the operating temperature of several devices, such as PV panels, and batteries, among others. Therefore, active and passive thermal management systems are required to maintain the operating temperature range of these devices [9].

1.2.3 Electrical power system

The MG for the base consists of power generation, storage, distribution, consumption, and its control and EMS. Power can be generated from different technologies like solar systems, nuclear and electrostatic, out of which solar is the most promising and abundantly available renewable energy because of the lack of atmosphere around the surface of the Moon [9–11]. Balance of power and supply of the required power during the nighttime is supported by several ESSs, such as regenerative fuel cells (RFCs), batteries, flywheel, and so on, can be used for several different purposes, out of which RFCs and batteries have shown to meet the requirements of the base [9]. The power can be transmitted from the point of generation to consumption using cables, RFs and lasers, out of which cables have a better specific mass. Power is required by several units in the base, such as the environment control and life support system (ECLSS) in the habitat, utilizing lunar resources, charging EVs and autonomous rovers, performing experiments, communicating with the ground stations and within the base, and electrostatic shielding [10]. The power consumption by each of these units is discussed further in the following subsections. Autonomous control and EMS inspired from the terrestrial approaches are desired for the base's MG due to significant communication delay in sending communication signals from the ground stations. Each of these aspects of the base's MG is discussed in detail in the following subsections.

1.2.3.1 Power generation technologies

Power for the base can be generated from the solar energy reaching the lunar surface [10], reactors based on nuclear fission [10, 28], and harnessing the static electricity from the regolith [11]. Several highly illuminated sites, as listed in Table 1.2, can utilize solar energy using PV arrays. Nuclear-based power sources have been used for several deep space missions where either solar power might not be enough to harness or be unreliable. Power can also be collected from the electrostatically charged lunar dust particles. The advantages and disadvantages of these power generation technologies are discussed in [9]. These power sources are discussed in further detail in the following subsections.

1.2.3.1.1 Nuclear fission-based reactor

Power from nuclear isotope-based sources is used in several deep space missions, such as *Cassini Probe* and *Mars Curiosity Rover* [10]. However, designing a reactor based on nuclear isotope-based technology to generate more than 1 kW of power is infeasible as it needs a considerable quantity of nuclear isotopes. Therefore, a nuclear fission-based reactor with Stirling technology called "Kilopower Reactor Using Stirling TechnologY (KRUSTY)" was developed [10, 28]. In this reactor, the core formed of uranium generates thermal energy, which is transferred to the Stirling engines using sodium heat pipes [29]. Effective validation of a 1 kW reactor stimulated the development of a 10 kW

module of the reactor, which can be combined to meet the requirement of more power on demand [29]. More details about KRUSTY reactors can be found in [29].

KRUSTY reactors come with the advantages of small size and low mass, are modular and can be combined for increased power demand and are unaffected by the condition of illumination at the location, making them preferable for deep space missions [9]. However, these reactors must be either installed at a safe distance from the base or appropriately shielded as long-term exposure to the radiations from these reactors may cause an adverse effect on the health condition of crew members [10, 30]. A 10 kW reactor module must be placed at a distance of 1.15 km from the base to keep the crew members' yearly radiation exposure below the acceptable level of 5 $rem/year$ [10]. The threshold of safe distance is directly proportional to installing additional modules of the reactor [10], creating hindrance in the expansion of the power sources and the base. Moreover, additional equipment is needed to transmit power from the reactors to the base. On the other hand, the reactors can also be shielded to reduce the separation distance and several shielding techniques are discussed in [9, 10], which also require additional equipment to shift lunar regolith. In addition, disposing of nuclear waste is yet to be investigated and can also prove to be challenging in a critical environment like space.

1.2.3.1.2 Lunar regolith electrostatic charge

The lunar regolith is continuously being hit by electrons and protons from the solar wind because of the lack of atmosphere, leaving the surface dust particles negatively charged [11]. The charge stored in the dust particles can be harnessed through capacitive coupling using a motorized thin-film array of capacitors. Observation made by NASA in a simulation study indicated that the regolith might be negatively charged with 700 V and 147 W per array of power might be collected by 40 capacitive array units [11]. However, this technology is still in the laboratory and several experiments are ongoing in this area [11]. A more detailed study about the technology can be found in [9, 11].

1.2.3.1.3 Solar photovoltaic

The generation of power from solar energy is a well-tested technology in space. On the base, PV panels can be installed on top of relocatable towers [31] to enhance the reception of solar energy at polar regions as explained in Section 1.2.2. Moreover, they do not pose any threat to the crew members' health and can be installed near the base without the need for any heavy equipment for installation, like nuclear reactors. The solar and nuclear power technology for lunar bases is compared in [9].

The solar energy near the polar regions is affected by the topography around the base location and not by the atmospheric conditions because of the lack of atmosphere around the surface of the Moon, as discussed in Section 1.2.2. Most of the space missions utilize the abundantly available energy from the Sun using multi-junction (MJ) PV

cells employing III-V semiconductor materials as they are highly efficient with a high ability to withstand cosmic radiations and an inexpensive well-establish production process [32]. The frequently used triple-junction (TJ) GaInP/GaAs/Ge architecture and upright metamorphic (UMM) PV cells have attained an efficiency of roughly 30% and 40%, respectively [9, 32, 33]. A detailed study on the efficiencies of PV cells for space applications and a comparison of PV technologies used in Earth and space can be found in [9, 10] and [9], respectively.

Although the lack of an atmosphere allows solar energy to reach the surface unhindered, it also allows small meteoroids and debris from space, ultraviolet and cosmic radiation, and nuclei/ion particles, deteriorating the PV cells. Among the several factors, deterioration in PV cells for space applications is primarily due to cosmic and nuclei/ion particle radiation. In addition, PV cells considerably degrade under the extreme operating temperature conditions and temperature cycles existing on the Moon [9, 34]. The span of temperature within which the PV arrays operate has the possibility to come close to the highest temperature of the surface varying from $-193.15°C$ to $-163.15°C$ in the close proximity of Shackleton crater [9, 26, 27]. A detailed discussion on the effect of the PV cells' lifetime for space applications due to operating temperature and radiation can be found in [9].

1.2.3.2 Power consuming units

The most evident power-consuming unit is the habitat of the crew members, which consists of ECLSS including an artificial atmosphere, thermal management, water and waste management, and biomass production and composting, among others [9, 35]. In addition, power is needed for refrigeration, food consumption and for running several electrical appliances, such as lights, cameras, computers, and scientific equipment for experiments [9]. Typically, $5 - 10\ kW$ of power is required for each crew member and approximately $28.05\ kW$ of power is required for a habitat accommodating a team of six crew members [10]. Moreover, charging stations are required for pressurized and non-pressurized rovers, EVs to perform EVA, support and maintenance tasks around the base, or transportation and remote-controlled or autonomous rovers for further exploration and collecting samples for experiments [9, 10, 36]. The charging frequency of EVs and rovers are influenced by their exploration path and range, loss in energy of the ESSs with time, rate of operation, ESS properties, and so on [9]. Furthermore, several units of the base must be in communication among themselves, and the ground station must also be capable of communicating with the base. The amount of power needed for operating the communication systems is decided by the range, bandwidth, rate, and frequency of the communicating signal [10].

To carry out lunar surface missions for a longer period of time, it might not always be feasible to depend on re-supply missions from Earth. Rather, it is desired to produce oxygen and water for consumption by crew members and propellants for further space travel in an infrastructure called in-situ resource utilisations (ISRUs) using resources

Table 1.4: Typical power demand ranges of different loads and elements influencing their power consumption [10, 36]

Unit	Active power (kW)	Survival power (kW)	Influencing elements
Habitat	$30-100$	$0.5-2$	Number of crew members ($5-10\ kW$ each)
Laboratory	$4-10$	$0.5-2$	Experiment type, objectives, and nature
Electric vehicle	$1-3$ (Unpressurized) $3-30$ (Pressurized)	$0.2-0.5$ (Unpressurized) $0.5-3$ (Pressurized)	Vehicle pressure and capacity
Autonomous/manual rover	$0.1-7$	less than $0.2-1$	Rover size and nature of experiments
Charging station	$1-10$	$0.5-2$	Rover and EV requirements
ISRU	$10-100$ (Thermal) $10-100$ (Electrical)	$1-5$	Oxygen, water and propellant production rate
Communication systems	$0.3-1$ per transmitter	Not applicable	Range, rate, bandwidth, frequency
Thermal systems	$1-2$	Not applicable	Maintaining equipment's safe operating temperatures and ensure trustworthy operation
Sensors and additional auxiliary equipment	$2-10$	Not applicable	Type, data acquisition and transmission rate and range

that are accessible in the local vicinity. ISRU is a high power-consuming unit, requiring electrical power to run the motors for the operations such as scooping the regolith, filtering and separating particles of required size, transporting them to a reactor using a conveyor belt, and performing electrolysis of the produced water. In addition, thermal power is needed in the reactor to perform the catalyzed hydrogen reduction reaction [10]. Electrical energy can also be utilized to power heaters to provide the required thermal power, resulting in higher electricity usage [9]. Alternatively, radiation from the Sun can also be concentrated using solar concentrators and guided using optical waveguides to meet the thermal power demands, and more details about them can be found in [37–39]. The rate at which the ISRU is operating and the method adopted for producing the required oxygen and water for the crew members may consume power from tens to hundreds of kilowatts [10]. The authors of [10] estimated that overall 25.8 kW of power must be supplied to the ISRU to maintain a rate of production at approximately 1.63 kg/h. The typical amount of power required by various other power-consuming units and the elements influencing their power demands are listed in Table 1.4 [10, 36]. Each power-consuming unit uses active power during the period when solar power is available, while they are either turned off or operate in a mode consuming less power during the period when the power from the PV arrays is not obtainable, called survival power. The essential survival power is provided by the ESS, and high power demand during this period when solar power is unavailable increases the size and mass of the ESS, affecting the expenses for the space mission as the expenditures related to space missions are directly proportional to size and mass of the payload. The different ESS technologies are discussed in the following section.

1.2.3.3 Energy storage systems

An ESS for planetary surface missions in space is preferred to have above 250 Wh/kg of specific energy, 500 Wh/l of energy density, 5 $years$ of calendar life, 1000 complete

cycle life, the ability to function even at temperatures below $-40°C$, and immensely resistant to deterioration because of harmful radiations from space [40]. An ESS having more specific energy and energy density allows storing more energy with less mass and volume [9]. Several ESSs, including batteries with recharging (secondary) and without recharging (primary) capabilities, fuel cells (FCs), flywheels, and capacitors, have been utilized for various space missions [8, 40] for different purposes and their advantages and disadvantages are discussed in [9]. Among them, batteries that can be recharged and FCs appear to have the possibility to meet the required characteristics and can support the power demand for a prolonged duration [40]. In the current scenario, secondary battery technologies based on nickel-hydrogen (Ni-H_2) and lithium-ion (Li-ion) are tried and tested for several space exploration missions. However, Li-ion are slowly displacing Ni-H_2 because of having more specific energy and energy density of approximately $\sim 100\ Wh/kg$ and $> 200\ Wh/l$ and their ability to function across a broader temperature scope compared to Ni-H_2 batteries [8, 9, 40]. However, several researchers are working to improve the operational capability of Li-ion batteries to even low temperatures of $-60°C$ to $-80°C$ [15, 40, 41]. In contrast, active thermal management techniques [42], such as resistive heaters, cryocoolers, and passive thermal management techniques [43], such as insulation with multiple shields, heat sinks are also being investigated and can also be implemented to ensure their operation within the desired operational temperature. Several kinds of Li-ion batteries and their technical specifications are listed in Table 1.5 [9].

For prolonged duration of stay, the power demand during the nighttime can be also supplied from FCs. The different types of FCs and their advantages and disadvantages are discussed in [9]. A FC combined with an electrolyzer and a system of storing multiple reactants in the fluid state makes the FC rechargeable and suitable for lengthy space expeditions and is called RFC [40, 41, 44, 45]. A detailed discussion on proton exchange membrane (PEM)-RFC and solid oxide (SO)-RFC is provided in [9, 46]. PEM-RFC appears to be quite beneficial and effective than SO-RFC for surface missions in terms of weight, charge and mechanism of pressurization [9, 40, 44, 46]. The permanently shadowed regions at the bottom of the Shackleton crater may temperatures as low as $-193.15°C$ to $-163.15°C$ [26] and can also provide cryogenic cooling temperatures ($-150°C$ to $-273°C$) for reactant storage tanks, without using any energy. However, additional equipment will be needed to carry the reactants upwards to the edge of the crater [8].

In straightforward comparison, RFCs have better specific energy and mass compared to batteries [10, 41, 44, 46]. The reason for this is that every component of the RFC, except the storage tanks, is engineered for a predetermined peak power level. Only enough reactants should be stored in the tanks to support the increased power demand for a prolonged operation duration. Therefore, with the increase in operational time at a fixed power level, an increase is observed in the RFC system's specific energy [10]. In addition, the energy storage (reactant tanks) and conversion (FC combined with

Table 1.5: Technical characteristics of various Lithium-ion based batteries [9]

Battery	Energy density (Wh/l)	Specific energy (Wh/kg)	Calendar life (Years)	Cycle life (cycles)	Operating temp. range (°C)
LFP (Long life)	$300-400$	$150-200$	20	$>100,000$	-10 to 25
LFP (with Alternate Anodes)	$300-400$	$250-300$	~ 5	<500	-40 to 30
LTO	$300-400$	$150-200$	20	$>100,000$	-10 to 25
NMC (Long life)	$300-400$	$150-200$	20	$>100,000$	-10 to 25
NMC (High Energy)	$300-400$	$150-200$	~ 5	>500	-40 to 30
NMC (with Alternate Anodes)	$300-400$	$250-300$	~ 5	<500	-40 to 30
LiPON	$300-400$	$250-350$	>20	$>100,000$	10 to 80
LLZO	$300-400$	$250-350$	>20	$>100,000$	10 to 80
LATP	$300-400$	$250-350$	>20	$>100,000$	10 to 80
LiS	$300-350$	$250-300$	~ 5	$100-500$	-40 to 30
LCO	$300-400$	$250-300$	~ 5	<500	-40 to 30
NCA	$300-400$	$250-300$	~ 5	<500	-40 to 30

LFP: Lithium Iron Phosphate; LTO: Lithium Titanium Oxide; NMC: Lithium Nickel Manganese Cobalt oxide; LiPON: Lithium Phosphorus Oxynitride; LLZO: Lithium Lanthanum Zirconium Oxide; LATP: Lithium Aluminum Titanium Phosphate; Li-S: Lithium – Sulfur; LCO: Lithium Cobalt Oxide; NCA: Lithium Nickel Cobalt Aluminum Oxide

electrolyzer) units are separate from each other and can be sized individually [44, 46], whereas both of them are integrated in a single unit in case of batteries [9, 44]. Regarding the weight of the system and the duration of discharge, a breakpoint of approximately $10-18h$ has been observed between RFCs and batteries [41]. The battery system mass is lower compared to the RFCs before the breakpoint but increases subsequently. However, RFCs exhibit a lower performance of charging compared to batteries [17]. Thus, batteries have the ability to recharge faster during short illumination periods.

1.2.3.4 Power distribution technologies

The generated or stored power requires a suitable means for distribution to the consumption units using AC, DC or a hybrid AC-DC system. A $50kW$ lunar EPS with a high voltage and frequency is simulated by the authors of [47]. It has been observed that, although a higher frequency of the power system decreases the capacitor and power converter size, the skin effect and reactive inductance of the line increase, thereby minimally affecting the mass of the entire system [8]. In addition, the oxides of iron found within the lunar regolith can cause inductive coupling with the transmission lines resulting in a significant loss of power [48]. On the other hand, the DC system is extensively used in space missions and is a well-tested technology. The human habitat in space, like the International Space Station (ISS), still uses $120VDC$ power for its EPS [8]. Moreover, DC systems have the advantage of uncomplicated design, fewer losses, no skin effect and compensation for reactive power [8, 15]. However, heavy industrial operations require driving motors, and AC motors are typically lighter and smaller compared to DC motors at comparable power and torque levels. Therefore, hybrid AC-DC systems might be beneficial, considering solid-state transformers, to operate the MG safely and reliably [49, 50].

On the base, it might be necessary to distribute the generated power to a distance of 0.1 km to 10 km using electrical cables carrying power, RF in the form of beam or lasers based on solid-state technology [9, 51]. The mass of a distribution system using power cables increases with the higher level of power. The cross-sectional area of the conductor might decrease while increasing the voltage level, whereas the thickness of the insulating material also increases, enhancing the mass of the overall power system [15, 51]. Alternatively, utilizing wireless transmission systems based on RF technologies are investigated in the literature to transmit power at 2.45 GHz or 5.8 GHz. Although 5.8GHz has more efficiency of free-space transmission, the mass of the system increases with the longer transmission distance because of more losses in free-space [51]. In addition to RF technologies, laser systems made from AlGaAs/Ge quantum well solid-state laser diode modules can also be used for wireless transmission systems. An active thermal management system is required to keep the temperature of the diode around 293 K to achieve a favorable efficiency of transmission [9, 51]. A detailed comparison in terms of the system power transfer efficiency and specific mass of the three distribution systems can be found in [9, 51]. Typically, power cables have the lowest specific mass for transmitting power of 10 kW over a span of 1 km with efficiency above 70%. Therefore, using a DC cable power distribution system for designing the MG might have the maximum efficiency at minimum mass. For heavy industrial operations, an AC-DC hybrid power distribution system using power cables is likely to be used to reap the benefits of the light mass and small size of AC motors.

1.2.3.5 Power systems design and operation

The safety and reliability of the space MG are ensured by having a robust topology design and operation control together with an efficient power distribution system. The MG topology affects the stability and resiliency of the MG. The operation control of an MGs includes coordination and control of converters, sharing the power demand utilizing several generators and resources, maintaining the required voltage (and frequency in case of AC), power and duration of charging/discharging of ESSs, and maintaining the power balance, among others.

Power electronic converter based islanded MGs have low system inertia and are vulnerable to stability due to frequent power fluctuations in case of minor faults and the controller's inability to handle sudden mismatches in power generation and demand. In case of a severe fault, the MG might also experience a complete power failure. To overcome this problem in terrestrial applications, several MGs are interconnected, establishing a system of multi-microgrids (MMGs), facilitating resource sharing and enhancing energy utilization. Less probable events such as meteoroid strikes may lead to equipment failure impacting the MG system severely and the critical loads can be supplied from the resources of another MG, thereby increasing the resiliency of the entire MMG system [52]. A lunar MMG system can be created by segregating the power-consuming units into several groups where each of the groups has its own power generation and

ESSs [21]. Therefore, a MMG system for the lunar base should be envisioned and such topologies are discussed in Section 1.2.3.5.1.

For operation control of MGs in space, such as the EPS of ISS, presently, three ground stations on Earth communicate the schedule of power-consuming units considering the requirements and constraints of several systems [53]. The instantaneous communication for space missions near the low Earth orbit makes it possible to schedule the power-consuming units on the ground and communicate with the spacecraft. For deep space missions, such as the missions to Moon and Mars, the communication delay may reach up to approximately 10 *sec* and 15 *minutes*, respectively [54, 55]. In the case of a base, direct line-of-sight communication might also not be possible during the mission period, requiring an orbiter to relay the communication signal, further increasing the communication delay. A delay in communication of even a few seconds can cause severe problems with control and power management, given that the operational time frames of these systems are less than a second. Therefore, self-reliant autonomous systems should be developed utilizing the capability of modern systems to compute critical calculations rapidly. During disastrous situations, self-governing systems can respond quickly in the order of a few milliseconds and adapt to swiftly evolving circumstances in space. For example, spacecraft such as *Dragon*, *Starship* and *Orion* are able to function independently for space transportation or cargo missions [56–58]. Therefore, an autonomous power controller (APC) is required to automatically coordinate and schedule the several power-consuming units and maintain the power balance [55]. The architecture of such APC is discussed in Section 1.2.3.5.2.

1.2.3.5.1 Multi-microgrid topologies

The lunar MMG topologies can be inspired by the different MMG topologies used for the terrestrial MMG systems. Commonly, in a single MG architecture, the power generation, storage and consumption units are connected to a single point of common coupling (PCC), while there are several PCC locations in an MMG system. A detailed description of various topologies for terrestrial MMG systems, along with their advantages and disadvantages, are discussed in [52]. Out of these topologies, grid series interconnected MGs and ring formation can be considered suitable for the formation of lunar MMG as depicted in Fig. 1.3a and Fig. 1.3b, respectively. In both grid series interconnected MGs and ring formation, detaching the defective part of the MMG system is possible while supplying power to the rest of the MMG system. There is an exclusive power line for sharing resources between any pair of MG in grid series interconnected MGs, increasing the reliability of the MMG system. However, the installation of such a system also requires high capital, and the disturbance might also extend to other MGs directly connected to the defective part of the MMG system. In the ring formation, power is shared via another MG in between the source and destination MGs, in case of which the power line must be designed to support the higher amount of power transfer [52]. A compromise is necessary between reliability, expenditure, and the challenges

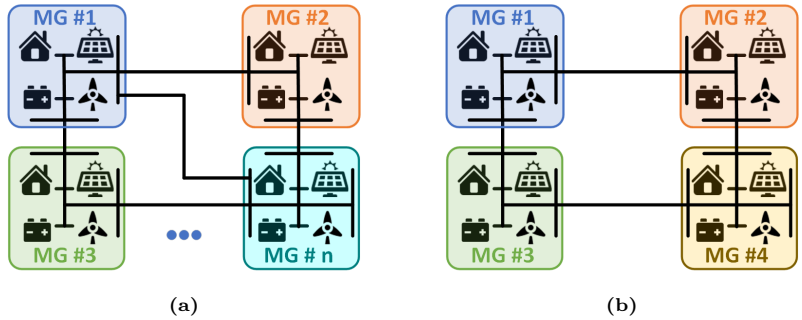

Fig. 1.3: Probable MMG topologies for a lunar base (a) grid series interconnected MG (b) ring formation

in implementing control and protection schemes [52].

1.2.3.5.2 Control framework

The operation and control system is one of the crucial design aspects for a safe, reliable and resilient MG. It includes controlling the operation mode of converters, sharing of power, maintaining the balance of power, ESS charging/discharging and maintaining state-of-charge (SoC), grid protection and self-restoration, and scheduling the power demand optimally, among others. For terrestrial MGs and MMGs systems, there are several control architectures, such as centralized, decentralized, distributed and hierarchical [52]. In a centralized architecture, information for all the MGs in an MMG system is collected, stored and processed in a single computation system, making it simple to implement while increasing the computational complexity of the controller. The operation of the whole system is jeopardized in case of a malfunction [52]. In decentralized architecture, the controllers do not communicate with each other, and the controller operates on the basis of variations in the voltage and frequency of the power grid. Decentralized architecture improves the independence of the MG and its protection from disruptions originating from external sources. However, the optimal state of operation with cooperation among the different MGs is not achieved. In a distributed architecture, the controllers communicate with each other to achieve a unanimous operating objective, facilitating flexibility with easy inclusion and operation of new MGs in the MMG system while having detrimental effects in case of communication lag or failure. In hierarchical architecture, the control complexity is categorized into several levels, namely primary, secondary and tertiary, with sharing of information among the different levels. In this architecture, the controller at the higher level creates references for the controllers at the lower level, considering the objectives and overall safety of the MMG system. The tertiary-level controller optimizes the management of power and energy of the MMG system, taking into consideration the long-term objectives of the

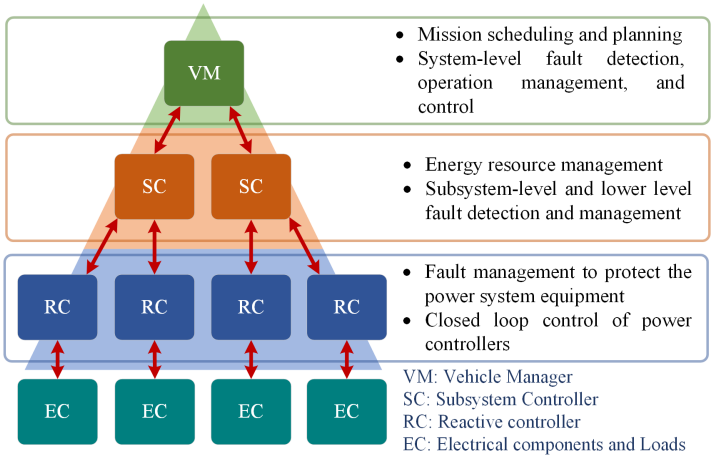

Fig. 1.4: Typical APC architecture for spacecraft

MMG system. The secondary-level controller is responsible for maintaining the voltage and power balance, while the lowest primary-level controller is responsible for controlling the power production and demand at the MG level using the power converters. The controllers also have a higher rate of operation and a lower scheduling horizon moving down the hierarchy. A detailed explanation of all control architectures is discussed in [52].

Similar to the terrestrial hierarchical control architecture, the authors of [55, 59, 60] proposed an APC architecture for spacecraft consisting of vehicle manager, subsystem, and reactive levels as depicted in Fig. 1.4. The main objective of the uppermost level controller vehicle manager is to plan and optimize the duration and time of operation of multiple power-consuming units and perform EMS considering the assigned priorities and constraints of each load and safety and timely execution of long-term objectives of the space mission [9]. Other than this, the vehicle manager is responsible for fault management, maintenance, mitigation, and recovery. In case of a system-level fault, the vehicle manager reconfigures the power distribution system to minimize or eliminate operation disruptions [9]. In addition, the control framework must also be able to handle unexpected operating conditions and allow simple expansion of the base assets and new operational requirements [9].

1.3 Research questions and hypothesis

Space MGs on the Moon need a variety of power generation, transmission, and storage technologies to fulfill the required power of the base and reliable control and EMS to

ensure the quality and continuity of the power supply. This thesis mainly develops a coordinated and efficient operation and energy management scheme for an optimally sized PV and battery for PV-battery-based lunar MGs, taking into consideration the crucial life-supporting systems and the daily operation of the base for maintaining the health of the crew members and accomplishing the mission's goals. The following are the research directions followed in this thesis:

- A PV-battery based MG needs an appropriately sized PV array area to supply the power demand and charge the battery during the periods when PV power is available. Enough energy should be stored in the battery to supply the required power during the time when PV power is unavailable. Moreover, there are several locations where the average Sun illumination is high, but the mass of the PV and battery systems is a crucial concern. This leads to the following research questions:
  - How to obtain the power generation profile of the PV system at any point of interest in the close proximity of lunar poles taking into consideration the solar elevation angle and the topography of the candidate site?
  - How the optimal area of the PV array and capacity of the battery can be determined to not only supply the power consumption during the periods in which the PV power is available but also to store adequate energy in the battery to supply the power demand when PV power is unavailable at each candidate site?
  - What are the most important factors that affect the size and mass of a MG formed using PV arrays and batteries at any possible site? And how can different locations be compared to select the most suitable location for a lunar base from the power generation and entire system mass points of view?
- There are several units in the base that consume power, and their operation is based on the availability of PV power, the total number of crew members, and the daily activities of the crew members. Moreover, several power-consuming units in the base interact with each other to maintain the life-sustaining conditions of the base and this interaction affects their mode and rate of operation. This leads to the following research questions:
  - How the interaction of several life-supporting subsystems can be modeled to be used for determining the power consumption profile of the base?
  - How do the number of crew members and their daily activities affect the operation rate and mode of several interacting power consuming units in different subsystems and their power consumption profile?
- The efficient operation management of the base is required to maintain the power balance and control the charging/discharging of the battery considering an appropriately sized PV array area and capacity of the battery, and power demand

profile of the base considering the interaction between several subsystems of the base. This leads to the following research questions:

- What is the optimal power management strategy to maintain the stored energy of the battery at a desired level while also providing the required power during the periods when PV power is unavailable?
- How does the reference storage level of the battery affect the mass of the PV-battery based MG system?

To tackle these research problems, the following methodologies are investigated in this thesis:

- Developing an optimization framework to optimally size the PV array area and battery capacity for a PV-battery based MG considering the profiles of Sun illumination time-series and power consumption at any candidate location.
- Identifying and modeling the interaction of life-supporting subsystems of the base to determine the operation mode and rate of the power consumption of the base.
- Developing an optimization framework to generate the optimal profile of power demand of the base considering the mutual influence of various subsystems and their operation rate and mode and the daily activities of the crew members to retain the intended levels of life-supporting resources in the base.
- Developing an operation management framework for the PV-battery based MG to obtain the optimal profiles of PV power generation and charging/discharging power of the battery while satisfying the system constraints and keeping the battery's stored energy at the intended level.
- Developing an index to compare different locations and identify the best candidate site to fulfill the requirements of the space mission with the least expenses.

The methodologies developed in this thesis are based on certain assumptions that are listed below:

- The Moon is bombarded with cosmic radiations and ions/nuclei particles from space due to the lack of an atmosphere. Although there are few studies modeling the degradation of the PV array and battery in a spacecraft due to cosmic radiations in the low-Earth orbit, a study on the degradation of PV array and battery due to cosmic radiations on the lunar polar regions is not still available. Therefore, this thesis does not consider the degradation of PV array and battery due to cosmic radiations from space.

- The mass of the PV-battery-based MG is determined by only considering the PV array and the battery mass. However, there are several other components, such as power converters, protection devices, and power cables, that need to be taken into consideration while determining the overall mass of the MG system.
- There is an interaction of several gases and other life-supporting resources in several subsystems of the base. However, the interaction of ISRU, habitat, and wastewater subsystem for maintaining only the oxygen and water in the base is considered in this thesis.
- At the start of the space mission, a certain amount of oxygen and water is required to support the lives of the crew members for some initial days before the oxygen and water production facility can start to operate. The initial levels of oxygen and water tanks for modeling the interaction among different subsystems of the base are determined arbitrarily.
- Demand-side management and load scheduling is an essential part of the optimal sizing and operation management of a power system as it optimally schedules the controllable loads maintaining the balance of power in the power system. Including an efficient demand-side management scheme can better utilize the available resources in space. However, this thesis does not consider demand management for the operation of the power system.

1.4 Outline of the thesis

This chapter of the thesis discussed the illumination and topographical conditions on the Moon and several technologies and devices needed to establish an MG on the Moon. It explained several generation, transmission and storage technologies of power available for MGs on the Moon. In addition, the several MMG topologies that can be implemented for establishing MMG system on the Moon along with their control framework are discussed.

Chapter 2 discusses the PV power generation profile using the Sun illumination time-series profile and the Sun elevation angle at the candidate location of the Moon. The several power-consuming units and their power demand during the availability and non-availability of PV power are discussed. An optimization framework is proposed to determine the optimal PV array area and capacity of the battery minimizing the mass of the PV and battery in a PV-battery MG system taking into account the time-series profile of Sun illumination and several technical constraints for battery and power balance. The simulation results of the proposed optimization framework are discussed and analyzed along with proposing the criterion to determine the location that serves the greatest power demand requiring the lowest aggregated mass of the PV-battery system.

Chapter 3 first introduces the need to consider the interaction among several subsystems of the base to maintain the critical resources supporting the life of crew members and its importance in determining the profile of power consumption of the base. The optimal profile of power consumption of the ISRU is determined using an optimization framework considering the daily activities of the crew members, their oxygen and water consumption profile and maintaining the oxygen and water tanks in the respective subsystems at a desired level. The overall power demand profile of the ISRU is determined taking into account the several other devices required for the operation of ISRU. The habitat power consumption profile is determined based on the daily schedule and activities of the crew members. An optimization framework is proposed for the operation management of both the PV-battery based ISRU and habitat MGs to maintain the stored energy of the battery at a desired level and determine the optimal PV power profile and battery charging/discharging profile by minimizing the PV array and battery mass. The simulation results for the operation management of both the ISRU and habitat MG are discussed. A comparison of several candidate sites in terms of PV array and battery system size and mass is discussed along with mass-per-unit-load (MPUL) and several other factors in determining the most suitable location for building a PV-battery based MG in the close proximity of Shackleton crater.

Chapter 4 first concludes the study with the primary inferences of the study. In addition, the contributions of the thesis are listed and described. The further directions of study are also discussed in this chapter.

Chapter 2: Optimal sizing and siting of PV-battery-based lunar MGs

This chapter elaborates on the framework to obtain the optimal size of the PV array and battery for the PV-battery-based lunar MG. The chapter starts by introducing the problem statement, the importance of determining the optimal size of PV array and battery and the hypothesis for the proposed solution. The rest of the sections of the chapter describes the methodology to obtain the profiles for power generation and demand of the base, the optimization framework to determine the size of the PV array and battery, the results of the optimization, and the parameter for selecting a site for the base. The Chapter 3 focuses on the operation management and EMS of a lunar MG considering the interaction between multiple power-consuming subsystems of the base.

2.1 Introduction

The space MG on the Moon requires an appropriate size of power generation and ESSs for supplying the power demand during daytime and nighttime and maintaining the power balance. Given the benefits of solar power generation and Li-ion batteries in comparison to nuclear fission-based reactors and RFCs [9], which are explored briefly in Section 1.2.3.1 and Section 1.2.3.3, respectively, PV arrays and Li-ion batteries are considered for power generation and energy storage in this thesis. During the daytime, it is desired that the PV system supply the power demand while the power is consumed from the batteries during the nighttime.

In the literature, several studies investigated the size of the ESS required to supply the power demand of the base. In [61], the authors used the DEM provided from the radars mounted on Earth and the average illumination at several sites to identify their highest and lowest ESS operation duration. The possibility of lowering the ESS size at a site by mounting PV arrays atop tall towers to enhance the condition of average illumination is examined in [16]. A comparison study of battery and RFC supported PV

system for 10 *years* by the authors of [17] showed that PV-RFC system has lower mass compared to battery supported system, but batteries have higher charging efficiencies than RFCs reducing the charging time duration of batteries. A power system based on PV arrays and batteries for a base near the rim of the Shackleton crater was also sized in [15] considering a constant solar illumination. The authors of [10] calculated the PV-battery system mass for a base located near the 30° lunar latitude having a fixed consumption of power at 25.8 kW for a duration of one lunar month ($\sim$ 708 h). Therefore, the studies in the literature considered either average or constant illumination, constant power demand or a non-polar location. However, several studies have shown that highly illuminated sites are near the poles and have small angles of elevation of the Sun with high elevated lands in the surrounding area that obstructs the solar energy at the sites [9] as discussed in Section 1.2.1 and Section 1.2.2. Moreover, it is more accurate to estimate a power demand profile according to the specific time and operational duration of multiple power-consuming units instead of an average or peak constant power demand of the base.

In this chapter, a methodology is discussed to estimate the PV power utilizing the time-series profile of Sun illumination at a site proposed in [19] taking into consideration the PV arrays mounted atop towers having heights of 10 m, 50 m, and 100 m. The power usage pattern of the base is obtained by considering the operational duration and time of multiple units within the base that consumes power [21]. The different power-consuming units are also divided into three groups, each having its own power generation and storage resources forming an MMG system. The MMG system in the base increases the reliability and resiliency of the MMG system [9] as discussed in Section 1.2.3.5. The chapter further discusses the proposed optimization function to minimize the PV array and battery mass of a PV-battery MG and the total cost per day of the battery to minimize the expenses of the space mission as the expenses rise with the growth in the weight of the payload [21]. *MATLAB-fmincon* optimization tool is utilized to find the solution to the optimization considering an optimization horizon of one year and five years [21]. Furthermore, yearly decline in the capacity of the battery because of calendar and cyclic aging is taken into account only for the case of five years. A comparison among 15 candidate sites (see Table 1.3) near the Shackleton crater is discussed in relation to the mass and area of the PV array, mass and capacity of the battery, mean illumination at the sites, most continuous period of darkness, and total power generation and demand served considering both the single MG and the MMG system. The chapter also discusses the proposed mass-per-unit-load (MPUL) criterion to locate the site with the lowest overall system mass supplying the greatest power demand [21].

The rest of the chapter is arranged as follows. The methodology to generate the PV power from the illumination time series profile is discussed in Section 2.2. Multiple units that consume power in a base and the methodology to generate the profile of power consumption of the base are discussed in Section 2.3. The model and optimization framework and the optimization results are discussed in Section 2.4, along

with several constraints and battery degradation. The site selection process is discussed in Section 2.5. Finally, Section 2.6 concludes the chapter with remarks.

2.2 PV power generation

Even though no atmosphere is present around the surface of the Moon to obstruct the solar radiations, the power generation from the solar radiation depends on several factors, such as the intensity of the solar radiation, the angle at which the PV arrays are inclined and their orientation, cell efficiency, and the elevation angle of the Sun, among others [10, 21]. The PV power generation on the Moon can be determined by the following [10, 21]:

$$P_{PV}^{t} = (1 - \chi_d) f_{sc} \eta_{sc} A_a I_s \sin(\alpha + \beta) \tag{2.1}$$

where I_s is considered almost equal to that of Earth at 1359 W/m^2 as the maximum variation on the Moon is approximately 0.56% of that of Earth [10, 21]. The illumination time-series profile [19] at the site is multiplied with the I_s to include the effect of shadows caused by the surrounding elevated terrains [21]. The illumination time-series for one year is shown in Fig. 2.1 [21]. At a particular latitude, the variation of α from the start to the end of the day can be determined by the following [10, 21]:

$$\alpha = \frac{\pi}{2} - \cos^{-1}\left[\sin(\phi)\sin(\psi) - \cos(\phi)\cos(\psi)\cos\left(\frac{2\pi t_i}{t_d}\right)\right] \tag{2.2}$$

Furthermore, the ψ can be determined by the following equation [10, 21]:

$$\psi = \psi_{max} \sin\left(\frac{2\pi d_n}{d_{nt}}\right) \tag{2.3}$$

In this study, χ_d is assumed to be zero taking into account that the PV arrays are installed near the base and the dust is removed at regular periods. All the parameters considered to calculate P_{PV}^{t} are listed in Table 2.1 [10, 21]. In space, MJ PV panels made up of GaInP/GaAs/Ge are extensively used as they possess high efficiency, resistance to radiation, and well-established procedures and techniques of production [21]. In Eq. (2.1), A_a is determined after solving the optimization problem.

The PV generation is also affected by the harsh operating conditions in space, as mentioned in Section 1.2.3.1.3. The temperature of the surface in the vicinity of the Shackleton crater are in the range of $-193.15°C$ to $-163.15°C$ [21, 26, 27]. Active [42] and passive [43] thermal management systems must be utilized to maintain the temperature of the PV cells within their operating range to save them from significant degradation due to extreme temperatures. Moreover, the PV cells also degrade due to cosmic and nuclei/particle radiation in space. However, the impact on PV cell due to extremely low temperatures and nuclei/particle radiations from space on the Moon is not included in this thesis as it has not yet been widely studied in the literature [21].

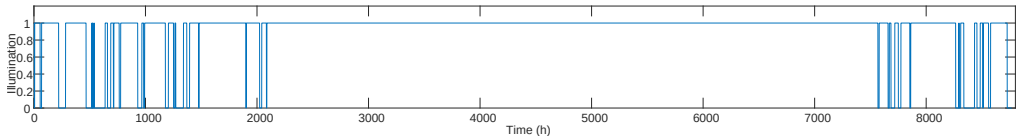

Fig. 2.1: Illumination time-series at Site #1 from July 6, 2023, to July 5, 2024. ("1" - illumination available and "0" - site shadowed

Table 2.1: Parameters for determining power output of PV array

Parameter	Value
χ_d	0
f_{sc}	0.89
η_{sc}	0.28
β	same as ϕ
t_d	708.33 h
ψ_{max}	0.0262 ($= 1.5°$)
d_{nt}	365.25 $days$

2.3 Power demand profile

The habitat is the most vital power-consuming unit in a base as it has to maintain the LSS for the crew members. The LSS includes maintaining the artificial atmosphere with life-supporting gases, habitable temperature and pressure in the habitat, food and water supply, and waste treatment, among others. In addition, biomass production is also considered a crucial LSS responsible for growing food for a longer duration of stay in space [21, 35]. Other than this, power is required for communication within the base and with the ground station, and for several electrical appliances, such as lights, computers, displays, and so on [21].

Furthermore, several specialized scientific appliances in the laboratory also need electrical power to perform scientific experiments in the base. It might be required to perform several EVA to collect samples, explore interesting locations, transportation and carry out maintenance tasks using pressurized or unpressurized EVs or rovers [10, 21]. Autonomous rovers can also be employed for some of the abovementioned activities. All the pressurized or unpressurized EVs, rovers and autonomous rovers need charging stations to charge their ESS [21].

Rather than depending on costly re-supply missions from Earth, it is desired to utilize the available minerals on the Moon to produce oxygen and water from the lunar regolith using ISRU [10, 21]. The ISRU is one of the major power-consuming units in the base consisting of a number of electrical motors to collect, vibrate to separate particles, and move the regolith to a reactor and carry out electrolysis to extract oxygen and propellants (hydrogen) from water [10, 21]. In addition to electrical power, thermal

power is also needed in the reactor to carry out catalyzed hydrogen reduction reaction of the regolith in the reactor. Solar energy can be utilized to supply the required thermal power using concentrators and optical waveguides [21, 37–39]. However, in this thesis, the thermal power is also considered to be supplied using electrical heaters [21].

All the units that consume power in a base are listed in Table 2.2 [10, 21, 36, 62]. The power-consuming units can have an active and survival state of power consumption. In the survival state, a non-critical power-consuming unit can either be switched off or operate in a low-powered state. During the nighttime, the power demand is to be supplied from the ESS, and a lower power consumption level reduces the size of the ESS. All the other critical power-consuming units consume active-state power throughout their operation duration [21]. It is to be noted that the power-consuming units are also divided into three groups, namely, habitat, laboratory and ISRU to investigate the case of a MMG system rather than examining only the case of including all of them within a single MG. Each of the groups has its own power generation and ESS to share resources in a time of emergency [21]. The power consumption of the habitat depends on the number of crew members as critical LSS are maintained in the habitat. It is assumed that approximately $10 - 30\ kW$ of power is required for $2 - 5$ crew members in the habitat [10, 21, 36]. The power usage of ISRU relies on the process and rate at which oxygen, water and propellants are produced and, therefore, has the possibility to lie within the range from tens to hundreds of kW [10, 21, 41]. Likewise, factors such as the type of lunar surface, distance traveled, frequency of experimentation, and the characteristics of the regolith influence the amount of power required by EV and rovers [9, 21, 36]. The factors affecting the consumption of power because of multiple units in the base are discussed in Section 1.2.3.2.

The pattern of power demand at various sites depends on the illumination time-series profile of the site and the time-of-use of the device [21]. It is assumed that the devices consume active-state/survival-state power during the period illumination is available/unavailable. The total power consumption at each hour (P_L^t) over 24 h is the summation of all the devices operating at that hour (t) and is determined as the following [21]:

$$P_L^t = \begin{cases} \sum_{u=1}^{U} P_u^a(t) & P_{PV}^t > 0 \\ \sum_{u=1}^{U} P_u^s(t) & P_{PV}^t = 0 \end{cases} \tag{2.4}$$

The power demand profile for each of the MGs in a MMG system, namely habitat, laboratory and ISRU, shown as "Section" in Table 2.2, is created in the same methodology as mentioned above [21].

Table 2.2: Different units that consumes power in various sections (Habitat (H), Laboratory (L), and ISRU (I)) of a base [10, 21, 36, 62]

Section			Device	Power (W)		Average daily use (h)	Time of use (h)
				Active-state	Survival-state		
H	L	I	Air compressor	3.5	3.5	24	0 – 24
H	L	I	Airlock vacuum pump	500	500	1	21 – 22
H	L	I	Airlock status LED	5	5	24	0 – 24
H	L	I	Artificial daylight LED	150	75	24	0 – 24
H			Water heater	4000	0	1	6 – 7
H			LSS	4500	3000	24	0 – 24
H			Induction oven	2000	0	1	8 – 9
H	L	I	Monitoring camera (9 Nos)	5	5	24	0 – 24
H	L		Laptop	60	60	12	9 – 21
H	L	I	LCD display	160	0	24	0 – 24
H	L	I	Lighting LED lamps (33 Nos)	20	10	4	20 – 24
H			Microwave	800	0	2	7 – 9
H	L		Projector	60	0	1	10 – 11
H			Crew Laptop-1	65	0	10	8 – 18
H			Crew Laptop-2	80	0	6	9 – 15
H			Crew Laptop-3	60	0	3	9 – 12
H			Crew Laptop-4	80	0	10	9 – 19
H			Crew Laptop-5	65	0	8	9 – 17
H			Crew Laptop-6	70	0	2	18 – 20
H			Crew Smartphone-1	2	0	1	19 – 20
H			Crew Smartphone-2	2	0	1	20 – 21
H			Crew Smartphone-3	5	0	2	20 – 22
H			Crew Smartphone-4	3	0	2	17 – 19
H			Crew Smartphone-5	2	0	3	18 – 21
H			Crew Smartphone-6	3	0	1	20 – 21
H	L		Camera-1	10	0	2	10 – 12
H	L		Camera-2	10	0	1	15 – 16
H	L		Camera-3	10	0	1	21 – 22
H			Treadmill	800	0	5	5 – 10
H	L		Refrigerator	10	10	24	0 – 24
H			Hair dryer	1200	0	1	8 – 9
H			Washing machine	2000	0	1	18 – 19
H			Vacuum cleaner	1.5	0	1	7 – 8
H	L	I	Electrical power system	200	200	24	0 – 24
H	L	I	Communication system internal components	1500	750	24	0 – 24
H	L	I	Communication system external components	1000	1000	24	0 – 24
H	L	I	Central computer	100	100	24	0 – 24
H	L		Spacesuit battery charger	140	140	6	23 – 5
H	L		Sample drill battery charger	2000	0	1	15 – 16
H	L	I	Active thermal control system-daytime	1200	900	24	0 – 24
H	L	I	Active thermal control system-nighttime	1900	1500	24	0 – 24
H	L	I	Sensors	4000	3000	24	0 – 24
	L		3D printer	700	0	12	9 – 21
	L		Welder	5000	0	1	11 – 12
	L		Laboratory electric arc furnace	5000	0	1	13 – 14
	L		Manufacturing device	2000	0	1	10 – 11
	L		Rover charging	7000	1000	6	23 – 5
	L		Pressurized EV charging	10 000	3000	6	23 – 5
	L		Unpressurized EV charging	3000	2000	6	23 – 5
		I	ISRU	65 000	500	24	0 – 24

2.4 Optimal sizing of PV and battery systems

This section explains the methodology to obtain the optimal PV array area and capacity of the battery using the proposed optimization function. The optimization considers

battery degradation and constraints related to battery and power balance, as discussed in the following sections.

2.4.1 Battery constraints

Among the several types of ESS, the Li-ion batteries have energy density and specific energy of approximately 200 Wh/l and $150 - 200$ Wh/kg, making it a suitable ESS to be used for the lunar MG [8, 10, 21, 40]. The battery charging/discharging can be determined using the following [21]:

$$\begin{aligned} \text{Charging: } E(t+1) &= E(t) + P_c^t \eta_c \Delta t \\ \text{Discharging: } E(t+1) &= E(t) - \frac{P_d^t}{\eta_d} \Delta t \end{aligned} \tag{2.5}$$

where the period between two successive instants is denoted by Δt. Charging/discharging power of battery, P_c^t and P_d^t, respectively, are constrained by [21]:

$$\begin{aligned} 0 \leq P_c^t &\leq P_c^{t,max} \\ 0 \leq P_d^t &\leq P_{d,}^{t,max} \end{aligned} \tag{2.6}$$

In addition, the restriction in the amount of energy stored within the battery is as follows [21]:

$$E^{min} \leq E(t) \leq E^{max} \tag{2.7}$$

where E^{min} and E^{max} is determined as the following:

$$\begin{aligned} E^{min} &= (1 - B_{dod})\, E_{cap} \\ E^{max} &= B^{max} E_{cap} \end{aligned} \tag{2.8}$$

The restriction on the battery's final energy at the end of the period of optimization is given by:

$$E(T) = (1 \pm \delta) E(0) \tag{2.9}$$

Flexibility on the final energy stored in the battery is introduced using δ varying between 0 and 1.

2.4.2 Battery degradation

The deterioration in battery performance is influenced by the number of cycles, called cyclic aging, and the duration for which the battery is operational, called calendar aging. Batteries are affected by their operating temperature, SoC, depth of discharge (DOD)

and duration of use [21, 63]. The total degradation in battery capacity caused by cyclic and calendar aging as suggested by the authors of [63] are given as follows:

$$\begin{aligned} L_{cyc} &= \sum_{i}^{N} n_i f_{cyc}\left(\rho_i, \lambda_i, T_{c,i}\right) \\ L_{cal} &= f_{cal}\left(t, \overline{\rho}, \overline{T}_c\right) \\ f_d &= L_{cyc} + L_{cal} \end{aligned} \tag{2.10}$$

where n_i is 0.5 or 1 depending on whether the cycle is half or full, respectively. Further, the f_{cyc} and f_{cal} is determined as follows [21, 63]:

$$f_{cyc}\left(\rho, \lambda, T\right) = S_\lambda(\lambda) S_\rho(\rho) S_T(T) \tag{2.11}$$

$$f_{cal}\left(t, \rho, T\right) = S_t(t) S_\rho(\rho) S_T(T). \tag{2.12}$$

where S_λ, S_ρ, S_T and S_t is determined as follows [21, 63]:

$$S_\lambda(\lambda) = \left(k_{\lambda 1} \lambda^{k_{\lambda 2}} + k_{\lambda 3}\right)^{-1} \tag{2.13}$$

$$S_\rho(\rho) = e^{k_\rho(\rho - \rho_{ref})} \tag{2.14}$$

$$S_T(T) = e^{k_T(T - T_{ref})\frac{T_{ref}}{T}} \tag{2.15}$$

$$S_t(t) = k_t t \tag{2.16}$$

Therefore, the decrease in battery capacity can be determined as follows [21, 63]:

$$E_{cap}^{new} = \left(1 - f_d\right) E_{cap} \tag{2.17}$$

In addition, the number of battery cycles is limited by [21]:

$$B_{cycles} < B_{totcycles} \tag{2.18}$$

where $B_{totcycles}$ is determined as [10, 21]:

$$B_{totcycles} = -0.0799 B_{dod}^3 + 20.035 B_{dod}^2 - 1757.6 B_{dod} + 57778 \tag{2.19}$$

The coefficients and parameters considered in this study are listed in Table 2.3 [21, 63]. The *rainflow cycle counting* algorithm is used to determine the battery's cycle number (half or full), B_{cycles}, DOD and mean SoC at the i^{th} cycle, and start and end time of battery cycle utilizing the SoC of the battery as input [21]. It is assumed that the battery is operating approximately at a temperature of $22°C$ using active and passive thermal management system [21].

Similar to PV cells, cosmic and nuclei/particle radiations in space also cause deterioration in the battery. While the batteries can be protected from detrimental space

Table 2.3: Degradation model parameters [21, 63]

Degradation coefficients	Value	Degradation coefficients	Value
$k_{\lambda 1}$	1.40×10^5	ρ_{ref}	0.5
$k_{\lambda 2}$	-5.01×10^{-1}	k_T	6.93×10^{-2}
$k_{\lambda 3}$	-1.23×10^5	T_{ref}	$25°C$
k_ρ	1.04	k_t	$4.14 \times 10^{-10} s^{-1}$

radiation by employing various methods of shielding, it is impossible to ensure full protection. Battery degradation models based on data collected from different spacecraft have restricted application areas, and other studies focus on battery electrolytes and electrode degradation [21]. Therefore, models for deterioration in batteries caused by cosmic radiation on the Moon need further research and are considered future work by the author.

2.4.3 Power balance constraint

The power balance is maintained using the following [21]:

$$P_{PV}^t = P_L^t + P_B^t \tag{2.20}$$

where during charging $P_B^t = P_c^t$ and while discharging $P_B^t = -P_d^t$.

2.4.4 Proposed optimal sizing algorithm

The expenses for the space mission depend on the mass of the PV arrays and the batteries as they need to be transported from the Earth to the Moon, along with several other structures for building the MG. Therefore, an optimization function is proposed in this study to minimize the area of the PV array, the capacity of the battery and the total cost per day (TCPD) of the battery. The solution to the optimization problem is an optimally sized PV array area and battery capacity. The proposed optimization function is given as [21]:

$$J(E_{cap}, A_a) = TCPD(r, l, E_{cap}, MC, FC) + M_B(E_{cap}) + M_{PV}(A_a) \tag{2.21}$$

where $TCPD$, M_B, and M_{PV} can be determined as [10, 21, 64]:

$$TCPD = \frac{1}{365}\big(AOTC(r, l, E_{cap}, FC) + E_{cap} \times MC\big) \tag{2.22}$$

$$M_B = \frac{E_{cap}}{S_b B_{dod}} \tag{2.23}$$

$$M_{PV} = \sigma_s A_a \tag{2.24}$$

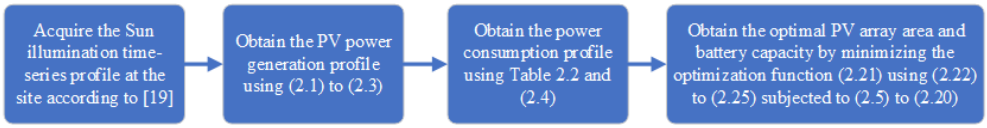

Fig. 2.2: Flow diagram to solve the optimization problem and determine the optimal PV array area and battery capacity

Table 2.4: Parameters considered in the optimization function [21]

Parameters	Value
r	6 %
l	1 (Optimization period: 1 year) 5 (Optimization period: 5 years)
FC	600 \$/kWh
MC	20 \$/kWh
B_{dod}	80 %
η_c	80 %
η_d	80 %
S_b	200 Wh/kg
σ_s	0.55 kg/m^2

The annualized one-time cost (AOTC) of the battery can be determined as [21, 64]:

$$AOTC = \frac{r(1+r)^l}{(1+r)^l - 1} FC \times E_{cap} \tag{2.25}$$

The optimal PV array area and battery capacity from the optimization function ensure that the PV array charges the battery before the solar energy becomes unavailable, during which the battery has to supply the power demand, maintaining the power balance of the system. The different parameters used for the optimization are listed in Table 2.4 [21, 64]. All the constraints related to battery and power balance, as discussed in Section 2.4.1 and Section 2.4.3, respectively, are considered in solving the optimization problem. The complete flow diagram of the optimization algorithm is shown in Fig. 2.2.

2.4.5 Simulation results and discussion

The non-linear optimization problem is solved using the *"interior point algorithm"* of the *Matlab-fmincon* tool for all the 15 candidate sites listed in Table 1.3. The optimization problem is solved by considering 1 year and 5 years periods of optimization. The degradation in battery capacity, as discussed in Section 2.4.2, is taken into consideration only for optimization period of 5 years. B_{dod} and B^{max} are assumed to be set to 80% and 90% to calculate E^{min} and E^{max} in Eq. (2.8), respectively. In addition, the PV arrays are mounted on 10, 50 and 100 m high towers are taken into consideration for

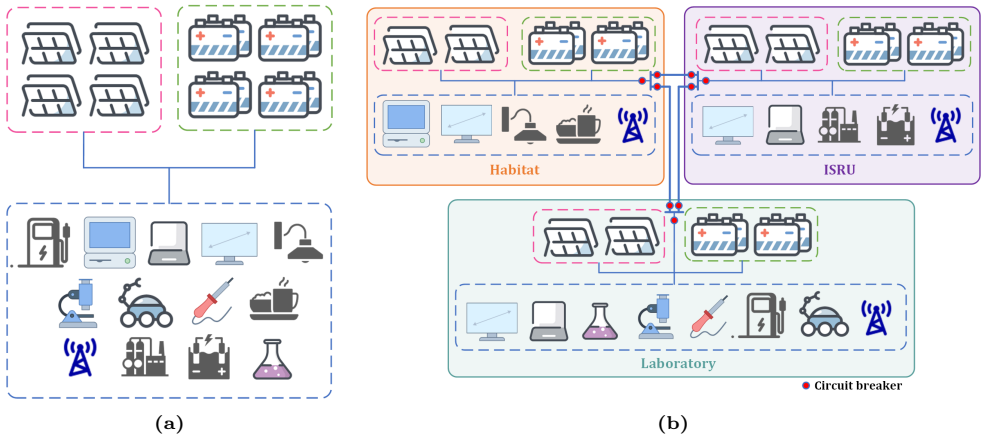

Fig. 2.3: Different lunar MG design approach (a) single MG (b) MMG system[1] [21]
[1] Icons from https://icons8.com

the study [21]. Moreover, the optimization results are analyzed considering both the single MG (see Fig. 2.3a) and MMG system (see Fig. 2.3b) as discussed in Section 2.3.

2.4.5.1 Single MG system design

All power-consuming units listed in Table 2.2 in single MG system are supplied from combined PV arrays and batteries as depicted in Fig. 2.3a. The stored energy level in the battery, power generation profile by the PV arrays, power demand profile and the charging/discharging power profile of the battery for the optimization horizon of 1 year ($\sim 8766\ h$) without taking into account the decline in the capacity of the battery and 5 years period of analysis ($\sim 43830\ h$) considering the decline in the capacity of the battery at site #2 are depicted in Fig. 2.4a and Fig. 2.4b, respectively. The methodology to determine the profile of power demand is described in Section 2.3. The profile of power generation from the PV arrays situated on 10 m high towers having an optimal A_a of 303.83 m^2 and 304.97 m^2 are obtained from the optimization solution for the period of optimization of 1 year and 5 years, respectively. From Fig. 2.4, it can be observed that the reduced level of power demand is provided from the batteries during the period when the generation from PV arrays are unavailable. The decrease in the stored energy level of the batteries can also be observed during this time period. Conversely, the battery is charged during the period PV power is available. In fig. 2.4b, a decrease in E^{max} and E^{min} can be observed after each year for 5 years caused by the degradation of battery capacity as a result of cyclic and calendar aging.

The optimal E_{cap} and A_a are found for all the 15 candidate sites as listed in Table 1.3 using the optimization framework for 1 year and 5 years as depicted in Fig. 2.5a,

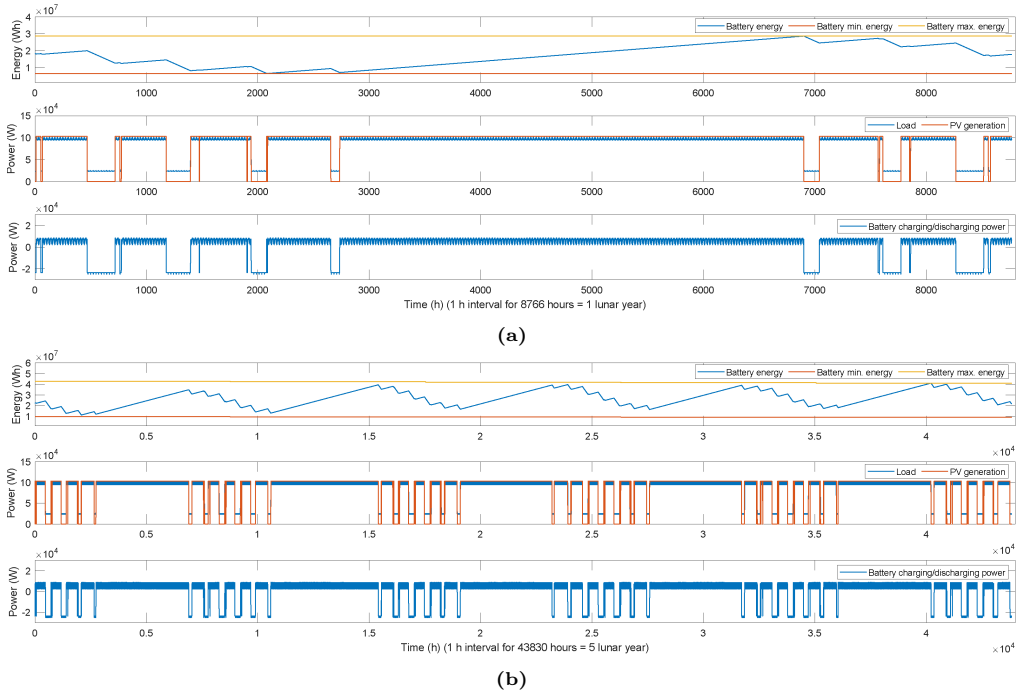

Fig. 2.4: Site #2 single MG design level of energy stored in the battery, profiles of power generation and consumption and charging/discharging power of the battery (a) 1 year without taking into account the decline in the capacity of the battery (b) 5 years taking into account the decline in the capacity of the battery with PV arrays mounted on 10 m high towers [21]

Fig. 2.5c, Fig. 2.6a and Fig. 2.6c, respectively. It was observed that the E_{cap} and A_a are in the order of 10^7 Wh and 10^2 m^2, respectively, for the period of optimization of both 1 year and 5 years. The M_B and M_{PV} from the optimal E_{cap} and A_a are found for all the 15 candidate sites using Eq. (2.23) and Eq. (2.24) for 1 year and 5 years as shown in Fig. 2.5b, Fig. 2.5d, Fig. 2.6b and Fig. 2.6d, respectively. It was observed that the M_B and M_{PV} is the order of 10^5 kg and 10^2 kg, respectively, for both the 1-year and 5-year optimization interval. The area of the PV array, the capacity of the battery and their masses are observed to be reduced as the tower height is increased. It is worth noticing that the area and mass of the PV array are almost the same for both the cases of 1-year and 5-years optimization duration, as deterioration in PV arrays is not considered in this study. However, an increase in battery capacity and mass is observed while increasing the period of optimization from 1 year to 5 years because of a decline in the capacity of the battery for the case of 5 years.

The entire mass of the PV-battery system for the MG at all the 15 candidate sites is

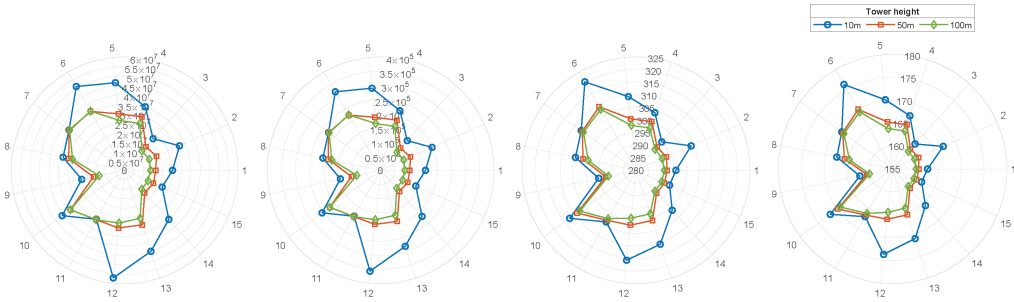

(a) Battery size (Wh) **(b)** Battery mass (kg) **(c)** PV array area (m^2) **(d)** PV array mass (kg)

Fig. 2.5: Capacity and mass of battery and area and mass of PV array for the single MG case and 1-year period of optimization without taking into account the decline in the capacity of the battery at various tower heights [21]

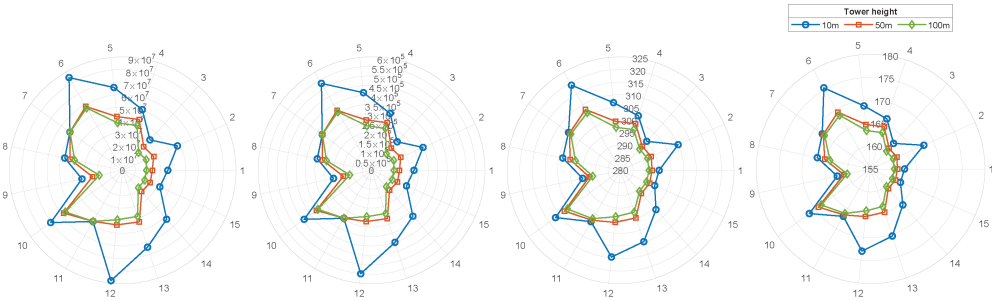

(a) Battery size (Wh) **(b)** Battery mass (kg) **(c)** PV array area (m^2) **(d)** PV array mass (kg)

Fig. 2.6: Capacity and mass of battery and area and mass of PV array for the single MG case and 5-years period of optimization with taking into account the decline in the capacity of the battery at various tower heights [21]

calculated by adding the PV and the battery mass is presented in Fig. 2.9a and Fig. 2.9b for both the 1 year and 5 years optimization horizons, respectively. It is observed from Fig. 2.9a and Fig. 2.9b that the total system mass decreases as the height of the tower is raised. This is because of the fact that, in general, the average illumination at the site enhances as the height of the tower is raised, as can be seen in Fig. 2.10a. Similarly, increasing the tower height also decreases the longest continuous dark period at the site as observed in Fig. 2.10b. From Fig. 2.10a and Fig. 2.10b, it can be observed that raising the height of the tower from 10 m to 50 m for the sites #2, #6, #12, #13, and #14 significantly increases the average illumination condition at the sites along with a considerable decrease in the longest continuous dark period. This rise in mean illumination and reduction in the longest continuous dark period also decreases

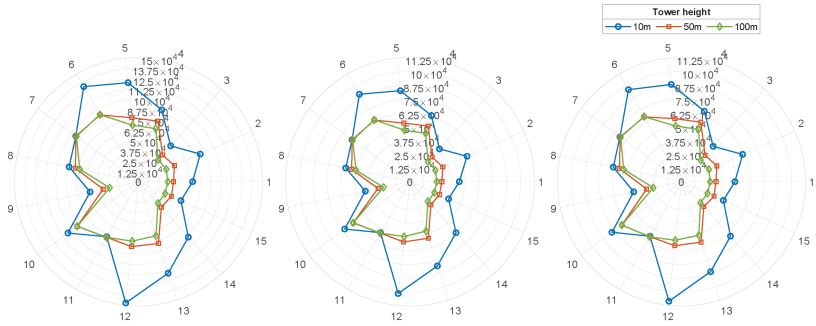

(a) Habitat **(b)** Laboratory **(c)** ISRU

Fig. 2.7: Entire mass of the PV array-battery system (in kg) for 1-year period of optimization considering different sections in the MMG system with PV arrays atop towers of different heights [21]

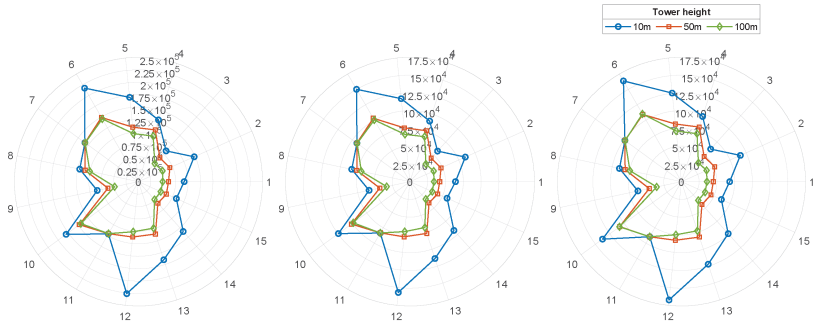

(a) Habitat **(b)** Laboratory **(c)** ISRU

Fig. 2.8: Entire mass of the PV array-battery system (in kg) for 5-years period of optimization considering different sections in the MMG system with PV arrays atop towers of different heights [21]

the combined weight of the system for the single MG case at these sites significantly for both 1-year and 5-year optimization periods as represented in Fig. 2.9a and Fig. 2.9b. The total mass of the PV-battery system decreases by approximately 50% if the tower height of the PV arrays installation is increased from 10 m to 50 m for both the 1-year and 5-year period of optimization. It can be observed from Fig. 2.10a that sites #1, #3, #9, and #15 have an illumination which is highest among other sites with towers of 10 m height and has the total system mass which is lowest among other sites. However, there is a negligible effect of raising the height of the tower from 10 m to 50 m on mean illumination and longest continuous dark period for sites #7 and #11. Therefore, increasing the tower height does not affect the overall weight of the PV-battery system at sites #7 and #11 for both 1-year and 5-year optimization periods. It is worth noticing that the mean illumination and the maximum duration of uninterrupted darkness are

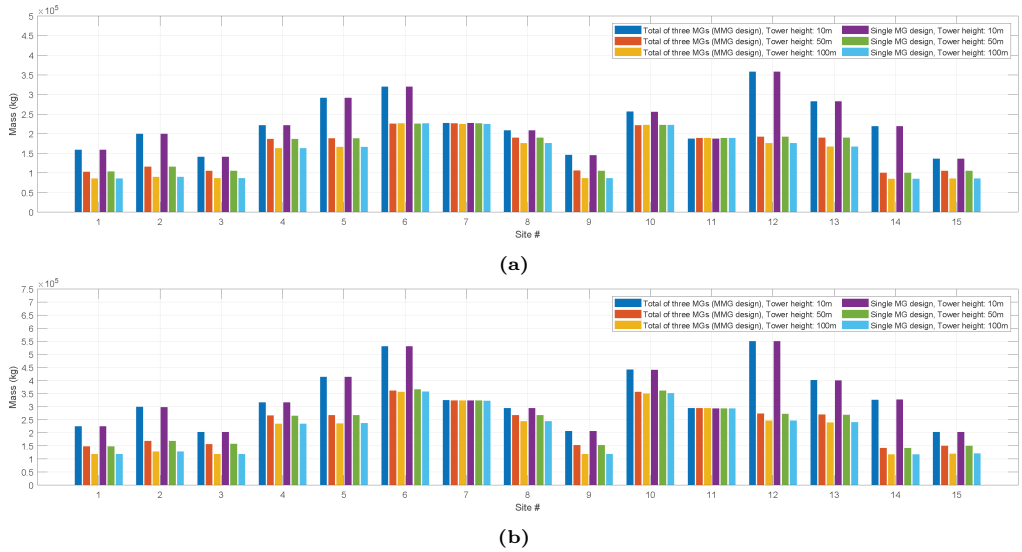

Fig. 2.9: Entire mass of the PV array-battery system (in kg) comparison of MMG and single MG system for (a) 1 year without (b) 5 years with taking into account the decline in the capacity of the battery

similar but not exactly the same for each of the 5 years. Thus, the optimal area of the PV array and the capacity of the battery for one of the years might be similar to those from other years but not identical.

2.4.5.2 MMG system design

In this study, the power-consuming units are divided into three sections, each section having its own PV array and battery system as discussed in Section 2.3, forming the habitat, ISRU, and laboratory MGs as depicted in Fig. 2.3b. Instead of a centralized PV-battery system as in a single MG design, the assets of each MG in the MMG system can be utilized by the other MGs in case of faults or disturbances, increasing the resiliency of the MMG system. The entire mass of the PV-battery system for the habitat, laboratory, and ISRU MGs at the 15 candidate sites are shown in Fig. 2.7 and Fig. 2.8 for 1-year and 5-year periods of optimization, respectively, which is in the order of 10^4 to 10^5 kg. It can be observed that the entire mass of the PV-battery system of the habitat MG is more than the laboratory and ISRU MGs for both cases, as the habitat MG consists of more critical power-consuming units that must be supplied from the batteries during the dark periods. The entire mass of the PV-battery system of the three MGs in the MMG system is compared with the single MG design in Fig. 2.9a and Fig. 2.9b for both assumed optimization periods. It is observed that, for both 1-year and 5-year horizons,

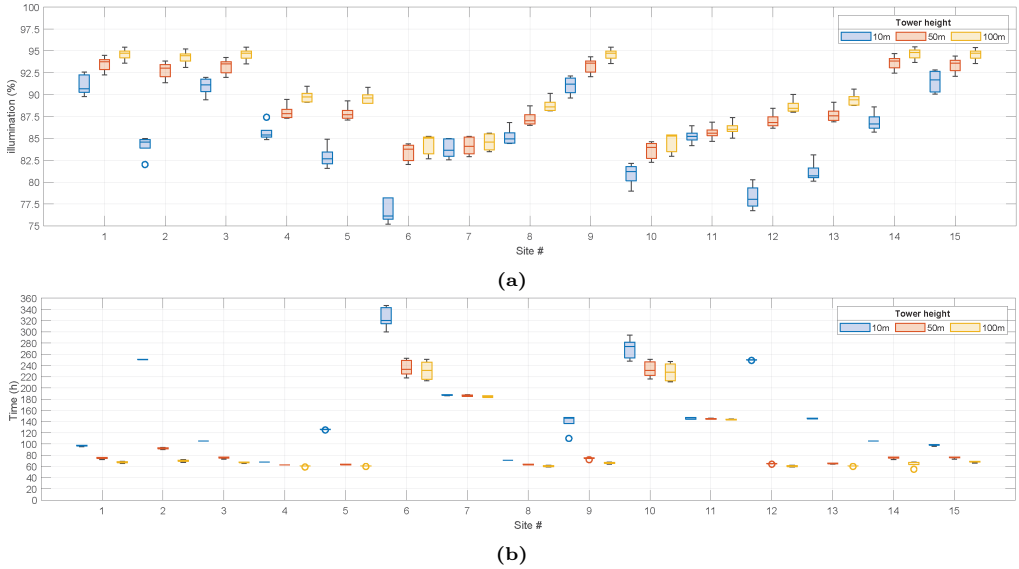

Fig. 2.10: (a) Illumination condition (b) Longest continuous dark period for different sites with PV arrays atop towers of different heights [21]

the combined mass of the MMG system design is nearly equal to the weight of a single MG configuration in all candidate locations. Thus, the MMG system design can increase the reliability of the power system without affecting the total mass of the PV-battery system.

It is worth noticing that raising the height of the towers with PV arrays improves the illumination condition of most of the sites, as can be seen in Fig. 2.10a, but a rise in the structural mass of the tower is also inevitable. On the other hand, a decrease of 10^4 kg to 10^5 kg in the weight of the battery is observed even though the mass of the towers becomes heavier. The tower can be made up of carbon composite structures [10] or using concrete produced from lunar regolith [65], in which transportation of towers from the Earth is not required. Other than mounting the PV arrays, the high towers have the advantage of using it for communication within the base, transmitting power using RF or lasers, and lighting the base area. Furthermore, the entire mass of the MMG system is calculated based on only the weight of PV and battery. However, given the extra weight of supplementary equipment like power cables, converters, devices for system protection, etc., it is anticipated that the total system mass for the design of MMG system will be larger. A more thorough investigation in this regard is considered a future work by the author.

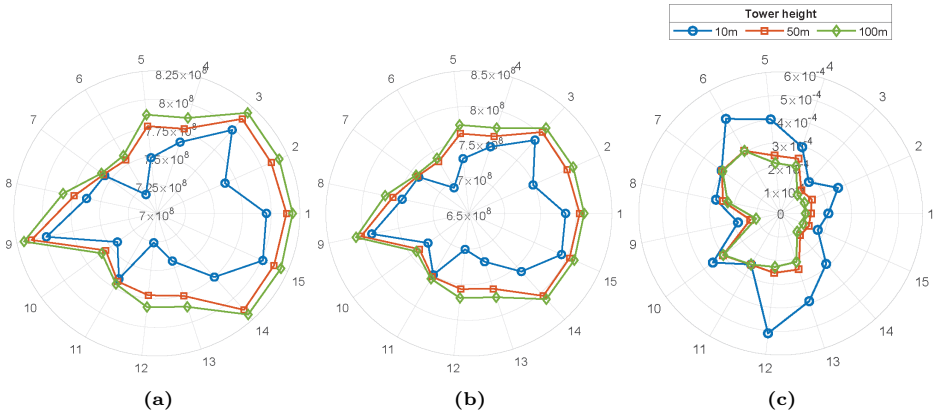

Fig. 2.11: (a) Total power generated by the PV arrays $[W]$ (b) total power supplied to loads $[W]$ (c) mass-per-unit-load $[kg/W]$ in case of the single MG configuration at various heights of tower considering 1 year period of optimization [21]

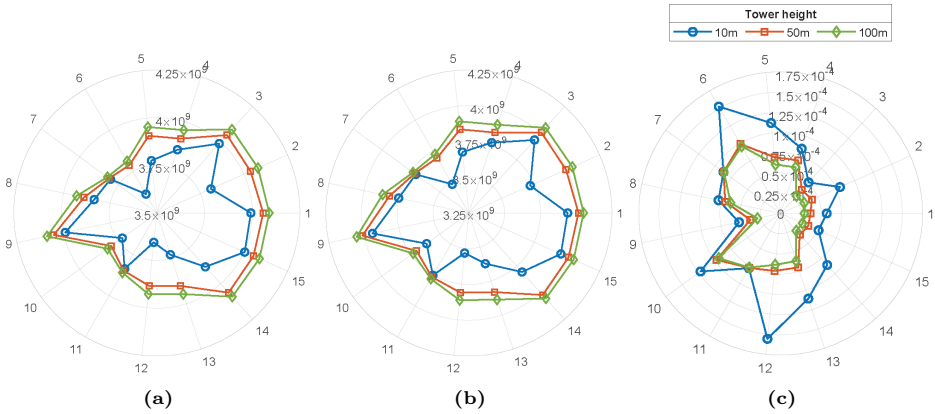

Fig. 2.12: (a) Total power generated by the PV arrays $[W]$ (b) total power supplied to loads $[W]$ (c) mass-per-unit-load $[kg/W]$ in case of the single MG configuration at various heights of tower considering a 5-year period of optimization [21]

2.5 Site selection

An ideal site for the base should not only have low PV-battery system mass but also serve a high total power demand. Therefore, the ratio between the combined system weight and the total power supplied to loads at a site is evaluated, called MPUL, to determine the location that serves the greatest power demand with the minimal overall

weight of the system. The MPUL of a site can be determined as follows [21]:

$$\text{MPUL} = \frac{\text{Total system mass}}{P_L^{total}} \tag{2.26}$$

where P_L^{total} can be determined as follows [21]:

$$P_L^{total} = \sum_{t=0}^{T} P_L^t \tag{2.27}$$

The Fig. 2.11 and Fig. 2.12 shows the total power generated from the PV, total consumption of power and the MPUL for the 15 candidate sites for 1-year and 5-year periods of optimization, respectively. It is observed from Fig. 2.11c and Fig. 2.12c that, the total power demand of roughly 7.8×10^8 W and 3.9×10^9 W is served by the sites #1, #3, #9, and #15 with a tower of 10 m height, which is among the highest compared to other sites for both 1-year and 5-year periods of optimization, respectively. Site #3 and #15 have MPUL of roughly 1.7×10^{-4} kg/W and 5.1×10^{-5} kg/W, which is the least among the 15 candidate sites for both 1-year and 5-year analysis periods, respectively. With PV arrays mounted at a height of 50 m using towers, low MPUL is observed in sites #1, #2, #3, #9, #14, and #15, among which lowest MPUL of 1.2375×10^{-4} kg/W is observed at site #14 for an analysis period of 1 year. Site #14 is observed to have the lowest MPUL of 3.53×10^{-5} kg/W also with an increased optimization horizon of 5 years and tower heights of 50 m as shown in Fig. 2.12c. With the increased tower height of 100 m, site #14 is observed to have the lowest MPUL of 1.0446×10^{-4} kg/W and 2.879×10^{-5} kg/W for 1-year and 5-year analysis periods, respectively.

2.6 Conclusion

In this chapter, the optimal area of the PV array and the capacity of the battery for a PV-battery-based MG were found using an optimization function to minimize the mass of the PV array, the mass of the battery and total cost per day of the battery for 15 potential locations in close proximity of the south pole. The time-series profile of Sun illumination at the site was utilized to determine the power generation from the arrays of PV installed at a height of 10, 50, and 100 m using towers. The area of the PV array and the capacity of the battery were optimally sized using the profile of power consumption, and generation from PV, and the time-of-use of multiple units that consumes power in the base. An analysis period of 1 year and 5 years were taken into account for finding the solution to the optimization problem, considering annual degradation in battery capacity caused by the calendar and cyclic aging for the case of 5 years. It was found that the entire mass of the PV-battery system of 15 candidate sites is roughly within 1.5×10^5 kg to 3.5×10^5 kg and 2×10^5 kg to 5.5×10^5 kg for

1-year and 5-year periods of optimization, respectively, taking into account that the PV arrays are mounted on 10 m high towers. By raising the height of the towers to 50 m and 100 m, the entire mass of the system approximately changes within 1×10^5 kg to 2.25×10^5 kg and 1.5×10^5 kg to 3.25×10^5 kg for analysis periods of 1 year and 5 years, respectively. One of the disadvantages of raising the height of the tower is the rise in the mass of the tower structure which would be added to the entire system mass. However, increasing the tower height also reduces the mass of the battery by 10^4 kg to 10^5 kg. Furthermore, high towers can also be utilized for wireless power transmission using RF and lasers, as well as for lighting and communication within the base. The potential of grouping multiple units that consume power into several sections, with each section having its own PV-battery unit to form a MMG was also investigated. It was noted that the entire mass of the PV-battery system accounting for only the mass of the PV array and battery, taking into consideration the MMG design is almost similar to the single MG design. In addition, a MPUL criterion was proposed to determine the location serving the greatest total power consumption with minimal overall system weight.

Chapter 3: Energy management system for lunar MG

This chapter enlightens the importance of having efficient operation management and EMS of the base, taking into consideration several interacting subsystems of the base. The chapter explores the problem statement and the proposed solution in the introduction section. The rest of the chapter presents the proposed model for interaction among multiple subsystems for the safe operation of the base, the proposed optimization framework to determine the profile of power demand of the base, the proposed optimization framework to obtain the operation management, and EMS of the base, the results of the optimization and the comparison of several sites in close proximity of the lunar south pole.

3.1 Introduction

In Table 2.2 of Chapter 2, it was considered that each power-consuming unit in the base has two states of power, namely, active and survival. Each power-consuming unit is considered to consume a constant level of power throughout its active or survival state of operation. Typically, a similar strategy is used while calculating the power budget of the space mission, where the power consumption of multiple power-consuming units is taken to be at a fixed average or maximum required power. However, most of the power-consuming units in a subsystem consume power depending on their rate and mode of operation. For instance, the power demand of the power-consuming units to maintain the artificial atmosphere depends on the consumption rate of several gases in the habitat. In a base, there are multiple subsystems that operate in tandem to maintain the ECLSS. There are also several interacting subsystems in the base, such as habitat, water, biomass production, and ISRU, among others. For instance, the production of oxygen and water in the ISRU depends on the oxygen and water requirement of the habitat. Along with ISRU, the biomass production subsystem can also supply oxygen for the crew members utilizing the photosynthetic photon flux (PPF) provided to the plants. The plants in the biomass production subsystem can also make use of the carbon

dioxide produced by the crew members. In addition, in a resource-scarce environment like space, recycling resources plays an important role. The wastewater produced in the base can also be filtered for reuse by the crew members. Thus, the power demand of the base is determined by the rate of oxygen and water consumption in the habitat, rate of PPF, oxygen production and carbon dioxide consumption rates by the plants, and wastewater production rate by the crew members, among others. Therefore, the operation mode and rate of several interacting subsystems in the base affect the power demand of the base.

Moreover, in low and medium Earth orbits-space missions, it is possible to communicate instantly with the ground stations. As space expeditions venture deeper into space, transmitting communication and command signals from ground stations is significantly delayed or even get hindered by celestial bodies, in case of which the information needs to be transmitted via a satellite, resulting in additional delay [55, 59, 66]. Even a slight delay of just a few milliseconds can have disastrous consequences for a space mission. In present days, the processing of large amounts of data is incredibly fast, which allows us to automatically decide and take action within a few milliseconds. Self-governing systems can quickly adjust to an unpredictable and rapidly altering environment in space. The newer generation spacecraft models, such as *Dragon* and *Starship* by *SpaceX* and *Orion* by NASA, have the ability to operate independently in carrying out space missions involving humans or cargo. Therefore, developing an APC for space MGs on the Moon is essential to guarantee a secure and reliable operation of the base.

In an interaction of several subsystems, the APC can coordinate the power and operation management of the base by scheduling the operating mode and rate of several interacting power-consuming units. An architecture to implement APC for spacecraft is proposed in [55, 59, 60] having three different levels for managing diverse problems, namely, vehicle manager, subsystem, and reactive levels. A similar approach is implemented in hierarchical control structure (HCS) for terrestrial MGs, where the three levels are called tertiary, secondary and primary. The vehicle manager and tertiary level are the topmost control levels of APC and HCS, respectively. Similar to the tertiary level, the vehicle manager is accountable for planning, scheduling and operating several subsystems with information on their power demand during specific time intervals.

In this chapter, the interaction among several subsystems for maintaining the oxygen and water requirement of the base is considered and an optimization framework for the optimal operation management of several interacting subsystems is proposed. The rest of the chapter is arranged as follows. The interaction within the various subsystems of the base for oxygen and water management of the base are discussed in Section 3.2. An optimization framework for generating the optimal power demand profile for ISRU is proposed in Section 3.3. The optimal sizing and operation management of MGs based on PV arrays and battery for the base is proposed in Section 3.4. The selection of sites based on the MPUL criteria is discussed in Section 3.5. Finally, Section 3.6 concludes the chapter with remarks.

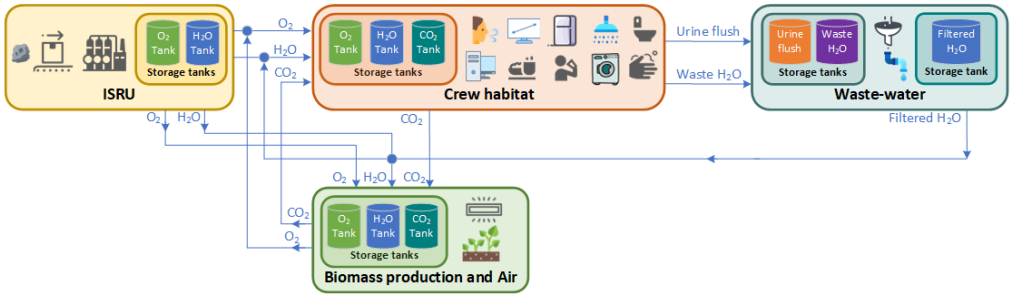

Fig. 3.1: Interacting subsystems for gases and water management in the base

3.2 Interacting subsystems for oxygen and water management

In a lunar base, there are several subsystems to maintain the ECLSS of the base. The oxygen and water management in the base includes managing the production of oxygen and water in the ISRU, consumption of oxygen and water in the habitat, production of oxygen in the biomass subsystem, wastewater production in the habitat, and production of freshwater from the wastewater filtration system in the wastewater subsystem, among others. Fig. 3.1 shows the interacting subsystems for operation management in the base.

The ISRU is accountable for producing water from the lunar regolith, which undergoes electrolysis to produce oxygen and hydrogen [9, 10]. The oxygen and water are assumed to be stored in tanks for later use in the base. It is desired to use hydrogen as a propellant for spacecraft and is not shown in the Fig. 3.1 as it is not used in the base. The process of producing oxygen and water requires the intake of regolith, performing catalyzed hydrogen reduction reaction and electrolysis of water, which consumes electrical power [10, 66]. The rate at which regolith is taken by the ISRU determines its operation rate and power consumption profile. The optimal profile of power consumption by the ISRU for producing the required oxygen and water is explored more thoroughly in Section 3.3. The total power demand profile of the ISRU includes power for running several other systems in the ISRU, which are discussed in Section 3.4.1.

The oxygen and water in the storage tanks of ISRU are used in biomass and habitat subsystems by the plants and crew members, respectively, as depicted in Fig. 3.1. It is presumed that the biomass and habitat subsystems consist of oxygen and water storage tanks which are transferred from the respective storage tanks of ISRU. Other than oxygen, there is another storage tank for carbon dioxide in both the biomass and habitat subsystems. The carbon dioxide that is released by the crew members is used by the plants in the biomass subsystem through the storage tanks. The artificial atmosphere consists of several other gases such as nitrogen, argon, and traces of other gases [67],

Table 3.1: Specification of the installed sensors at MPP

Parameter	Value
Supply Voltage	110 V to 230/240 V
Supply frequency	50/60 Hz
Maximum Measurement	120 A
Operating temperature	$-40°/-20°C$ to $20°C$
RF output power	1 to 12 mW
Radio protocol	Wi-Fi 802.11 b/g/n
Radio frequency	$2412-2472$ MHz
Operating range	Outdoors - up to 50 m Indoors - up to 30 m
Self-power consumption	< 1 W

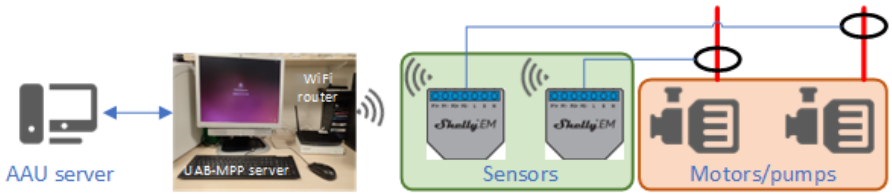

Fig. 3.2: Architecture of the data collection for energy consumption of the MPP

which are not considered in the modeling of the interacting subsystems in this thesis.

Identification of the rate of oxygen, carbon dioxide, and water usage by various plants in the biomass production subsystem to produce food is still under laboratory tests. Such a testing facility called Micro-Ecological Life Support System Alternative (MELiSSA) pilot plant that is established by ESA in collaboration with Universitat Autònoma de Barcelona, Spain. The MELiSSA pilot plant (MPP) is a self-sustainable closed ecological LSS to maintain the artificial environment and provide recycled water and food without any exchange of resources (except energy) from outside the loop. The plants are also provided with various PPF varying the composition and intensity of artificial lights to investigate the effect of lighting conditions on the growth, consumption of gases and water, and production of gases by the plants. Power is consumed to maintain the artificial lighting conditions and an environment composed of several gases. Developing a complete model of power and energy consumption of the biomass production subsystem to maintain the artificial lighting conditions and environment is under investigation by the author and is not considered as a part of the interacting subsystems of the base in this thesis.

To develop the model, several sensors have been installed in the MPP to measure the power requirement of several devices and to monitor the energy required for different processes and conditions. The sensors collect several data, such as the voltage, current,

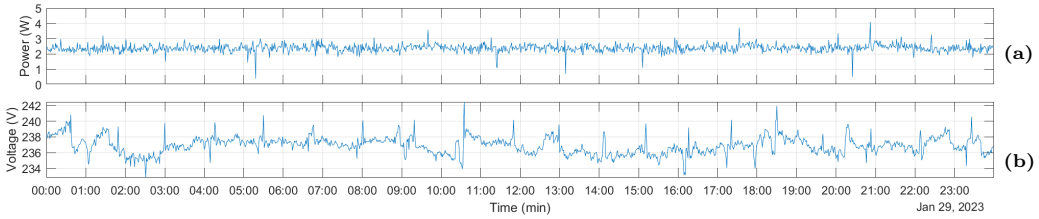

Fig. 3.3: (a) Instantaneous power (b) voltage supplied to one of the pumps at standby mode in MPP for one day

instantaneous power, power factor, and energy consumption, among others, of different pumps, motors, and auxiliary equipment required for the operation of the plant. Some of the specifications of the sensors are listed in Table 3.1. The data is communicated over WiFi to the router connected to the server installed at the plant. The collected data is stored locally on the server. From the server, the data can also be downloaded on the server installed at the IoT house laboratory at AAU Energy, Aalborg University (AAU), Denmark. The complete architecture of collecting the data is shown in Fig. 3.2. The power and voltage supplied to one of the pumps in standby mode of operation for one day are shown in Fig. 3.3. The collected data is used for the development of the power demand model for the biomass production subsystem to be integrated into the model of other interacting subsystems of the base. This is ongoing research by the author, and its time schedule is beyond the time horizon of this thesis.

In the habitat, different gases are transferred from the respective storage tanks to maintain a safe level of gas pressure and composition. In the current design, it is assumed that the biomass production subsystem is the only subsystem that consumes carbon dioxide produced in the habitat. In this thesis, the carbon dioxide cycle is not taken into account and will not be further discussed. A simplified block diagram of several interacting subsystems is shown in Fig. 3.4. The crew members consume oxygen for their daily activities from the habitat oxygen storage tank (see Section 3.3.1 for more details). Water is also used for drinking and several other purposes in the habitat, and the produced wastewater is filtered in the wastewater subsystem. The wastewater subsystem stores the filtered water in a tank which is resupplied in the habitat for further use. The system for managing the water resources of the base is further discussed in Section 3.3.2. The consumption rates of oxygen and water, along with the wastewater generation and filtration rates, determine the rate at which oxygen and water must be transferred to the respective storage tanks of the habitat. The habitat is also equipped with several other power-consuming devices, which are required for LSS of the crew members and the operation of the base. The power demand of the habitat is discussed in detail in Section 3.4.2.

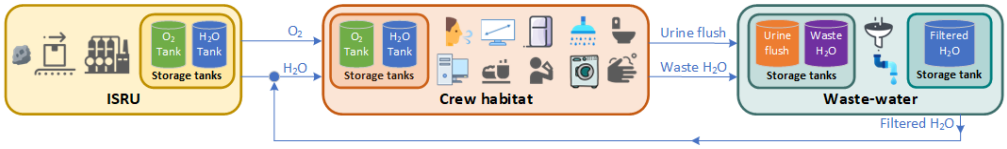

Fig. 3.4: Simplified interaction of subsystems for oxygen and water management in the base

3.3 ISRU optimal power demand profile

The authors of [10] propose the model to determine the power demand of ISRU for producing oxygen and water from lunar regolith. The process involves scooping, transporting, vibrating, magnetically separating and transferring the ilmenite from the regolith to the reactor. Catalyzed hydrogen reduction reaction in the reactor produces water which undergoes electrolysis to generate oxygen. Electrical power is utilized for the process of electrolysis and for the motors to scoop, transport, vibrate, magnetically separate, and transfer the ilmenite to the reactor. The reactors required thermal power to perform the reduction reaction. Thermal power can be supplied from the energy of the Sun utilizing concentrators to gather sunlight and guide them using optical waveguides [37–39]. However, in this study, it is assumed that electrical heaters provide the required thermal power consuming electrical power [10, 21]. Therefore, the thermal power and the electrical power are combined together to determine the total power consumption of the ISRU, as shown in Fig. 3.5 [66]. From Fig. 3.5, it can be observed that the rate at which water and oxygen are produced increases linearly with the increase in the rate of ilmenite replenished in the reactor (V_{ir}) from 0 to 1. It is worth noticing that both water and oxygen are generated at any given rate of regolith intake. The rate at which water is produced is always higher than the rate of oxygen production, as shown in Fig. 3.5. With the increase of V_{ir}, the total power consumption of ISRU also increases, and at intake rates more than 0.75, the total power demand of the ISRU is more than 10^3 kW. A large PV-battery system is necessary to meet such a high demand for power, and installing such a huge power generation and storage system can prove to be difficult. Therefore, the maximum power consumption of the ISRU is restricted by limiting the maximum V_{ir}, fulfilling oxygen and water requirements of the base [66]. The oxygen and water produced by the ISRU are consumed in the habitat, as discussed in the following subsections.

3.3.1 Maintaining artificial atmosphere in habitat

To support the life of crew members, it is crucial to maintain the pressure, temperature, humidity, and composition of gases. This study focuses solely on monitoring and controlling the levels of oxygen pressure and concentration within the habitat. The level

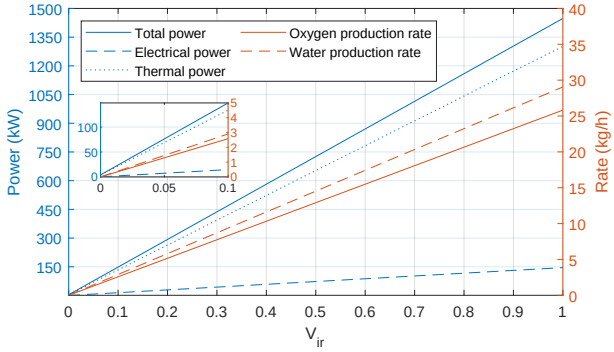

Fig. 3.5: ISRU power demand of ISRU and production rate of oxygen and water with different rates of ilmenite intake (V_{ir}) [66]. Inset figure: V_{ir} varying from 0 to 0.1.

Table 3.2: Daily activity schedule of crew members and oxygen consumption rate of one crew member for each activity [66, 68, 69]Table 3-25 (p. 49) of [68]

Time (h)	Activity	Oxygen consumption (g/min)
00:01 - 06:00	Sleep	0.37
06:01 - 07:00	Post sleep task–Nominal	0.59
07:01 - 08:00	Exercise	3.99
08:01 - 09:00	Exercise recovery	0.59
09:01 - 21:00	Nominal	0.59
21:01 - 22:00	Pre-sleep task–Nominal	0.59
22:01 - 00:00	Sleep	0.37

Table 3.3: Habitat atmosphere pressure and composition [68]

Component	Pressure (kPa)			Concentration (%)
	Lower	Nominal	Upper	Nominal
Oxygen	20.7	21.2	50.6	20.9
All gases	48.0	70.3	102.7	100.0

of oxygen in the habitat depends on the several tasks performed by the crew members during the day. To preserve the health of the crew members during their stay in space, it is recommended that crew members get sleep of 8 h, engage in aerobic exercises of 1 h, take 1 h for exercise recovery, and spend 13.5 h on nominal other activities [66, 68]. A schedule for each of these daily activities and the oxygen consumption rate for each of these activities is listed in Table 3.2 [66, 68, 69]. Using Table 3.2, the daily oxygen consumption profile for four crew members in the habitat is generated as shown

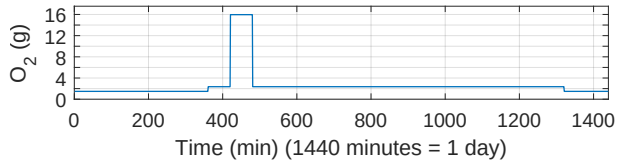

Fig. 3.6: Daily oxygen usage profile by a team of four crew members [69]

in Fig. 3.6 [66, 69]. In this study, the mission is considered to be 708 h long, which is approximately 1 lunar month. The oxygen consumption profile of the habitat for the whole duration of the mission is formed by repeating the daily oxygen consumption profile shown in Fig. 3.6.

The *Ideal Gas Law* ($pV = nRT$) is utilized to regulate the required level of pressure and concentration of oxygen in the habitat. NASA human research program has developed a facility called Human Exploration Research Analog (HERA) for carrying out analog missions to experiment on isolation and other conditions during space exploration. The HERA consists of four chambers, namely, core, loft, airlock and hygiene module, which has a total volume of 148.6 m^3 and maintains a temperature of 295.37 K, which is also taken into consideration in this study. Table 3.3 lists the oxygen pressure and concentration considered in this study. The amount of oxygen consumption and infusion in the habitat is measured as n *mols* and Algorithm 1 [66] maintains the required pressure and concentration of oxygen in the habitat. The O_2^{out} determines the amount of oxygen that is consumed in the base, which is translated in terms of $n_{O_2}^{out}$. The amount of $n_{O_2}^{in}$ infused in the habitat is calculated by comparing $pV_{O_2}^{err}$, $T_{hab_{O_2}}$, and $O_2^{in_{max}}$.

The habitat oxygen tank fulfills the oxygen consumption in the habitat which is refilled from the ISRU oxygen tank as shown in Fig. 3.4. Algorithm 2 [66] transfers the required amount of oxygen from the oxygen tank of ISRU to habitat after comparing the $T_{hab_{O_2}}^{err}$, $T_{ISRU_{O_2}}^{min}$, and $O_{2_{ISRU-hab}}^{max}$.

3.3.2 Water management system in habitat

Supplying the required amount of water in the habitat is as crucial as maintaining the oxygen levels in the habitat. The water in the habitat is used from the habitat water tank several purposes such as drinking, rehydrating the food, maintaining personal hygiene and showering, urine, and urinal flush, among others [66, 68, 69] which generates wastewater. The amount of water consumption and wastewater generation by one crew member for several activities in the habitat is listed in Table 3.4 [66, 68–70]. The water consumption, wastewater and urine wastewater generation profile by four crew members in the habitat following the schedule of daily activities as listed in Table 3.5 is shown in Fig. 3.7a, Fig. 3.7b, and Fig. 3.7c, respectively.

Algorithm 1 Proposed algorithm for maintaining the desired level of pV of oxygen in the habitat [66]

Input: CM, O_2^{out}, pV_{O_2}, $pV_{O_2}^{ref}$, $T_{hab_{O_2}^{ref}}$, $O_2^{in_{max}}$, $T_{hab_{O_2}}^{min}$, M_{O_2}

Set: $\Delta_m = 1min$
$n_{O_2}^{out} = O_2^{out}/M_{O_2}$
$pV_{O_2}^{err} = pV_{O_2}^{ref} - pV_{O_2}$
if $pV_{O_2}^{err} > 0$ **then**
  $n_{O_2}^{in} = pV_{O_2}^{err}/(RT\Delta_m)$
  $O_2^{in} = n_{O_2}^{in} M_{O_2}$
  if $T_{hab_{O_2}} - \left(O_2^{in}\Delta_m\right) > T_{hab_{O_2}}^{min}$ *and* $O_2^{in} < O_2^{in_{max}}$ **then**
    $T_{hab_{O_2}} = T_{hab_{O_2}} - \left(O_2^{in}\Delta_m\right)$
    $pV_{O_2} = pV_{O_2} - n_{O_2}^{out} RT\Delta_m + n_{O_2}^{in} RT\Delta_m$
  else if $T_{hab_{O_2}} - \left(O_2^{in}\Delta_m\right) \leq T_{hab_{O_2}}^{min}$ *and* $O_2^{in} < O_2^{in_{max}}$ **then**
    $O_2^{in} = \left(T_{hab_{O_2}} - T_{hab_{O_2}}^{min}\right)/\Delta_m$
    $T_{hab_{O_2}} = T_{hab_{O_2}} - \left(O_2^{in}\Delta_m\right)$
    $n_{O_2}^{in} = O_2^{in}/M_{O_2}$
    $pV_{O_2} = pV_{O_2} - n_{O_2}^{out} RT\Delta_m + n_{O_2}^{in} RT\Delta_m$
  else if $T_{hab_{O_2}} - \left(O_2^{in}\Delta_m\right) > T_{hab_{O_2}}^{min}$ *and* $O_2^{in} \geq O_2^{in_{max}}$ **then**
    $O_2^{in} = O_2^{in_{max}}$
    $T_{hab_{O_2}} = T_{hab_{O_2}} - \left(O_2^{in}\Delta_m\right)$
    $n_{O_2}^{in} = O_2^{in}/M_{O_2}$
    $pV_{O_2} = pV_{O_2} - n_{O_2}^{out} RT\Delta_m + n_{O_2}^{in} RT\Delta_m$
  else if $T_{hab_{O_2}} - \left(O_2^{in}\Delta_m\right) \leq T_{hab_{O_2}}^{min}$ *and* $O_2^{in} \geq O_2^{in_{max}}$ **then**
    $O_2^{in} = \left(T_{hab_{O_2}} - T_{hab_{O_2}}^{min}\right)/\Delta_m$
    $T_{hab_{O_2}} = T_{hab_{O_2}} - \left(O_2^{in}\Delta_m\right)$
    $n_{O_2}^{in} = O_2^{in}/M_{O_2}$
    $pV_{O_2} = pV_{O_2} - n_{O_2}^{out} RT\Delta_m + n_{O_2}^{in} RT\Delta_m$
  else
    $O_2^{in} = 0$
    $n_{O_2}^{in} = O_2^{in}/M_{O_2}$
    $pV_{O_2} = pV_{O_2} - n_{O_2}^{out} RT\Delta_m + n_{O_2}^{in} RT\Delta_m$
else
  $O_2^{in} = 0$
  $pV_{O_2} = pV_{O_2} - n_{O_2}^{out} RT\Delta_m$

The Fig. 3.4 shows that individual tanks are used to store the wastewater produced within the habitat. To promote recycling of resources within the base and reduce the dependency on the water produced from the ISRU, wastewater is to be filtered using

Algorithm 2 Proposed algorithm to transfer oxygen from ISRU oxygen tank to the crew habitat oxygen tank [66]

Input: $T_{ISRU_{O_2}}$, $T^{min}_{ISRU_{O_2}}$, $T^{ref}_{hab_{O_2}}$, $T_{hab_{O_2}}$, $O^{max}_{2_{ISRU-hab}}$
Set: $\Delta_h = 1h$
$T^{err}_{hab_{O_2}} = T^{ref}_{hab_{O_2}} - T_{hab_{O_2}}$
$O_{2_{ISRU-hab}} = T^{err}_{hab_{O_2}}/\Delta_h$
if $T^{err}_{hab_{O_2}} > 0$ and $O_{2_{ISRU-hab}} \leq O^{max}_{2_{ISRU-hab}}$ and $\left(T_{ISRU_{O_2}} - \left(O_{2_{ISRU-hab}}/10^3\right)\Delta_h\right) \geq T^{min}_{ISRU_{O_2}}$ **then**
  $T_{ISRU_{O_2}} = T_{ISRU_{O_2}} - \left(\left(O_{2_{ISRU-hab}}/10^3\right)\Delta_h\right)$
  $T_{hab_{O_2}} = T_{hab_{O_2}} + \left(O_{2_{ISRU-hab}}\Delta_h\right)$
else if $T^{err}_{hab_{O_2}} > 0$ and $O_{2_{ISRU-hab}} \leq O^{max}_{2_{ISRU-hab}}$ and $\left(T_{ISRU_{O_2}} - \left(O_{2_{ISRU-hab}}/10^3\right)\Delta_h\right) < T^{min}_{ISRU_{O_2}}$ **then**
  $O_{2_{ISRU-hab}} = \left(\left(T_{ISRU_{O_2}} - T^{min}_{ISRU_{O_2}}\right) \times 10^3\right)/\Delta_h$
  $T_{ISRU_{O_2}} = T_{ISRU_{O_2}} - \left(\left(O_{2_{ISRU-hab}}/10^3\right)\Delta_h\right)$
  $T_{hab_{O_2}} = T_{hab_{O_2}} + \left(O_{2_{ISRU-hab}}\Delta_h\right)$
else if $T^{err}_{hab_{O_2}} > 0$ and $O_{2_{ISRU-hab}} > O^{max}_{2_{ISRU-hab}}$ and $\left(T_{ISRU_{O_2}} - \left(O_{2_{ISRU-hab}}/10^3\right)\Delta_h\right) \geq T^{min}_{ISRU_{O_2}}$ **then**
  $T_{ISRU_{O_2}} = T_{ISRU_{O_2}} - \left(\left(O^{max}_{2_{ISRU-hab}}/10^3\right)\Delta_h\right)$
  $T_{hab_{O_2}} = T_{hab_{O_2}} + \left(O^{max}_{2_{ISRU-hab}}\Delta_h\right)$
else if $T^{err}_{hab_{O_2}} > 0$ and $O_{2_{ISRU-hab}} > O^{max}_{2_{ISRU-hab}}$ and $\left(T_{ISRU_{O_2}} - \left(O_{2_{ISRU-hab}}/10^3\right)\Delta_h\right) < T^{min}_{ISRU_{O_2}}$ **then**
  $O_{2_{ISRU-hab}} = \left(\left(T_{ISRU_{O_2}} - T^{min}_{ISRU_{O_2}}\right) \times 10^3\right)/\Delta_h$
  $T_{ISRU_{O_2}} = T_{ISRU_{O_2}} - \left(\left(O_{2_{ISRU-hab}}/10^3\right)\Delta_h\right)$
  $T_{hab_{O_2}} = T_{hab_{O_2}} + \left(O_{2_{ISRU-hab}}\Delta_h\right)$

appropriate filtration techniques to generate freshwater for further use in the habitat. A new process of filtering wastewater, called the alternative water processor (AWP), is being developed to substitute the existing water recovery system (WRS) on the ISS for extended duration of space exploration missions [71–73]. The WRS is equipped with urine processor assembly (UPA) to process the pretreated urine wastewater to produce distillate which goes into water processor assembly (WPA) for further processing along with the rest of the wastewater as shown in Fig. 3.8 [66, 74]. The UPA and WPA have a power consumption of 315 Wh/h and 320 Wh/h, respectively, during their period of operation. Additionally, other control modules require 108 Wh/h of power, resulting in a total maximum power consumption of 743 Wh/h when the whole WRS is operational. In the standby mode, the entire WRS consume a power of 297 Wh/h [75]. The WRS is assumed to have the ability to treat 2.5 kg/h of urine and latent wastewater with a

Table 3.4: Rates of water consumption and wastewater generation for various activities by one crew member. [66, 68–70][Table 4-20 (p. 72), Table 4-21 (p. 73)] of [68]

Water consumption (kg/day)		Wastewater generation (kg/day)	
Activity	Amount	Activity	Amount
Drinking (DW)	2.00	Urine	1.50
Food rehydration (FR)	0.50	Oral hygiene	0.37
Urinal flush (UF)	0.50	Hand wash	4.08
Personal hygiene (PH)	0.40	Shower	1.08
Shower (SH)	1.08	Crew latent humidity condensate	2.27

Table 3.5: Daily schedule of activities followed by the crew members for consumption of water and wastewater generation [66, 69, 70]

Time (h)	Activity
00:01 - 06:00	None
06:01 - 07:00	DW+PH+UF+FR+SH or DW+PH+UF+FR
07:01 - 08:00	None
08:01 - 09:00	DW
09:01 - 12:00	None
12:01 - 13:00	DW+PH+UF+FR
13:01 - 15:00	None
15:01 - 16:00	DW+UF
16:01 - 18:00	None
18:01 - 19:00	DW+PH+UF+FR or DW+PH+UF+FR+SH
19:01 - 21:00	None
21:01 - 22:00	DW+PH+UF
22:01 - 00:00	None

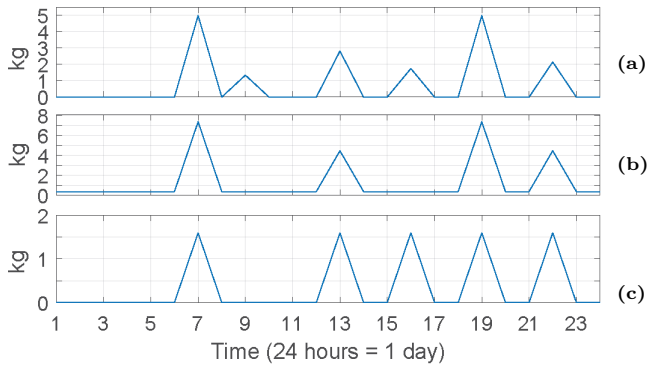

Fig. 3.7: Daily (a) consumption of water, (b) generation of wastewater, and (c) generation of urine wastewater profiles for four crew members

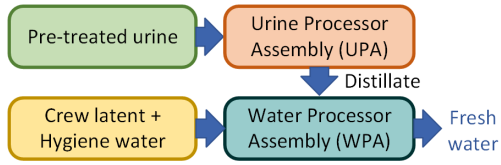

Fig. 3.8: General block diagram of WRS to recover water from the wastewater in the ISS

recovery rate of around 81% of the input [66, 75]. Algorithm 3 [66, 70] proposes the algorithm to filter wastewater using the WRS to produce freshwater. The operation of WRS depends on the current levels of T_{UF}, T_{WW}, and T_{FW} and their respective desired levels of T_{UF}^{ref}, T_{WW}^{ref}, and T_{FW}^{ref}.

The habitat water tank fulfills the consumption of water within the habitat which is refilled from both the ISRU water tank and freshwater tank in the wastewater subsystem as depicted in Fig. 3.4. Algorithm 4 proposes the methodology to resupply the water from the ISRU and freshwater tank in the wastewater subsystem. The algorithm compares the $T_{hab_{H_2O}}^{err}$, $W_{FW_{out}}^{max}$, T_{FW}^{min}, $W_{ISRU_{H_2O_{out}}}^{max}$, and $T_{ISRU_{H_2O}}^{min}$ to transfer freshwater from either or both of ISRU and freshwater tank in the wastewater subsystem. In this algorithm, utilizing the filtered water stored in the wastewater subsystem is emphasized rather than depending on the ISRU water storage tank.

3.3.3 Proposed power demand profile optimization algorithm

The operation of the ISRU is managed in the tertiary level controller of the APC. It ensures the safe operation of the base by supplying the required amount of power at the time of need and maintaining a safe amount of oxygen and water in the respective tanks of both ISRU and habitat. The proposed optimization framework considers the required oxygen and water levels in the respective reservoirs of both ISRU and habitat and determines the optimal power demand of the ISRU. The Sun illumination time-series profile is considered to determine the available power at the candidate location using the methodology proposed in [19]. The proposed optimization function is given as [66]:

$$J\left(V_{ir}, O_{2_{ISRU-hab}}^{max}, W_{FW_{out}}^{max}, W_{ISRU_{out}}^{max}\right) = \left(T_{ISRU_{O_2}}^{ref} - T_{ISRU_{O_2}}\right) + \left(T_{hab_{O_2}}^{ref} - T_{hab_{O_2}}\right) + \left(T_{ISRU_{H_2O}}^{ref} - T_{ISRU_{H_2O}}\right) + \left(T_{hab_{H_2O}}^{ref} - T_{hab_{H_2O}}\right) \quad (3.1)$$

The oxygen to the habitat oxygen tank is supplied from the ISRU oxygen tank following Algorithm 2. The water to the water tank of the habitat is supplied from both

Algorithm 3 Proposed wastewater and urine wastewater filtration algorithm and produce freshwater [66, 70]

Input: T_{UF}, T_{UF}^{ref}, T_{UF}^{min}, T_{WW}, T_{WW}^{ref}, T_{WW}^{min}, T_{FW}, T_{FW}^{max}, T_{WRS}^{ph}
Set: $\Delta_h = 1h$
$T_{UF}^{err} = T_{UF}^{ref} - T_{UF}$
$T_{WW}^{err} = T_{WW}^{ref} - T_{WW}$
$T_{FW}^{err} = T_{FW}^{ref} - T_{FW}$
$C_{WRS} = 0.81 \times \left(T_{WRS}^{ph}\Delta_h\right)$
if $P_W^{avail} \geq 743$ and $T_{UF} > T_{UF}^{min}$ and $T_{UF} \geq \left(T_{WRS}^{ph}\Delta_h\right)$ and $T_{UF}^{err} < 0$ and $T_{WW} > T_{WW}^{min}$ and $T_{WW} \geq \left(T_{WRS}^{ph}\Delta_h\right)$ and $T_{WW}^{err} < 0$ and $(T_{FW} + C_{WRS}) \leq T_{FW}^{max}$ and $T_{FW}^{err} > 0$ **then**
  $C_{UF} = (T_{UF}^{err}/(T_{UF}^{err} + T_{WW}^{err})) \times \left(T_{WRS}^{ph}\Delta_h\right)$
  $C_{WW} = (T_{WW}^{err}/(T_{UF}^{err} + T_{WW}^{err})) \times \left(T_{WRS}^{ph}\Delta_h\right)$
  $T_{UF} = T_{UF} - C_{UF}$
  $T_{WW} = T_{WW} - C_{WW}$
  $WW_{total} = C_{UF} + C_{WW}$
  $C_{FW} = 0.81 \times WW_{total}$
  $T_{FW} = T_{FW} + C_{FW}$
  $P_W = 320 + 315 + 108$
else if $P_W^{avail} \geq 743$ and $T_{UF} > T_{UF}^{min}$ and $T_{UF} \geq \left(T_{WRS}^{ph}\Delta_h\right)$ and $T_{UF}^{err} < 0$ and $(T_{FW} + C_{WRS}) \leq T_{FW}^{max}$ and $T_{FW}^{err} > 0$ **then**
  $C_{UF} = T_{WRS}^{ph}\Delta_h$
  $T_{UF} = T_{UF} - C_{UF}$
  $WW_{total} = C_{UF}$
  $C_{FW} = 0.81 \times WW_{total}$
  $T_{FW} = T_{FW} + C_{FW}$
  $P_W = 320 + 315 + 108$
else if $P_W^{avail} \geq 428$ and $T_{WW} > T_{WW}^{min}$ and $T_{WW} \geq \left(T_{WRS}^{ph}\Delta_h\right)$ and $T_{WW}^{err} < 0$ and $(T_{FW} + C_{WRS}) \leq T_{FW}^{max}$ and $T_{FW}^{err} > 0$ **then**
  $C_{WW} = T_{WRS}^{ph}\Delta_h$
  $T_{WW} = T_{WW} - C_{WW}$
  $WW_{total} = C_{WW}$
  $C_{FW} = 0.81 \times WW_{total}$
  $T_{FW} = T_{FW} + C_{FW}$
  $P_W = 320 + 108$
else
  $C_{UF} = 0$
  $C_{WW} = 0$
  $WW_{total} = C_{UF} + C_{WW}$
  $C_{FW} = 0.81 \times WW_{total}$
  $P_W = 297$

Algorithm 4 Proposed algorithm to refill water from water tanks of the ISRU and freshwater tanks to the water tank of the habitat [66, 70]

Input: $T_{hab_{H_2O}}$, $T^{ref}_{hab_{H_2O}}$, T_{FW}, T^{min}_{FW}, $T_{ISRU_{H_2O}}$, $T^{min}_{ISRU_{H_2O}}$, $W^{max}_{FW_{out}}$, $W^{max}_{ISRU_{H_2O_{out}}}$
Set: $\Delta_h = 1h$
$T^{err}_{hab_{H_2O}} = T^{ref}_{hab_{H_2O}} - T_{hab_{H_2O}}$
if $T^{err}_{hab_{H_2O}} > 0$ and $T_{FW} > T^{min}_{FW}$ **then**
  if $T^{err}_{hab_{H_2O}} < \left(W^{max}_{FW_{out}}\Delta_h\right)$ and $\left(T_{FW} - T^{err}_{hab_{H_2O}}\right) > T^{min}_{FW}$ **then**
    $TOT_{H_2O_{out}} = TOT_{H_2O_{out}} + T^{err}_{hab_{H_2O}}$
    $T_{FW} = T_{FW} - T^{err}_{hab_{H_2O}}$
  else if $T^{err}_{hab_{H_2O}} < \left(W^{max}_{FW_{out}}\Delta_h\right)$ and $\left(T_{FW} - T^{err}_{hab_{H_2O}}\right) \leq T^{min}_{FW}$ **then**
    $TOT_{H_2O_{out}} = TOT_{H_2O_{out}} + \left(T_{FW} - T^{min}_{FW}\right)$
    $T_{FW} = T^{min}_{FW}$
  else if $T^{err}_{hab_{H_2O}} \geq \left(W^{max}_{FW_{out}}\Delta_h\right)$ and $\left(T_{FW} - \left(W^{max}_{FW_{out}}\Delta_h\right)\right) > T^{min}_{FW}$ **then**
    $TOT_{H_2O_{out}} = TOT_{H_2O_{out}} + \left(W^{max}_{FW_{out}}\Delta_h\right)$
    $T_{FW} = T_{FW} - \left(W^{max}_{FW_{out}}\Delta_h\right)$
  else if $T^{err}_{hab_{H_2O}} \geq \left(W^{max}_{FW_{out}}\Delta_h\right)$ and $\left(T_{FW} - \left(W^{max}_{FW_{out}}\Delta_h\right)\right) \leq T^{min}_{FW}$ **then**
    $TOT_{H_2O_{out}} = TOT_{H_2O_{out}} + \left(T_{FW} - T^{min}_{FW}\right)$
    $T_{FW} = T^{min}_{FW}$
$T^{err}_{hab_{H_2O}} = T^{err}_{hab_{H_2O}} - TOT_{H_2O_{out}}$
if $T^{err}_{hab_{H_2O}} > 0$ and $T_{ISRU_{H_2O}} > T^{min}_{ISRU_{H_2O}}$ **then**
  if $T^{err}_{hab_{H_2O}} < \left(W^{max}_{ISRU_{H_2O_{out}}}\Delta_h\right)$ and $\left(T_{ISRU_{H_2O}} - T^{err}_{hab_{H_2O}}\right) > T^{min}_{ISRU_{H_2O}}$ **then**
    $TOT_{H_2O_{out}} = TOT_{H_2O_{out}} + T^{err}_{hab_{H_2O}}$
    $T_{ISRU_{H_2O}} = T_{ISRU_{H_2O}} - T^{err}_{hab_{H_2O}}$
  else if $T^{err}_{hab_{H_2O}} < \left(W^{max}_{ISRU_{H_2O_{out}}}\Delta_h\right)$ and $\left(T_{ISRU_{H_2O}} - T^{err}_{hab_{H_2O}}\right) \leq T^{min}_{ISRU_{H_2O}}$ **then**
    $TOT_{H_2O_{out}} = TOT_{H_2O_{out}} + \left(T_{ISRU_{H_2O}} - T^{min}_{ISRU_{H_2O}}\right)$
    $T_{ISRU_{H_2O}} = T^{min}_{ISRU_{H_2O}}$
  else if $T^{err}_{hab_{H_2O}} \geq \left(W^{max}_{ISRU_{H_2O_{out}}}\Delta_h\right)$ and $\left(T_{ISRU_{H_2O}} - \left(W^{max}_{ISRU_{H_2O_{out}}}\Delta_h\right)\right) > T^{min}_{ISRU_{H_2O}}$ **then**
    $TOT_{H_2O_{out}} = TOT_{H_2O_{out}} + \left(W^{max}_{ISRU_{H_2O_{out}}}\Delta_h\right)$
    $T_{ISRU_{H_2O}} = T_{ISRU_{H_2O}} - \left(W^{max}_{ISRU_{H_2O_{out}}}\Delta_h\right)$
  else if $T^{err}_{hab_{H_2O}} \geq \left(W^{max}_{ISRU_{H_2O_{out}}}\Delta_h\right)$ and $\left(T_{ISRU_{H_2O}} - \left(W^{max}_{ISRU_{H_2O_{out}}}\Delta_h\right)\right) \leq T^{min}_{ISRU_{H_2O}}$ **then**
    $TOT_{H_2O_{out}} = TOT_{H_2O_{out}} + \left(T_{ISRU_{H_2O}} - T^{min}_{ISRU_{H_2O}}\right)$
    $T_{ISRU_{H_2O}} = T^{min}_{ISRU_{H_2O}}$
$T_{hab_{H_2O}} = T_{hab_{H_2O}} + TOT_{H_2O_{out}}$

Table 3.6: Decision variables and bounds

Decision variables	V_{ir}	$O^{max}_{2_{ISRU-hab}}$ (g)	$W^{max}_{FW_{out}}$ (kg)	$W^{max}_{ISRU_{out}}$ (kg)
Lower bound	0	0	0	0
Upper bound	0.05	500	5	10

Algorithm 5 Proposed optimization framework to determine the power demand of ISRU

Input: T_H, CM, V, pV_{O_2}, $pV^{min}_{O_2}$, $pV^{max}_{O_2}$, $T^{ref}_{hab_{O_2}}$, $T^{min}_{hab_{O_2}}$, $T^{max}_{hab_{O_2}}$, $T^{ref}_{ISRU_{O_2}}$, $T^{min}_{ISRU_{O_2}}$, $T^{max}_{ISRU_{O_2}}$, $T^{ref}_{hab_{H_2O}}$, $T^{min}_{hab_{H_2O}}$, $T^{max}_{hab_{H_2O}}$, $T^{ref}_{ISRU_{H_2O}}$, $T^{min}_{ISRU_{H_2O}}$, $T^{max}_{ISRU_{H_2O}}$, Latitude and longitude of the candidate site

Step 1: Create Sun illumination time-series profile using [19]

Step 2: Create consumption profile of oxygen and water, and wastewater production profile using Table 3.2, and Table 3.4, respectively

Step 3: Minimize the optimization function in eq. (3.1) subjected to $pV^{min}_{O_2} \leq pV_{O_2} \leq pV^{max}_{O_2}$ and running Algorithm 1 every minute and Algorithm 2, Algorithm 3, Algorithm 4 every hour

the water tank of the ISRU and the freshwater tank in the wastewater subsystem following Algorithm 4. It is noteworthy that regolith intake in the ISRU results in the production of both water and oxygen. Therefore, hourly V_{ir} is the decision variable to produce oxygen and water and store them in the respective tanks of ISRU to maintain the intended storage levels of $T_{ISRU_{O_2}}$ and $T_{ISRU_{H_2O}}$. The decision variable $O^{max}_{2_{ISRU-hab}}$ regulates the highest rate of oxygen transfer from ISRU to habitat oxygen tank in Algorithm 2. $W^{max}_{FW_{out}}$ is the decision variable for regulating the highest rate of freshwater supply to the water tank of the habitat from the freshwater tank of the wastewater subsystem in Algorithm 4. The hourly $W^{max}_{ISRU_{out}}$ is the decision variable for regulating the highest rate of resupplying the water from the water tank of the ISRU to habitat in Algorithm 4. The maximum and minimum bounds of each of the decision variables are mentioned in Table 3.6. The optimal hourly power demand profile of ISRU is determined from the hourly optimal V_{ir} profile which produces the required oxygen and water for the base.

The entire optimization framework with its steps is described in Algorithm 5. The framework receives all the necessary parameters and keeps iterating until it reaches an optimal outcome. Algorithm 1 executes every minute to regulate the necessary pV_{O_2} levels in the habitat. Algorithm 2, Algorithm 3, and Algorithm 4 executes every hour to regulate the appropriate levels of respective oxygen and water tanks in the both the ISRU and habitat.

Table 3.7: Assumed levels of several tanks and habitat pV_{O_2} in the base

Tank	Minimum	Initial	Reference	Maximum
$T_{ISRU_{O_2}}$ $[kg]$	25	50	200	250
$T_{ISRU_{H_2O}}$ $[kg]$	50	50	$1.125 \times T^{ref}_{ISRU_{O_2}}$	250
$T_{hab_{O_2}}$ $[g]$	500	5×10^4	5.4×10^4	1×10^5
$T_{hab_{H_2O}}$ $[kg]$	10	100	500	600
T_{UF} $[kg]$	0	0	50	500
T_{WW} $[kg]$	0	0	50	500
T_{FW} $[kg]$	50	0	900	1000
pV_{O_2} $[Pa.m^3]$	6.50×10^5	6.56×10^5	6.56×10^5	6.62×10^5

3.3.4 Simulation results and discussion

The optimization framework determines the optimal power demand profile of ISRU by maintaining the desired oxygen and water level in the respective tanks of ISRU and habitat. The *'interior-point'* algorithm in the *MATLAB-fmincon* toolbox is used to find the solution to the non-linear optimization problem. The daily consumption profiles of oxygen and water, wastewater and urine wastewater generation profile as shown in Fig. 3.6, Fig. 3.7a, Fig. 3.7b, and Fig. 3.7c, respectively, are extended by repeating them for the entire optimization horizon of 708 h. The optimization takes into account the sun illumination time-series profile at site #1 (longitude 222.6627° and latitude −89.4511° from Table 1.3) for a duration of 708 h (= 1 lunar month). Fig. 3.9a shows the generated PV power profile with PV arrays on top of towers with 10 m height for an array area of 300 m^2. There are several duration when the PV power is not available. The operation of regolith intake is stopped during these periods with no power generation, as shown in Fig. 3.9b to reduce the power consumption from the battery. In this time period, oxygen and water are not produced from the ISRU and only the survival power is supplied to the ISRU as shown in Fig. 3.9c.

The minimum, initial, desired and maximum levels of several tanks are listed in Table 3.7. The $T^{ref}_{ISRU_{H_2O}}$ is set to $1.125 \times T^{ref}_{ISRU_{O_2}}$ as the amount of water produced by ISRU is 1.125 times greater compared to the amount of oxygen produced using the same V_{ir}. Initially, V_{ir} reaches its maximum allowable limit of 0.05 as restricted in Table 3.6 to reach the required levels of oxygen and water in the respective tanks of ISRU as shown in Fig. 3.9d and Fig. 3.9g, respectively. Therefore, the power demand of ISRU is also higher, as shown in Fig. 3.9c. However, as soon as the required levels of oxygen and water are reached in the respective ISRU tanks, the V_{ir} and the power consumed by the ISRU are reduced despite the availability of PV power. Throughout the optimization period, an increase in power consumption of ISRU is again observed a few hours before the dark periods so as to prepare the oxygen and water tanks of the ISRU (see Fig. 3.9e and Fig. 3.9h) as the oxygen and water will not be produced during the dark period

when power from PV array is not generated. An increase in the power consumption of ISRU is also observed after the periods of no PV power generation to increase the production of oxygen and water to reach the desired level of the respective tanks in the ISRU. The amount of oxygen transfer from the oxygen tank of ISRU to the habitat is shown in Fig. 3.9f, which is in accordance with the profile of daily oxygen usage of the habitat.

The water in the water tank of the habitat is supplied from the freshwater tank of the wastewater subsystem and the water tank of the ISRU. During the first few hours of operation, the amount of water in the habitat water tank reduces (see Fig. 3.9i) as there is no supply of water from either freshwater tank or ISRU water tank as observed in Fig. 3.9k and Fig. 3.9l, respectively. The amount of freshwater is observed to be at 0 kg during the first few hours of operation in Fig. 3.9j as the T_{UF} and T_{WW} have not yet reached the T_{UF}^{ref} and T_{WW}^{ref}, respectively, and the WRS is in standby operation mode. The freshwater tank in the wastewater subsystem starts filling when the filtration process starts in WRS. The freshwater tank starts supplying water to the water tank of the habitat once the T_{FW} reaches T_{FW}^{min} as observed by comparing Fig. 3.9j and Fig. 3.9k. The ISRU water tank supplies water to the water tank of the habitat once the $T_{ISRU_{H_2O}}$ is close to $T_{ISRU_{H_2O}}^{ref}$ as observed by comparing Fig. 3.9h and Fig. 3.9l.

The level of stored oxygen in the habitat oxygen tank, $T_{hab_{O_2}}$, reaches the desired level within the first few hours of operation as shown in Fig. 3.10a. Taking into account that the maximum and minimum pressure of oxygen in the habitat is at 21.4 kPa and 21 kPa, respectively, the pV_{O_2} stays between the $pV_{O_2}^{max}$ and $pV_{O_2}^{min}$ as shown in Fig. 3.10b. Fig. 3.10c and Fig. 3.10d shows that the pressure and concentration level of oxygen inside the habitat is regulated to remain roughly at the standard level of 21.2 kPa and 20.9%, respectively. The $T_{hab_{O_2}}$, pV_{O_2}, pressure, and concentration level of oxygen also follow the daily oxygen consumption profile of the habitat where the sudden decrease in levels is due to the heavy consumption of oxygen during exercise sessions of the crew members.

From the simulation results, it can be concluded that the proposed optimization framework produces an optimal profile of optimal power consumption by the ISRU, as shown in Fig. 3.9c, by keeping the amount of oxygen and water of the respective ISRU and habitat tanks at the desired level. It was observed from Fig. 3.9c that 4.086 kW, 25.144 kW, and 76.267 kW, are the minimum, average, and maximum power demand of ISRU, respectively. The upper bound of regolith intake rate (V_{ir}) regulates the maximum power consumption of the ISRU. However, Reducing the upper bound of V_{ir} would also result in a decline in the highest rates of oxygen and water production and additional time would be needed to attain the required amount of oxygen and water levels in the ISRU tank. To control the sudden surges in power and increase resource utilization, solving a multi-criteria optimization problem taking into account an optimal trade-off between power demand and tracking efficiency is considered a future focus of the author.

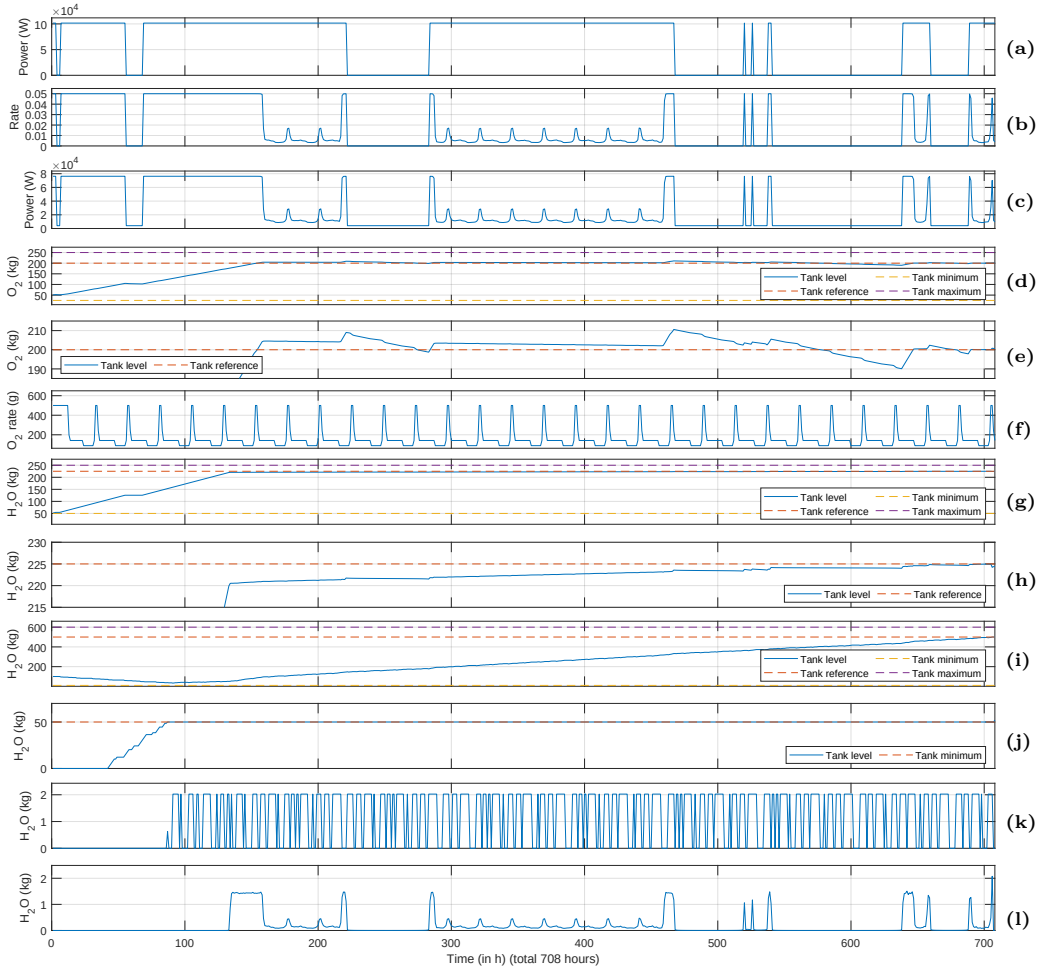

Fig. 3.9: (a) Unoptimized PV power profile at site #1 having 300 m^2 array area (b) Regolith intake (V_{ir}) (c) optimal ISRU power consumption profile (d) amount of oxygen in the ISRU oxygen storage tank (e) zoomed plot of ISRU oxygen storage tank (f) amount of oxygen transfer from ISRU to habitat oxygen tank (g) amount of water in the ISRU water storage tank (h) zoomed plot of ISRU water storage tank (i) amount of water in the habitat water storage tank (j) amount of freshwater in the wastewater subsystem tank (k) amount of freshwater transfer to the water tank of the habitat from the wastewater subsystem (l) amount of water transfer to the water tank of the habitat from the water tank of the ISRU

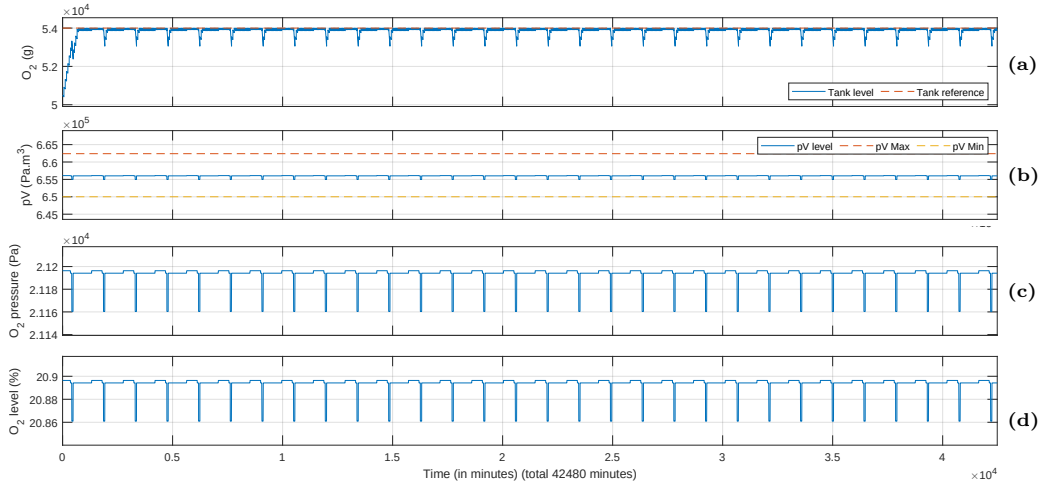

Fig. 3.10: (a) Amount of oxygen in the habitat tank (b) Level of pV_{O_2} in the habitat (c) pressure of oxygen in the habitat (d) Concentration of oxygen in the habitat

3.4 Optimal sizing and operation management of PV-battery based MGs

The expenses for a space mission are influenced by both the weight and storage space for the payload. Therefore, various ingenious approaches, such as using reusable launching systems, have been designed to lower the expenses associated with space expeditions. The expenses for a space mission are significantly affected by the size and weight of both the PV array and the battery in a PV-battery based MG. With the optimal size of the PV array and battery system, the power balance in the MG is also to be maintained, taking into consideration the charging/discharging of the battery. A MMG system composed of two MGs, namely ISRU and habitat, each with its individual PV-battery system, is taken into consideration. This section describes the proposed optimization framework for optimally managing the operation of both the PV-battery based MGs. The following subsections describe the methodology to formulate the profile of total power consumption of the ISRU and habitat, and the optimization framework for the optimal operation management for both the ISRU and habitat MGs.

3.4.1 ISRU power consumption profile

The profile of required power by the ISRU to maintain the desired levels of oxygen and water in the ISRU tanks is shown in Fig. 3.9c. Nevertheless, a number of additional devices are necessary for the proper functioning of the ISRU. A list of such devices is

Table 3.8: Power consumed by various additional devices in ISRU

Device	Power (W)	
	Active	Survival
Electrical power system	200	200
Communication system internal components	1500	750
Communication system external components	1000	1000
Central computer	100	100
#9 Monitoring camera	5	5
Air compressor	3.5	3.5
Airlock status LED	5	5
Artificial daylight LED	150	75
Airlock vacuum pump	500	500
#33 Lighting LED lamps	20	10
LCD display	160	0
Lunar day thermal control system	1200	900
Lunar night thermal control system	1900	1500
Sensors	4000	3000
Total	**10743.5**	**8048.5**

provided in the Table 3.8, which has active and survival-state operational modes and is assumed to operate during the whole optimization horizon (T_H). The essential devices operate at their full ability consuming the active-state power when the power from the PV arrays is available. During the periods when no PV power is available, the essential devices consume the power from the battery to continue operating and the devices which are not essential but important consume a lower power called survival-state while the non-essential devices are turned off to reduce the power consumption from the battery. In total, around 11 kW and 8 kW of active and survival power, respectively, are consumed as observed from Table 3.8. Thus, the active and survival-state power consumed by the additional devices is included in the overall power consumption profile as follows [69, 76]:

$$P^t_{ISRU} = \begin{cases} P^t_{V_{ir}} + 11000 & P^t_{PV} > 0 \\ P^t_{V_{ir}} + 8000 & P^t_{PV} = 0 \end{cases} \tag{3.2}$$

The power consumption profile of the ISRU after including the active and survival state power of additional devices is shown in Fig. 3.11b and is utilized for the optimal sizing and operation management of the PV-battery based ISRU MG.

3.4.2 Habitat power demand profile

There are various devices in the habitat that require power to support several operations, such as operating the LSS, filtering wastewater, facilitating equipment for exercise, conducting scientific experiments, communicating among several units in the base

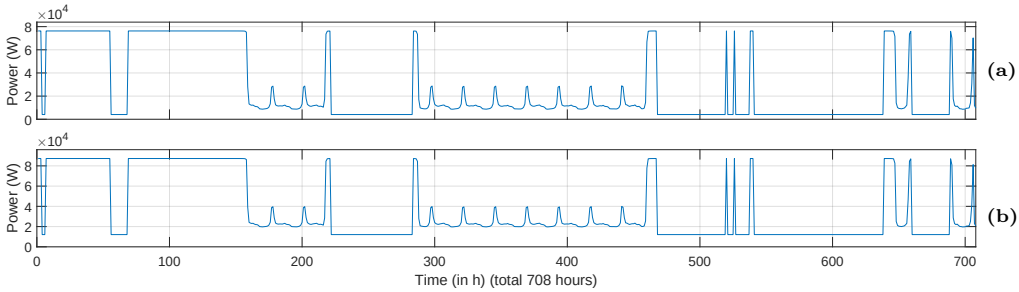

Fig. 3.11: Power consumption profile of ISRU (a) for keeping the oxygen and water tanks of the ISRU at the desired levels (b) taking into consideration the power consumed by additional devices

and ground station, and charging EVs and rovers for exploration, among others. The wastewater collected in the habitat undergoes a filtration process using the WRS of the wastewater subsystem in the habitat. The power consumption for the operation of WRS is described in Section 3.3.2. The profile of consumed power by the wastewater subsystem is obtained while the optimization problem for the optimal power consumption profile of ISRU is being solved. It is because of the interaction among the wastewater and ISRU subsystem for managing the water requirement of the base, and freshwater from the wastewater subsystem is supplied to the water tank of the habitat along with the water from water tank of the ISRU. It is assumed that the wastewater subsystem is provided with the required power from the habitat MG as the wastewater subsystem is operating within the habitat. The wastewater subsystem consists of wastewater, urine wastewater and freshwater tanks, as shown in Fig. 3.12. The water filtration process to maintain the desired levels of the three tanks and the consumption of power by the wastewater subsystem is described in Algorithm 3 [66, 70]. During the first few hours of operation, it can be observed from Fig. 3.12a that the wastewater subsystem consumes standby power of 297 Wh/h as the WRS is not operational [69]. Once the desired level of wastewater in the wastewater tank is reached, the WPA starts its operation and 428 Wh/h of power is consumed as observed by comparing Fig. 3.12a and Fig. 3.12c. The wastewater subsystem starts to consume 743 Wh/h of power once the set level of urine wastewater is attained, as both UPA and WPA start to function, as observed by comparing Fig. 3.12a and Fig. 3.12b [69]. It is worth noticing that although the WRS is active and generating freshwater, the contents of the freshwater tank are at the minimum level (see Fig. 3.12d) since freshwater is provided to the water tank of the habitat following Algorithm 2 [66, 70] and also shown in Fig. 3.9k [69].

The various devices consuming power in the habitat are listed in Table 3.9 [10, 21, 36, 62, 69]. The Fig. 3.13 shows the hourly power consumption profile of the habitat, which is determined based on the time at which the different devices are used, their active or survival-state mode of operation and the wastewater subsystem power consumption

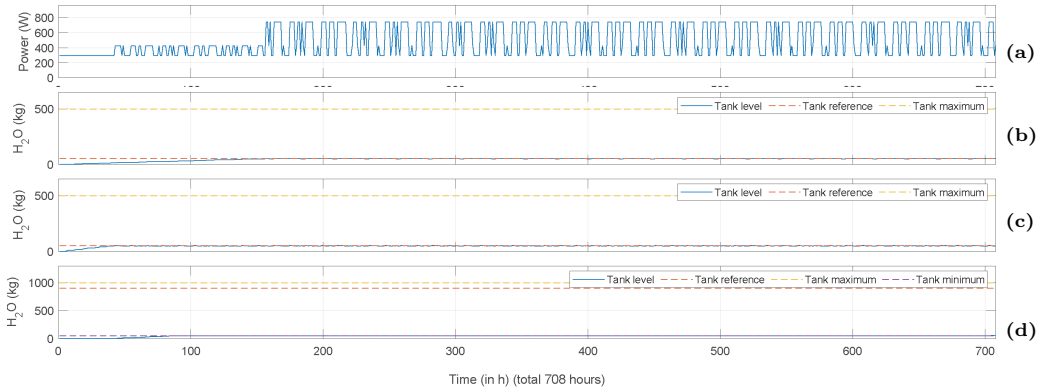

Fig. 3.12: (a) Power consumption profile of the wastewater subsystem (b) Amount of urine wastewater (c) Amount of Wastewater (d) Amount of filtered freshwater

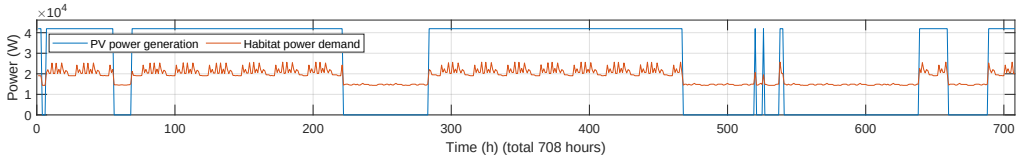

Fig. 3.13: Power consumption profile of habitat and PV power generation with array area of 123.87 m^2 at site #1 (longitude 222.6627° and latitude −89.4511°)

profile (see Fig. 3.12a) [69]. According to [10], roughly $5-10$ kW of power is consumed by every crew member in the habitat. In this study, the habitat is assumed to be accommodating four crew members and is consuming roughly 20 kW of power.

3.4.3 Proposed optimal sizing and operation management algorithm

The operational mode, time and duration of various units that consume power in the base are planned and organized by the APC optimally utilizing the resources and keeping a balance between power generation and demand. The objective of the proposed optimization framework is to minimize the mass of the PV array and the battery and the total surplus PV power, keeping the stored energy of the battery at a desired level. The proposed optimization function is given as [76]:

$$J\left(E^{init}, E_{cap}, A_a, \delta_{P_{PV}}^{shed}\right) = M_B + M_{PV} + \left(E(t) - E^{ref}\right)^2 + P_{PV}^{shed} \tag{3.3}$$

Table 3.9: The time-of-use and power consumption of several devices in the habitat [10, 21, 36, 62, 69]

Device	Active-state power (W)	Survival-state power (W)	Average daily use (h)	Time of use (h)
Air compressor	3.5	3.5	24	0 - 24
Airlock vacuum pump	500	500	1	21 - 22
Airlock status LED	5	5	24	0 - 24
Artificial daylight LED	150	75	24	0 - 24
Water heater - 1	4000	0	1	6 - 7
Water heater - 2	4000	0	1	18 - 19
LSS	4500	3000	24	0 - 24
Induction oven	2000	0	1	8 - 9
Monitoring camera (9 Nos)	5	5	24	0 - 24
Laptop	60	60	12	9 - 21
LCD display	160	0	24	0 - 24
Lighting LED lamps (33 Nos)	20	10	4	20 - 24
Microwave	800	0	2	7 - 9
Projector-1	60	0	1	10 - 11
Projector-2	60	0	1	11 - 12
Crew Laptop-1	65	0	10	8 - 18
Crew Laptop-2	80	0	6	9 - 20
Crew Laptop-3	60	0	3	9 - 21
Crew Laptop-4	80	0	10	8 - 19
Crew Smartphone-1	2	0	1	19 - 20
Crew Smartphone-2	2	0	1	20 - 21
Crew Smartphone-3	5	0	2	19 - 21
Crew Smartphone-4	3	0	2	17 - 19
Camera-1	10	0	2	10 - 12
Camera-2	10	0	1	15 - 16
Camera-3	10	0	1	21 - 22
Camera-4	10	0	1	11 - 12
Camera-5	10	0	1	13 - 15
Camera-6	10	0	1	17 - 18
Treadmill	800	0	1	7 - 8
Refrigerator-1	10	10	24	0 - 24
Refrigerator-2	10	10	24	0 - 24
Hair dryer-1	1200	0	1	6 - 7
Hair dryer-2	1200	0	1	18 - 19
Washing machine	2000	0	1	19 - 20
Vacuum cleaner	1.5	0	1	19 - 20
Electrical power system-1	500	500	24	0 - 24
Electrical power system-2	300	300	24	0 - 24
Communication system internal components	2500	1500	24	0 - 24
Communication system external components	3000	3000	24	0 - 24
Central computer	100	100	24	0 - 24
Spacesuit battery charger	140	140	6	23 - 5
Sample drill battery charger	2000	0	2	21 - 23
Active thermal control system-daytime	1200	900	24	0 - 24
Active thermal control system-nighttime	1900	1500	24	0 - 24
Sensors	4000	3000	24	0 - 24
3D printer	700	0	12	9 - 21
Welder	5000	0	1	11 - 12
Laboratory electric arc furnace	5000	0	1	14 - 15
Manufacturing device	2000	0	1	16 - 17
Rover charging	7000	1000	6	23 - 5
Pressurized EV charging	10 000	3000	6	23 - 5
Unpressurized EV charging	3000	2000	6	23 - 5

where M_B and M_{PV} can be determined as [10, 21, 76]:

$$M_B = \frac{E_{cap}}{S_b B_{dod}} \tag{3.4}$$

Table 3.10: Lower and upper bounds of the decision variables [76]

Decision variable	Lower bound	Upper bound
E^{init} (%)	0	100
E_{cap} (Wh)	1×10^5	1×10^8
A_a (m^2)	satisfy highest ISRU power consumption	330
$\delta_{P_{PV}}^{shed}$ (%)	0	100

$$M_{PV} = (\sigma_a + \sigma_s)\, A_a \tag{3.5}$$

where S_b, σ_a, and σ_s are assumed to be 200 Wh/kg, 1.59 kg/m^2, and 0.55 kg/m^2, respectively [10, 69, 76].

The optimization function is subjected to several battery constraints from Eq. (2.5) to Eq. (2.9) as discussed in Section 2.4.1 [21, 76]. The power balance in the MG is maintained as [76]:

$$\left(\left(1 - \delta_{P_{PV}}^{shed,t}\right) \times P_{PV}^{t}\right) - P_{ISRU}^{t} - P_{B}^{t} = 0 \tag{3.6}$$

where a normalized value for $\delta_{P_{PV}}^{shed}$ is considered denoting the fraction of total PV power which is shed every hour, and $P_B^t = P_c^t$ or $P_B^t = -P_d^t$ while charging or discharging, respectively [76].

The optimization function minimizes the M_B and also assures supplying the required power during the dark period when the PV power is unavailable. The M_B is proportional to the E_{cap}, which is one of the decision variables of the optimization problem. Reducing the PV array mass ensures an optimal PV array area to produce sufficient power to meet the power demand and charge the battery to satisfy the demand during dark periods. The hourly $\delta_{P_{PV}}^{shed}$ allows keeping the battery stored energy at a desired level. The decision variable E^{init} is allowed to take any value while maintaining the initial and final level of the stored energy according to the constraint in Eq. (2.9) [76]. Table 3.10 lists the bounds of several decision variables of the optimization problem [76]. The lower bound for A_a is set such that the PV power supplies the highest power consumption of the ISRU. This strategy reduces the use of batteries, and a majority of the power demand is supplied by the power generated from the PV arrays when PV power is available. In a situation with a brief period of illumination between two considerably long periods of darkness, the optimal area of the PV array might increase to quickly store charge to the battery [76]. Fig. 3.14 shows the optimization framework to identify the optimal PV array area and battery capacity and optimal operation management with optimal PV power generation and battery charging/discharging profile [76].

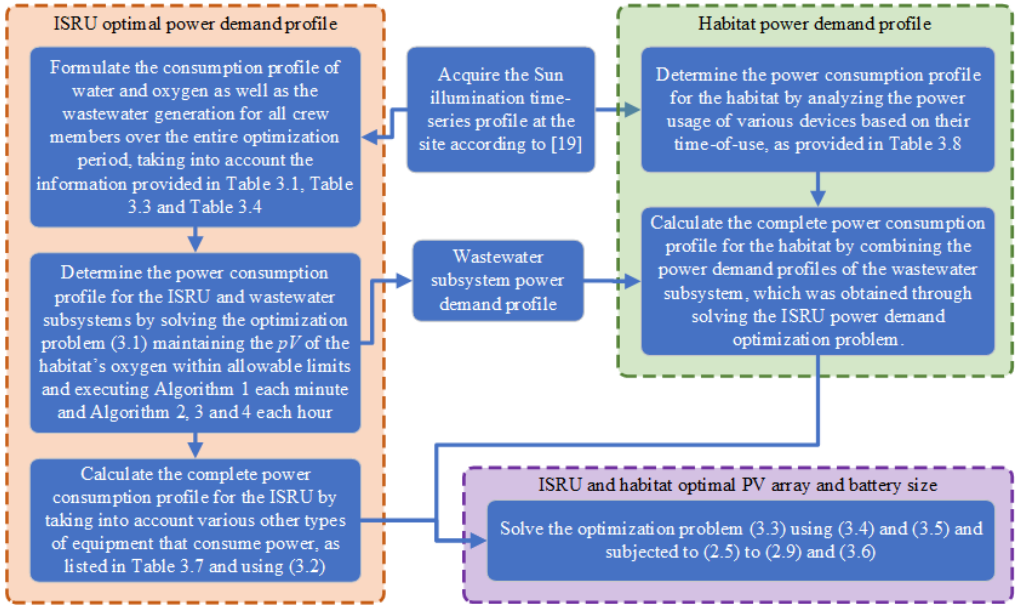

Fig. 3.14: Flow diagram to obtain the optimal operation of the ISRU and habitat MGs

3.4.4 Simulation results and discussion

For the simulation, the Sun illumination time-series profile at site #1 (longitude 222.6627° and latitude −89.4511° from Table 1.3) with PV arrays on top of towers with 10 m height is considered [19, 76]. The *'interior-point'* algorithm in the *MATLAB-fmincon* toolbox is used to solve the non-linear optimization problem for an optimization horizon of 708 h. The battery parameters B^{max}, B_{dod}, η_c, η_d, and δ are assumed to be 90%, 80%, 80%, 80%, and 1%, respectively [69, 76]. The simulation considers the power consumption profile for ISRU and habitat MGs as shown in Fig. 3.11b and Fig. 3.13, respectively. Although two MGs, namely habitat and ISRU, are considered, there is no sharing of resources between the two MGs.

3.4.4.1 ISRU operation management

Four schemes are considered for examining the ISRU MG. The analysis of the first scheme considers minimizing the total surplus PV power with the lower bound of PV array area set to a value that produces the amount of PV power to meet the highest power consumed by the ISRU. The first scheme is analyzed with three distinct cases of stored energy reference levels of the battery at 50% (case−1), 25% (case−2), and 85% (case−3) of E_{cap}.

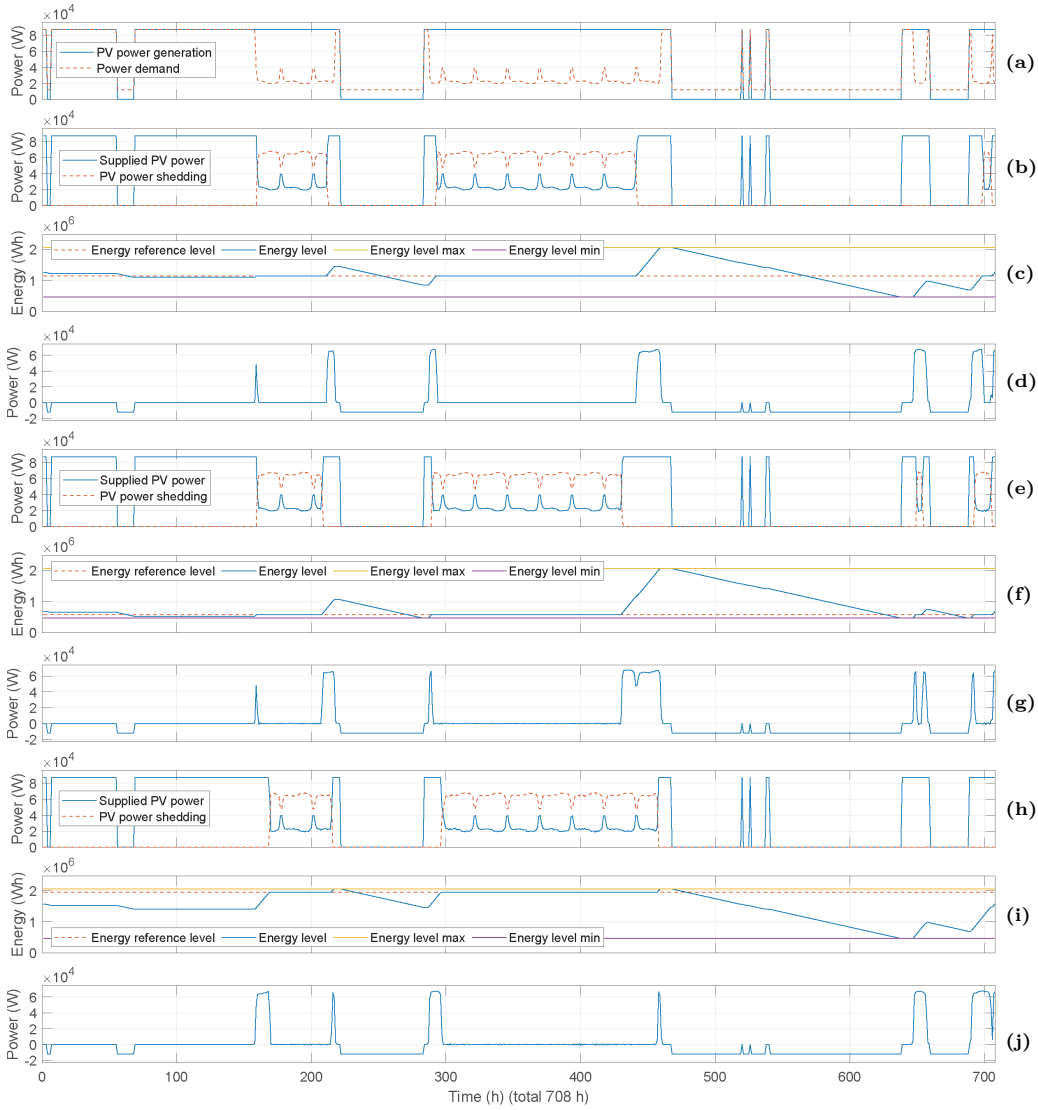

Fig. 3.15: (a) PV power and consumption profile for all the three cases of scenario 1 (b) Optimal PV power reference and surplus PV power profile for case−1 of scheme 1(c) Stored energy profile of the battery for case−1 of scheme 1 (d) Power profile for charging/discharging the battery for case−1 of scheme 1 (e) Optimal PV power reference and surplus PV power profile for case−2 of scheme 1 (f) Stored energy profile of the battery for case−2 of scheme 1 (g) Power profile for charging/discharging the battery for case−2 of scheme 1 (h) Optimal PV power reference and surplus PV power profile for case−3 of scheme 1 (I) Stored energy profile of the battery for case−3 of scheme 1 (j) Battery Power profile for charging/discharging the battery for case−3 of scheme 1 [76]

The optimal area of the PV array is found as a solution of the optimization problem as 257.7 m^2 in each of the cases of scheme #1. The power produced by the PV arrays having an area of 257.7 m^2 is shown in Fig. 3.15a [76]. It can be observed that the power generation from the PV arrays are almost equivalent to the highest power required by the ISRU. The ISRU power consumption and PV power generation reaches a highest peak of 8.7267×10^4 W and 8.7273×10^4 W, respectively [76].

The periods of time for which the generation from the PV arrays is more than the power demand of the ISRU, it is observed that in all three cases of scheme #1, the power from the PV arrays are utilized to charge the battery or shed the surplus PV power generation as shown in Fig. 3.15b, Fig. 3.15e, and Fig. 3.15h. During a few initial hours of operation, the PV power generation is completely used in supplying the power demand of the ISRU. At around 160 h, the power demand is less than the power generation (see Fig. 3.15a) and the excess power generation is used for providing charging power to the battery and the desired storage energy level of the battery is reached in all three cases as observed in Fig. 3.15c, Fig. 3.15f, and Fig. 3.15i. Once the battery storage energy reaches the desired levels, the surplus PV power generation is shed to maintain the battery storage energy level at the desired level. Just before the extended darkness periods, the battery storage energy increases from the desired level in all three cases to prepare for supplying the power demand during the upcoming period when PV power is unavailable. A downfall in battery stored energy level in all three cases in the absence of PV power signifies that the power consumption of ISRU is supplied from the batteries. The profiles of charging/discharging of the battery for case−1, case−2, and case−3 can be observed in Fig. 3.15d, Fig. 3.15g, and Fig. 3.15j, respectively. After the extended darkness periods, such as at 280 h and 640 h, the ISRU consumes a high power to reach the desired levels of the oxygen and water tanks as observed by comparing Fig. 3.9c, Fig. 3.9e, and Fig. 3.9h. After supplying the required power demand, the surplus power from the PV is supplied for charging the battery to reach the desired stored energy level in all three cases. Once the desired stored energy level is reached, the surplus PV power is shed to maintain the battery stored energy at the desired level.

The optimal PV power profile for all three cases is determined by subtracting the PV power generation (shown in Fig. 3.15a) and the surplus PV power shed profile as observed in Fig. 3.15b, Fig. 3.15e, and Fig. 3.15h. The results of Fig. 3.15 suggest that the proposed optimization strategy can effectively manage the power balance and operation of the MG. It is worth noticing that the battery capacity and mass are the same for all three cases of *Scheme* #1 as listed in Table 3.11 [76].

Furthermore, three additional schemes were compared with *Scheme* #1 to analyze the effect of shedding the surplus PV power generation and keeping the lower bound of the PV array area to a value that provides enough power to meet the highest power demand of the ISRU as follows:

- *Scheme* #2: Shedding the surplus PV power, keeping $E^{ref} = 50\% \times E_{cap}$, and

Table 3.11: Comparison of PV array area and battery capacity and their mass at various optimization conditions [76]

Scenario	Consideration		PV array		Battery	
	PV shedding	A_a lower bound	Area (m^2)	Mass (kg)	Capacity (Wh)	Mass (kg)
1	Yes	maximum power demand of the ISRU	257.7	551.478	2.2930×10^6	14 331.0254
2	Yes	0 m^2	249.3449	533.5981	2.3564×10^6	14 727.6102
3	No	0 m^2	163.5221	349.9374	7.2667×10^6	45 417.0311
4	No	maximum power demand of the ISRU	257.7	551.478	2.2194×10^8	1 387 132.1689

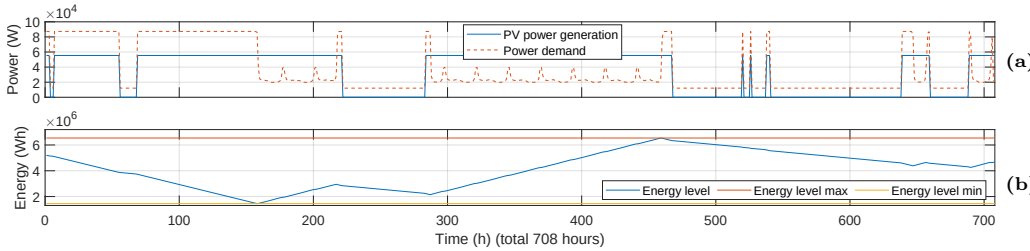

Fig. 3.16: Profiles for *Scheme* #3 (a) Power consumption and PV power generation profile (b) Stored energy level of the battery [76]

lower bound of $A_a = 0\ m^2$.

- *Scheme* #3: Without shedding the surplus PV power, keeping $E^{ref} = 50\% \times E_{cap}$, lower bound of $A_a = 0\ m^2$, and $\delta = 10\%$ in Eq. (2.9).
- *Scheme* #4: Without shedding the surplus PV power, keeping $E^{ref} = 50\% \times E_{cap}$, setting lower bound of A_a to a value that generates sufficient PV power to meet the highest power consumed by the ISRU, and $\delta = 10\%$ in Eq. (2.9).

Compared to *Scheme* #1, the battery mass for *Scheme* #2 increased by 396.5848 kg. The mass of the PV array is reduced by 17.8799 kg, which is insignificant considering the increase in battery mass. Although, the PV power profile is observed to be similar to Fig. 3.15b as in *Scheme* #1, the stored energy level and charging/discharging power profile of the battery denoted a discharge in the early hours at the starting of operation. This discharge of the battery is due to the fact that the highest power consumption by the ISRU during a few initial hours is 8.7267×10^4 W which is more than the maximum power of 8.4444×10^4 W generated by the PV [76].

In *Scheme* #3, removing the condition of shedding the surplus PV generation decreased the mass of the PV array by 201.5406 kg while increasing the mass of the battery by 31086.0057 kg compared to *Scheme* #1. Since it is not possible to shed the surplus PV power when the generation is more than the demand, the surplus power is stored in the battery to maintain the power balance. The stored energy level of the battery along with the generated PV power profile is shown in Fig. 3.16 [76]. *Scheme* #4 also

exhibited an increased capacity of the battery to store the surplus power from PV, increasing the mass of the battery by 1.372×10^6 kg compared to *Scheme 1* [76]. From this analysis, it can be inferred that implementing an approach to optimally utilize the surplus power from the PV arrays to boost the stored energy level in the battery and shed the rest of the surplus generation can significantly decrease the size and mass of the battery [76].

3.4.4.2 Habitat operation management

The habitat MG is also simulated with the same conditions as *Scheme* #1 of the ISRU MG but with the habitat power consumption profile as shown in Fig. 3.13. In this case, even though the lower bound of the PV array area is set to a value that produces the maximum power consumption of the habitat, the optimal PV array area generates much more PV power than the consumption. This is because more PV power is required to charge the battery during the time when PV power is available, as the stored power from the battery is used to supply the power demand during the dark periods. It can be observed by comparing Fig. 3.17b and Fig. 3.17c that surplus PV power is shed once the stored energy of the battery reaches the desired level after the initial few hours of operation. The surplus power generation is utilized for charging the battery before the extended periods without PV power. During the periods without PV power, the battery is discharged to supply the power consumption of the habitat as depicted in Fig. 3.17c and Fig. 3.17d. For a few hours after approximately 280 h, the surplus PV power generation is utilized to charge the battery to the desired stored energy level. Once the stored energy level is reached, the surplus PV power is shed. The habitat MG at site #1 has an optimal PV array area of 123.87 m^2 having a mass of 265.09 kg. The optimal capacity of the battery for the habitat MG at site #1 is 2.67×10^6 Wh having a mass of 16729.7 kg. The capacity and mass of the battery for the habitat MG are more than the ISRU because habitat MG consists of more essential power-consuming devices than ISRU that need power from the battery during the periods when the generation of power from the PV array is unavailable.

Even though the capacity and mass of the battery can be decreased by discarding surplus PV power, neglecting available supplies in an environment with limited resources such as space would be unreasonable. Alternative types of ESS such as RFCs can be recharged from the surplus PV power [76]. In a situation of instrument breakdown, the availability of diverse ESS provides better flexibility in managing operations. Furthermore, the possibility of implementing efficient load scheduling to use the surplus PV power is also being considered for investigation in the future by the author [76].

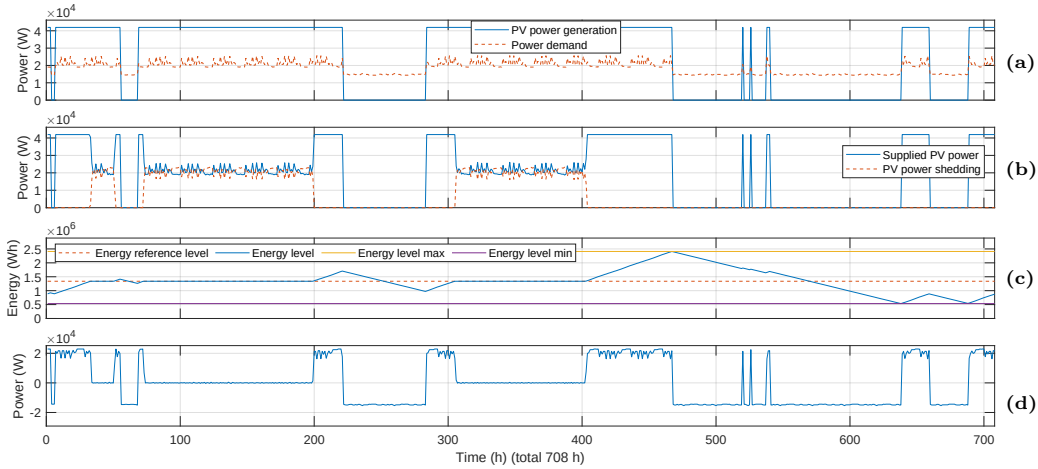

Fig. 3.17: Habitat MG at site #1 (a) PV power generation and power demand profile with optimal array area of 123.87 m^2 (b) Optimal PV power reference and surplus PV power profile keeping the battery stored energy level at 50% (g) Battery stored energy level profile keeping the battery stored energy level at 50% (h) Charging/discharging power profile of the battery keeping the battery stored energy level at 50%.

3.5 Site selection

The sites listed in Table 1.3 are compared in terms of PV array area and mass, battery capacity and mass, average illumination and longest continuous period of darkness of the sites, total power demand served and PV power supplied at the site, and MPUL as shown in Fig. 3.18 [69]. The MPUL of the sites are determined using the methodology described in Section 2.5. The optimal capacity of the battery at the sites listed in Table 1.3 are shown in Fig. 3.18e, which is used to determine the mass of the battery at the respective sites using Eq. (3.4) and are shown in Fig. 3.18a [69]. It is observed that the capacity and mass of the battery are in the order of 10^6 Wh and 10^4 kg, respectively, for both the ISRU and habitat MGs [69]. The combined battery mass for the ISRU and habitat MG gives the total mass of the battery at different sites in Fig. 3.18a, which is also observed to be in the order of 10^4 kg. The optimal PV array area at various possible locations are depicted in Fig. 3.18f, which is used to determine the weight of the PV system at the respective sites using Eq. (3.5) and are shown in Fig. 3.18b [69]. It is noted that the area of the PV array is in the order of 10^2 m^2 and PV mass are in the order of 10^2 kg and 10^3 kg, for both the ISRU and habitat MGs [69]. The aggregated mass of the PV system for the ISRU and habitat MG gives the total mass of the PV at different sites in Fig. 3.18b, which is also observed to be in the order of 10^2 kg and 10^3 kg. The area and mass of the PV array for the ISRU MG is higher compared to the

habitat MG as ISRU utilizes the energy from the Sun to produce enough oxygen and water for the base.

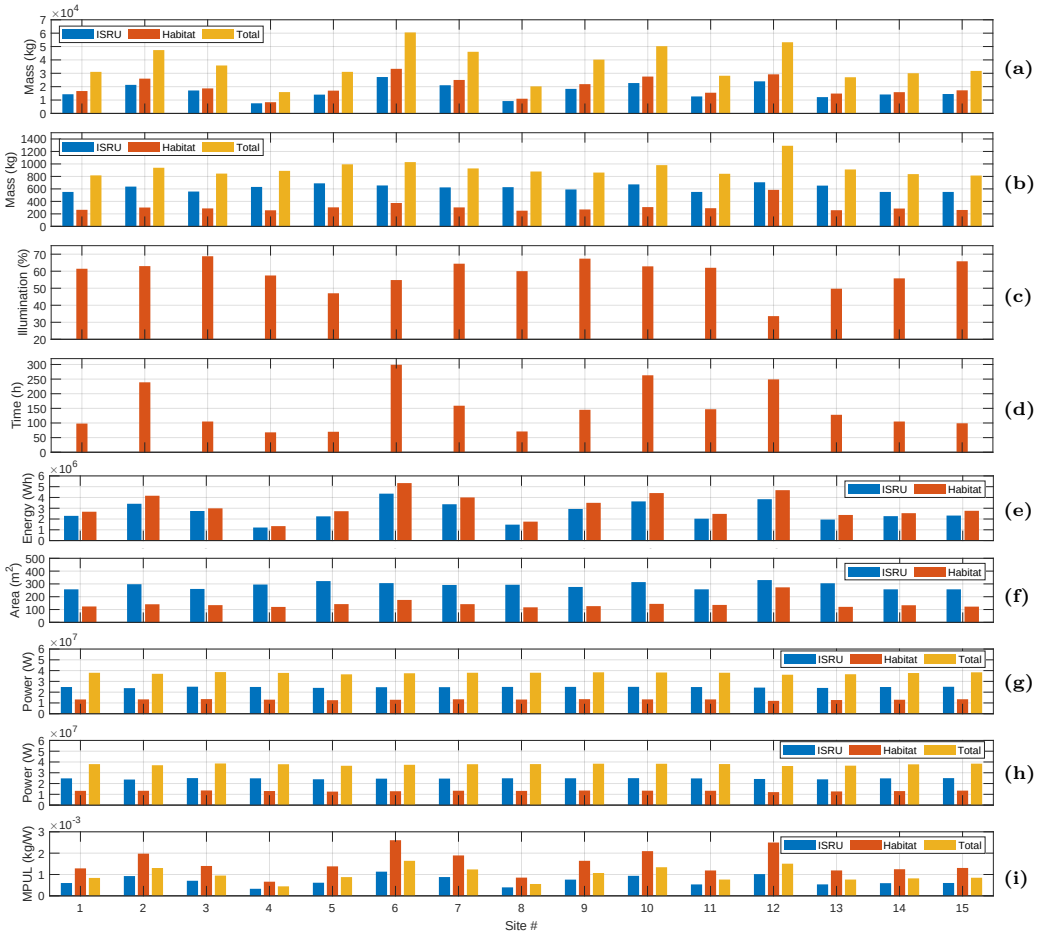

Fig. 3.18: Sites listed in Table 1.3 compared in terms of (a) battery mass (b) PV array mass (c) average illumination (d) longest continuous period of darkness (e) battery energy (f) PV array area (g) total power demand served (h) total PV power supplied (i) mass-per-unit-load (MPUL) for an optimization horizon of 1 month from July 6, 2023, to August 5, 2023

The average illumination at the sites for a 1 month period starting from July 6, 2023 and ending on August 5, 2023 is shown in Fig. 3.18c, while the longest continuous period of darkness is shown in Fig. 3.18d [69]. The average illumination at site #3 and #9 is observed to be approximately 68%, which is significantly more than site #4.

However, site #4 requires lower capacity of battery and has less battery mass compared to site #3 and #9. On the other hand, site #3 and #9 are observed to have the longest continuous period of darkness of 105 h and 145 h, respectively, whereas, it is for 68 h at site #4. Site #5 has the longest continuous period of darkness of 70 h, which is comparable to site #4, but site #5 has an average illumination of 47.03% in contrast to site #4 exhibiting an average illumination of 57.48%. Thus, site #5 has more capacity and mass of battery in comparison to site #4, despite both sites having a comparable longest continuous period of darkness. As a result, it can be inferred that the capacity and mass of the battery for a PV-battery based MG are influenced by both average illumination and the longest continuous period of darkness at each site [69].

The mass of the battery is found to be much heavier than the mass of the PV array for a PV-battery based MG on the Moon. It can be seen in Fig. 3.18a that site #4 has the lowest mass of battery for the ISRU and habitat MGs with a mass of 7563.46 kg and 8379.9 kg, respectively, having a total battery mass of 15943.4 kg for the combined two MGs. Site #8 is observed to be the nearest comparable site having a mass of battery for the ISRU and habitat MG as 9237.65 kg and 10981 kg, respectively, and total battery mass of the combined two MGs as 20218.7 kg [69].

The Fig. 3.18g and Fig. 3.18h shows the aggregated power requirement served and total power provided by the PV array generation, respectively, at the 15 candidate sites. The most total power demand of 38616.949 kW is served by site #3. The MPUL of all the sites listed in Table 1.3 as compared in Fig. 3.18i are in the order of 10^{-3} kg/W [69]. Site #4 is observed to have the least MPUL for both the ISRU and habitat MG as 0.330×10^{-3} kg/W and 0.662×10^{-3} kg/W, respectively, and MPUL for the total combined two MGs is 0.444×10^{-3} kg/W [69].

Fig. 3.19 shows the approximate locations of the sites listed in Table 1.3 [69]. Site #4, with the least amount of battery mass and MPUL, is located at the edge of the Shackleton crater, which typically receives a high illumination.

3.6 Conclusion

In this chapter, the several interacting subsystems in the lunar base were studied and the operation management of the base considering oxygen and water supply in the base was investigated. A methodology was proposed to generate the profiles for oxygen and water consumption and wastewater generation of the base. Several algorithms were proposed to maintain the pressure and concentration of oxygen in the habitat, refill the consumed oxygen in the habitat oxygen tank from the ISRU oxygen tank, filter wastewater for reusing freshwater in the habitat, refill the consumed water in the water tank of the habitat from both the freshwater and ISRU water tank. An optimization function was proposed to maintain the required levels of the oxygen and water tanks of the ISRU and habitat subsystems, maintaining the safe conditions and operation of the base. The optimization framework considered the time-series profile of the solar

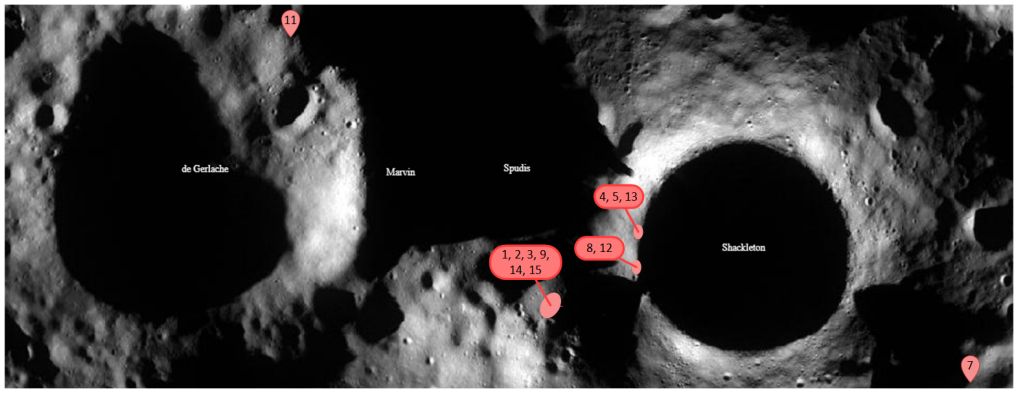

Fig. 3.19: Approximate locations of the sites listed in Table 1.3[1]
[1] Snapshot from https://quickmap.lroc.asu.edu/ (Accessed on 16/2/2023)

illumination at the site. The optimization considered PV arrays mounted on 10 m high towers and an optimization horizon of 708 h (= 1 month). The optimization framework resulted in generating the optimal power demand profile for the ISRU. A methodology to create the profile of the power demand for the habitat was discussed, taking into consideration various power-consuming devices in the habitat and their duration of use depending on several activities of the crew members. The power demand profile of the ISRU and habitat was considered for managing two PV-battery based MGs, namely ISRU and habitat MG, with each of them having their individual PV array and battery system. An optimization function was proposed to determine the optimal area of the PV array and capacity of the battery and operate the MGs optimally by maintaining the stored energy of the battery at a desired level considering the time-series profile of solar illumination at the site for an analysis period of 708 h. The optimization framework resulted in generating a surplus PV power profile which is either shed or used to charge and prepare the battery ahead of extended long darkness periods when PV power is not available and the battery is used to supply the critical loads. It was observed that storing the surplus PV power unnecessarily increased the battery capacity. Instead of shedding the surplus PV power, the possibility of utilizing the surplus power to charge other ESSs or implement load scheduling is to be investigated by the author in the future. Furthermore, 15 candidate sites near the Shackleton crater with high average illumination were compared and the site with the least battery mass was observed to have a mass of 7563.46 kg and 8379.9 kg for the ISRU and habitat MG, respectively. Finally, a comparison of MPUL revealed that the site with least MPUL has a MPUL of 0.330×10^{-3} kg/W and 0.662×10^{-3} kg/W for the ISRU and habitat MGs, respectively.

Chapter 4: Closing remarks

4.1 Overall conclusion

Several space agencies are interested in expanding human civilization further into space by establishing a human base on the Moon. Developing such a system in outer space primarily requires maintaining the artificial LSS for the crew members. Several systems for maintaining the LSS, communicating with the ground station, and performing scientific explorations, among others, require electrical power to operate. Therefore, electrical power systems consisting of power generation, transmission, and storage technologies with efficient control and energy management systems are required on the Moon. Several technologies for power generation, transmission, storage, and control framework for space MGs on the Moon, along with the different power-consuming units, were discussed in [9].

To establish a PV-battery based MG for the base, an appropriate methodology is required to determine the optimal area of the PV array and the capacity of the battery and coordinate among the several power-consuming units. Moreover, the illumination of the candidate sites near the lunar polar regions was observed to be affected by the topology of the surrounding region. Therefore, this thesis considered the time-series profile of solar illumination at the candidate locations to determine the availability of PV power. It was assumed that PV arrays are installed on top of towers of height 10, 50, and 100 m to harvest more solar power. A methodology was presented to obtain the profile of power consumption of multiple power-consuming units of the base assuming two states of power consumption for the loads depending on the availability of PV power [21]. An optimization framework was proposed to identify the optimal area of the PV arrays and the capacity of the battery minimizing the mass of the PV array and battery and the battery total cost per day [21]. An analysis period of 1 year and 5 years were taken into account in which the annual decline in the capacity of the battery because of the calendar and cyclic aging was taken into consideration for the case of 5-year horizon. A comparison was performed among 15 different candidate sites in the close proximity of the Shackleton crater. The mass of the PV-battery system varied roughly from 1.5×10^5 kg to 3.5×10^5 kg and from 2×10^5 kg to 5.5×10^5 kg for analysis

periods of 1 year and 5 years, respectively, assuming towers of 10 m height for the PV arrays. It was observed that the longest continuous period of darkness also affects the size and mass of the PV and battery, along with the average illumination at the sites. Raising the height of the towers to 50 m and 100 m increased the average illumination for some of the sites and also reduced the longest continuous period of darkness, resulting in reduced PV-battery system mass varying from 1×10^5 kg to 2.25×10^5 kg and from 1.5×10^5 kg to 3.25×10^5 kg for optimization horizons of 1 year and 5 years, respectively. The units that consume power in the base were also distributed among three sections to form an MMG system to enhance the system reliability and resiliency, keeping the total PV-battery system mass approximately the same. Although more investigation is required for the MMG system as, additional power cables and converters and protection systems might increase the overall system mass. A criterion is established by considering the total power requirement fulfilled and the overall mass of the system, called MPUL, was proposed to determine the location that fulfills the highest power requirements with the minimum overall system weight.

It was noted that a more accurate power consumption profile can be obtained by considering the operation mode and rate of the subsystems. Also, the interaction between several subsystems for oxygen and water management of the base was taken into account [66]. The profile for consumption of oxygen and water in the habitat was modeled according to the several tasks performed by the crew members on a daily basis to account for the rate of operation of several power-consuming units. A profile for wastewater produced in the habitat was also considered and the freshwater obtained after filtering the wastewater was assumed to be reused in refilling the habitat water tank. Several algorithms were proposed to supply oxygen and water from the respective ISRU and wastewater tanks to the habitat tanks and to maintain the required pressure and concentration of oxygen in the habitat [66, 70]. An optimization framework was proposed to maintain the desired level of oxygen and water in the respective tanks of ISRU and habitat to determine the profile of power consumed by the ISRU and the maximum rate of transfer of oxygen and water to the habitat tanks [66]. The optimization considered the Sun illumination time-series profile at a site with towers of 10 m height for the PV arrays for an optimization horizon of 1 lunar month. It was observed that with the optimal operating strategy, the base is prepared for the upcoming extended long duration of darkness by storing more oxygen and water in the respective tanks of ISRU. Similarly, the power demand profile of the habitat was also determined depending on the daily activities of the crew members and the usage time of several power-consuming devices in the habitat [76]. The optimal power demand profile of the ISRU and the habitat were further used for optimal sizing and operation management of the base. Two MGs were considered, namely the ISRU and the habitat, each one having a separate PV-battery system. An optimization framework was proposed for optimal operation of the MGs by optimally sizing the PV array area and battery capacity, keeping the stored energy of the battery at the desired level while minimizing the total surplus PV power

generation and mass of the PV array and battery. The optimization was carried out for a horizon of 708 h with PV arrays on top of towers of height 10 m. It was observed that the batteries are charged with more energy than the desired level prior to extended periods of darkness when PV power is going to be unavailable to ensure continuity of power supply. It was also noticed that shedding the surplus power reduces the battery size as the surplus power is not stored in the battery. Instead of wasting the surplus PV power in an environment with limited access to energy resources, such as space, more efficient operation strategies can be developed for scheduling the controllable loads and deploying other types of ESS, such as RFCs. In addition, a comparison study for investigating the PV array and battery mass for 15 candidate sites was performed [69], which revealed that the site with the least battery mass has a battery mass of 7563.46 kg and 8379.9 kg for the ISRU and habitat MGs, respectively. The PV array mass for the ISRU and habitat MGs are 631.61 kg and 257.40 kg, respectively. The ISRU and habitat MGs at the same site also had the MPUL of 0.330×10^{-3} kg/W and 0.662×10^{-3} kg/W, respectively.

4.2 Contribution

Establishing a MG for a human base in the space environment involves supporting invaluable human lives in a harsh and unforgiving environment. This thesis first provided a summary of the main requirements of a PV-battery based MG on the Moon. Installing a PV-battery based MG requires an estimation of the power demand profile and a proper methodology to determine the optimal PV array area and battery size to supply the power demand. The main contribution of this thesis is developing a coordinated control and operation management system for multiple units that consume power in a human base on the Moon supplied by a PV-battery based MGs, to ensure the safety and vital LSS of the crew members. The following are the sub-objectives fulfilled to achieve the main goal of this thesis:

- **Determining the optimal size of the PV array and battery system:** The thesis proposed an optimization framework to optimally size the PV array area and battery capacity to minimize the mass of the PV array and battery, and the total cost per day of the battery using the Sun illumination time series profile and the angle of Sun elevation at a candidate site on the Moon.
- **Modeling the interaction among different subsystems:** In the thesis, the interaction among ISRU, habitat, and wastewater subsystems were modeled for managing the oxygen and water supply in the base.
- **Deriving the optimal power demand profile of the ISRU:** The thesis proposed an optimization framework to determine the optimal power demand profile of the ISRU keeping the desired levels of stored oxygen and water in the respective

ISRU and habitat tanks while taking into account the required pressure and concentration of oxygen in the habitat, and the profile of consumption of oxygen and water because of the daily tasks performed by the crew members in the habitat, as well as the time-series profile of the solar illumination at a candidate site on the Moon. Several algorithms to maintain the required pressure and concentration of oxygen in the habitat, supply oxygen from the oxygen tank of ISRU to the habitat, perform filtration of the wastewater to produce freshwater, supply water to the habitat water tank from the ISRU water tank and freshwater tank were also proposed which are vital to determine the optimal power profile of the ISRU.

- **Optimal operation management:** The thesis proposed an optimization framework to determine the optimal operating strategy of a PV-battery based MG for maintaining the stored energy of the battery at a desired level by optimally sizing the PV array and battery and minimizing the total surplus PV power generation along with the mass of the PV array and battery taking into account the optimal power demand profile of the ISRU, thereby, generating the optimal PV power profile and charging/discharging profile of the battery.
- **Mass-per-unit-load (MPUL):** The thesis proposed a criterion called MPUL to compare different candidate locations and determine the locations that fulfill the highest power requirement with the minimum PV-battery based MG total system mass.

4.3 Future work

In this thesis, optimal sizing, siting, and operation management of a lunar MG was accomplished considering several specific requirements of the power systems in the space environment. According to the study conducted in this thesis, the following directions are proposed for future research in this area:

- **Battery degradation due to cosmic radiation:** Although several research has been focused on the deterioration of batteries in spacecraft, these degradation models have restricted usage in specific applications. A more specific study analyzing the effect of cosmic radiation reaching the lunar polar regions and its effect on battery degradation is required.
- **Integrating the biomass production subsystem into the oxygen and water management system:** Further analysis is required to identify the amount and rate of oxygen, carbon dioxide, and water consumption and oxygen generation by various plants. Moreover, the amount of power consumed for maintaining the artificial atmosphere and lighting conditions needs further study.

- **Parameter sensitivity:** A study has to be performed to analyze the effect of initial levels of several storage tanks in determining the optimal power demand profile of the ISRU.
- **Forming an MMG system:** To enhance the reliability and resiliency of the lunar base, power and resource sharing in an MMG system needs to be established considering the safe operation of the base. Further investigation is required with respect to the mass of the overall MMG system, accounting for the extra power cables, converters, and protection devices required to form an MMG system.
- **Demand-side management:** A multi-objective optimization strategy is required to manage sudden surges and the peak-to-average ratio of the power demand profile, taking into consideration a compromise between following the desired references and power demand. Formulating a methodology to flexibly schedule loads and charge diversified ESSs is essential for better management of the available resources and to reduce the peak-to-average ratio.

Chapter 5: References

References

[1] National Aeronautics and Space Administration (NASA). NASA artemis. [Online]. Available: https://www.nasa.gov/specials/artemis/

[2] National Aeronautics and Space Administration (NASA), "Artemis III: NASA's First Human Mission to the Lunar South Pole | NASA," (Accessed on 03/10/2023). [Online]. Available: https://www.nasa.gov/feature/artemis-iii

[3] European Space Agency (ESA). Imagining a moon base. [Online]. Available: https://www.esa.int/Science_Exploration/Human_and_Robotic_Exploration\/Imagining_a_Moon_base

[4] JAXA. The jaxa space exploration innovation hub center co-produces results on remote and automatic control to build lunar base. [Online]. Available: https://global.jaxa.jp/press/2019/03/20190328a.html

[5] N. Connor. China prepares for manned moon landing. [Online]. Available: https://www.telegraph.co.uk/news/2017/06/07/china-prepares-moon-landing/

[6] D. Etherington. Spacex wants to land starship on the moon before 2022, then do cargo runs for 2024 human landing. [Online]. Available: https://techcrunch.com/2019/10/25/spacex-wants-to-land-starship-on-the-moon-before-2022-then-do-cargo-runs-for-2024-human-landing/

[7] T. Mogg. Prime delivery, straight from the moon? bezos dreams of heavy industry in space. [Online]. Available: https://www.digitaltrends.com/cool-tech/jeff-bezos-reaffirms-plan-for-moon-colony/

[8] Z. Khan, A. Vranis, A. Zavoico, S. Freid, and B. Manners, "Power system concepts for the lunar outpost: A review of the power generation, energy storage, Power Management and Distribution (PMAD) system requirements and potential technologies for development of the lunar outpost," *AIP Conference Proceedings*, vol. 813, no. 1, pp. 1083–1092, 2006.

[9] D. Saha, N. Bazmohammadi, J. M. Raya-Armenta, A. D. Bintoudi, A. Lashab, J. C. Vasquez, and J. M. Guerrero, "Space microgrids for future manned lunar bases: A review," *IEEE Open Access Journal of Power and Energy*, vol. 8, pp. 570–583, 2021.

[10] A. J. Colozza, "Small Lunar Base Camp and In Situ Resource Utilization Oxygen Production Facility Power System Comparison," 2020. [Online]. Available: https://ntrs.nasa.gov/citations/20200001622

[11] S. H. Choi, G. C. King, H.-J. Kim, and Y. Park, "Electrostatic power generation from negatively charged, simulated lunar regolith," 2010. [Online]. Available: https://ntrs.nasa.gov/citations/20100032922

[12] E. Mazarico, G. Neumann, D. Smith, M. Zuber, and M. Torrence, "Illumination conditions of the lunar polar regions using lola topography," *Icarus*, vol. 211, no. 2, pp. 1066–1081, 2011.

[13] P. Gläser, J. Oberst, G. Neumann, E. Mazarico, E. Speyerer, and M. Robinson, "Illumination conditions at the lunar poles: Implications for future exploration," *Planetary and Space Science*, vol. 162, pp. 170–178, 2018.

[14] E. J. Speyerer and M. S. Robinson, "Persistently illuminated regions at the lunar poles: Ideal sites for future exploration," *Icarus*, vol. 222, no. 1, pp. 122–136, 2013.

[15] A. D. Bintoudi, C. Timplalexis, G. Mendes, J. M. Guerrero, and C. Demoulias, "Design of space microgrid for manned lunar base: Spinning-in terrestrial technologies," in *2019 European Space Power Conference (ESPC)*. IEEE, 2019, pp. 1–8.

[16] J. Fincannon, "Characterization of lunar polar illumination from a power system perspective," in *46th AIAA Aerospace Sciences Meeting and Exhibit*, 2008, p. 447.

[17] J. Freeh, "Analysis of stationary, photovoltaic-based surface power system designs at the lunar south pole," in *AIAA SPACE 2008 Conference & Exposition*, 2009, p. 7810.

[18] J. Fincannon, "Lunar south pole illumination: review, reassessment, and power system implications," in *5th International Energy Conversion Engineering Conference and Exhibit (IECEC)*, 2007, p. 4700.

[19] J. M. R. Armenta, N. Bazmohammadi, D. Saha, J. C. Vasquez, and J. M. Guerrero, "Optimal multi-site selection for a pv-based lunar settlement based on a novel method to estimate sun illumination profiles," *Advances in Space Research*, 2023.

[20] PDS Geosciences Node Data and Services: LRO LOLA. (Accessed on 12/12/2020). [Online]. Available: https://pds-geosciences.wustl.edu/lro/lro-l-lola-3-rdr-v1/lrolol_1xxx/data/lola_gdr/polar/img/

[21] D. Saha, N. Bazmohammadi, J. M. Raya-Armenta, A. D. Bintoudi, A. Lashab, J. C. Vasquez, and J. M. Guerrero, "Optimal sizing and siting of pv and battery based space microgrids near the moon's shackleton crater," *IEEE Access*, vol. 11, pp. 8701–8717, 2023.

[22] H. Benaroya, "Reliability and damage," in *Building Habitats on the Moon*. Springer, 2018, pp. 249–285.

[23] C. Tamponnet, "Life support systems for lunar missions," *Advances in Space Research*, vol. 18, no. 11, pp. 103–110, 1996.

[24] J. Oberst, A. Christou, R. Suggs, D. Moser, I. Daubar, A. McEwen, M. Burchell, T. Kawamura, H. Hiesinger, K. Wünnemann *et al.*, "The present-day flux of large meteoroids on the lunar surface—a synthesis of models and observational techniques," *Planetary and Space Science*, vol. 74, no. 1, pp. 179–193, 2012.

[25] W. Schonberg, F. Schäfer, and R. Putzar, "Some comments on the protection of lunar habitats against damage from meteoroid impacts," *Journal of Aerospace Engineering*, vol. 23, no. 1, pp. 90–97, 2010.

[26] E. Sefton-Nash, M. Siegler, and D. Paige, "Thermal extremes in permanently shadowed regions at the lunar south pole," in *Proceedings of the 44th Lunar and Planetary Science Conference*. Lunar and Planetary Institute, 2013, p. 2617.

[27] D. M. Hurley, M. Sarantos, C. Grava, J.-P. Williams, K. D. Retherford, M. Siegler, B. Greenhagen, and D. Paige, "An analytic function of lunar surface temperature for exospheric modeling," *Icarus*, vol. 255, pp. 159–163, 2015.

[28] D. Palac, L. Mason, M. Houts, and S. Harlow, "Fission surface power technology development update," in *AIAA SPACE 2010 Conference & Exposition*, 2011, p. 8711.

[29] M. Gibson and P. Schmitz, "Higher power design concepts for nasa's kilopower reactor," in *2020 IEEE Aerospace Conference*. IEEE, 2020, pp. 1–9.

[30] M. Kaczmarzyk and M. Musiał, "Parametric study of a lunar base power system," *Energies*, vol. 14, no. 4, p. 1141, 2021.

[31] R. Pappa, C. Taylor, J. Warren, M. Chamberlain, S. Cook, S. Belbin, R. Lepsch, D. Tiffin, B. Doggett, M. Mikulas, I. Wong, D. Long, D. Steinkoening, A. Pensado, J. Blandino, and J. Haste, "Relocatable 10 kW Solar Array for Lunar South Pole Missions - NASA Technical Reports Server (NTRS)," Mar 2021, (Accessed on 03/30/2023). [Online]. Available: https://ntrs.nasa.gov/citations/20210011743

[32] X. Zhao, A. Aierken, M. Heini, M. Tan, Y. Wu, S. Lu, R. Hao, J. Mo, Y. Zhuang, X. Shen, Y. Xu, Q. Lei, and Q. Guo, "Degradation characteristics of electron and proton irradiated InGaAsP/InGaAs dual junction solar cell," *Solar Energy Materials and Solar Cells*, vol. 206, p. 110339, 2020.

[33] G. Hongliang, S. Linfeng, S. Qiang, Z. Qiming, W. Yiyong, X. Jingdong, G. Bin, and Z. Yanqing, "Degradation of up-grown metamorphic ingap/ingaas/ge solar cells by low-energy proton irradiation," *Solar Energy Materials and Solar Cells*, vol. 191, pp. 399–405, 2019.

[34] E. F. Lisbona, "llf-2 - calibration, testing and monitoring of space solar cells," in *Solar Cells*, T. Markvart and L. Castañer, Eds. Oxford: Elsevier Science, 2005, pp. 475–503.

[35] C. Ciurans, N. Bazmohammadi, J. C. Vasquez, G. Dussap, J. M. Guerrero, and F. Gòdia, "Hierarchical control of space closed ecosystems: Expanding microgrid concepts to bioastronautics," *IEEE Industrial Electronics Magazine*, vol. 15, no. 2, pp. 16–27, 2021.

[36] H. J. Fincannon, "Lunar Environment and Lunar Power Needs," pp. 1–5, 2020. [Online]. Available: https://ntrs.nasa.gov/citations/20205002224

[37] A. J. Colozza, R. S. Heller, W. A. Wong, and A. F. Hepp, "Solar energy systems for lunar oxygen generation," *48th AIAA Aerospace Sciences Meeting Including the New Horizons Forum and Aerospace Exposition*, no. April, p. 1166, 2010.

[38] T. Nakamura and B. K. Smith, "Solar power system for lunar ISRU applications," *48th AIAA Aerospace Sciences Meeting Including the New Horizons Forum and Aerospace Exposition*, p. 1162, Jan 2010.

[39] P. E. C. Gordon, A. J. Colozza, A. F. Hepp, R. S. Heller, and R. Gustafson, "Thermal Energy for Lunar In Situ Resource Utilization : Technical Challenges and Technology Opportunities," *Cleveland, Ohio, USA: National Aeronautics and Space Administration, Glenn Research Center.*, 2011.

[40] J. Blosiu, R. Bugga, E. Brandon, M. Smart, J. Elliott, J. Castillo, T. Yi, L. Lee, M. Piszczor, T. Miller, C. Reid, C. Taylor, S. Liu, U. S. Army, E. Plichta, C. Iannello, P. M. Beauchamp, and J. A. Cutts, "Energy Storage Technologies for Future Planetary Science Missions Work Performed under the Planetary Science Program Support Task," no. JPL D-101146, Dec 2017. [Online]. Available: https://solarsystem.nasa.gov/resources/549/energy-storage-technologies-for-future-planetary-science-missions/

[41] L. Mason and M. Rucker, "Common power and energy storage solutions to support lunar and Mars surface exploration missions," *Proceedings of the International Astronautical Congress, IAC*, pp. 1–7, 2019. [Online]. Available: https://ntrs.nasa.gov/citations/20190032521

[42] "7.0 Thermal Control | NASA," https://www.nasa.gov/smallsat-institute/sst-soa-2020/thermal-control, (Accessed on 07/22/2021).

[43] A. Pérez, M. Benavides, H. Rozas, S. Seria, and M. Orchard, "Guidelines for the characterization of the internal impedance of lithium-ion batteries in phm algorithms," *International Journal of Prognostics and Health Management*, vol. 9, no. 3, 2018.

[44] M. C. Guzik, R. Gilligan, P. Smith, and I. Jakupca, "Energy storage for lunar surface exploration," in *2018 AIAA SPACE and Astronautics Forum and Exposition*, 2018, p. 5106.

[45] S. Okaya, "Regenerative fuel cell for high power space system applications," in *11th International Energy Conversion Engineering Conference*, 2013, p. 3923.

[46] M. C. Guzik, I. Jakupca, R. Gilligan, W. R. Bennett, P. J. Smith, and J. Fincannon, "Regenerative fuel cell power systems for lunar and martian surface exploration," in *AIAA SPACE and Astronautics Forum and Exposition*, 2017, p. 5368.

[47] A. Birchenough and D. Hervol, "Test results from a simulated high voltage lunar power transmission line," in *AIP Conference Proceedings*, vol. 969, no. 1. American Institute of Physics, 2008, pp. 593–601.

[48] T. Mintz, E. A. Maslowski, A. Colozza, W. McFarland, K. P. Prokopius, P. J. George, and S. W. Hussey, "Simulation of a lunar surface base power distribution network for the constellation lunar surface systems," *Glenn Research Center, Cleveland, Ohio*, 2010.

[49] D. V. Pombo, "A hybrid power system for a permanent colony on mars," *Space: Science & Technology*, vol. 2021, 2021.

[50] S. P. Barave and B. H. Chowdhury, "Hybrid ac/dc power distribution solution for future space applications," in *2007 IEEE Power Engineering Society General Meeting.* IEEE, 2007, pp. 1–7.

[51] T. W. Kerslake, "Lunar surface-to-surface power transfer," in *AIP Conference Proceedings*, vol. 969, no. 1. American Institute of Physics, 2008, pp. 466–473.

[52] D. Saha, N. Bazmohammadi, J. C. Vasquez, and J. M. Guerrero, "Multiple microgrids: A review of architectures and operation and control strategies," *Energies*, vol. 16, no. 2, p. 600, 2023.

[53] R. May, J. F. Soeder, R. Beach, P. George, J. D. Frank, M. Schwabacher, S. P. Colombano, L. Wang, and D. Lawler, "An architecture to enable autonomous control of a spacecraft," in *12th International Energy Conversion Engineering Conference*, 2014, p. 3834.

[54] D. Gingras, P. Allard, T. Lamarche, S. G. Rocheleau, S. Gemme, L. Deschênes-Villeneuve, and E. Martin, "Lunar rover remote driving using monocameras under multi-second latency and low-bandwidth: Field tests and lessons learned," in *Submitted to International Symposium on Artificial Intelligence, Robotics and Automation in Space (i-SAIRAS),(Montreal, Canada)*, 2014.

[55] J. T. Csank, J. F. Soeder, M. A. Carbone, M. G. Granger, B. J. Tomko, M. J. Muscatello, and J. C. Follo, "A Control Framework for Autonomous Smart Grids for Space Power Applications," *70th International Astronautical Congress (IAC)*, 2019.

[56] NASA, "SpaceX Operations | NASA," Jul 2021, (Accessed on 03/10/2023). [Online]. Available: https://www.nasa.gov/feature/spacex-operations

[57] SpaceX, "Starship Users Guide," Mar 2020, (Accessed on 03/10/2023). [Online]. Available: https://www.spacex.com/media/starship_users_guide_v1.pdf

[58] All Points Logistics, "The Autonomy of NASA's Orion Spacecraft Shines Spotlight on Software, Modeling, and Simulation - All Points Logistics," (Accessed on 03/10/2023). [Online]. Available: https://www.allpointsllc.com/the-autonomy-of-nasas-orion-spacecraft-shines-spotlight-on-software-modeling-and-simulation-2/

[59] J. T. Csank, J. F. Soeder, J. C. Follo, M. J. Muscatello, M. A. Carbone, and Y. H. Hau, "An autonomous power controller for the NASA human deep space gateway," in *International Energy Conversion Engineering Conference*, no. GRC-E-DAA-TN56670, 2018.

[60] J. F. Soeder, A. Mcnelis, R. Beach, N. McNelis, T. Dever, L. Trase, and R. May, "Overview of intelligent power controller development for human deep space exploration," in *12th International Energy Conversion Engineering Conference*, 2014, p. 3833.

[61] J. Fincannon, "Lunar polar illumination for power analysis," in *6th International Energy Conversion Engineering Conference (IECEC)*, 2008, p. 5631.

[62] M. Kaczmarzyk, A. Starakiewicz, and A. Waśniowski, "Internal heat gains in a lunar base—a contemporary case study," *Energies*, vol. 13, no. 12, p. 3213, 2020.

[63] B. Xu, A. Oudalov, A. Ulbig, G. Andersson, and D. S. Kirschen, "Modeling of lithium-ion battery degradation for cell life assessment," *IEEE Transactions on Smart Grid*, vol. 9, no. 2, pp. 1131–1140, 2018.

[64] S. X. Chen, H. B. Gooi, and M. Q. Wang, "Sizing of energy storage for microgrids," *IEEE Transactions on Smart Grid*, vol. 3, no. 1, pp. 142–151, 2012.

[65] S. Ruppert, A. Ross, J. Vlassak, and M. Elvis, "Towers on the moon: 1. concrete," *arXiv preprint arXiv:2103.00612*, 2021.

[66] D. Saha, N. Bazmohammadi, A. Lashab, J. C. Vasquez, and J. M. Guerrero, "Power and energy management system of a lunar microgrid - part i: Optimal power demand of isru," *IEEE Transactions on Aerospace and Electronic Systems*, 2023, (Submitted).

[67] NASA, "Human Integration Design Handbook (HIDH) - revision 1," Jun 2014. [Online]. Available: https://www.nasa.gov/sites/default/files/atoms/files/human_integration_design_handbook_revision_1.pdf

[68] M. K. Ewert, T. T. Chen, and C. D. Powell, "Life support baseline values and assumptions document - NASA Technical Reports Server (NTRS)," Feb 2022. [Online]. Available: https://ntrs.nasa.gov/citations/20210024855

[69] D. Saha, N. Bazmohammadi, J. C. Vasquez, and J. M. Guerrero, "Optimal pv and battery sizing for a space microgrid near the lunar south pole considering isru, habitat and water subsystem power demand," in *International Conference on Environmental Systems*, no. ICES-2023-250, 2023, (Submitted).

[70] D. Saha, N. Bazmohammadi, A. Lashab, J. C. Vasquez, and J. M. Guerrero, "Lunar habitat wastewater subsystem power and water management," in *2023 International Conference on Power, Instrumentation, Energy and Control (PIECON)*, 2023, pp. 1–6.

[71] D. J. Barta, K. D. Pickering, C. Meyer, S. Pensinger, L. Vega, M. Flynn, A. Jackson, and R. Wheeler, "A biologically-based alternative water processor for long duration space missions - NASA Technical Reports Server (NTRS)," May 2015. [Online]. Available: https://ntrs.nasa.gov/citations/20150014482

[72] C. E. Meyer, S. Pensinger, N. Adam, K. D. Pickering, D. Barta, S. A. Shull, L. M. Vega, K. Lange, D. Christenson, and W. A. Jackson, "Results of the alternative water processor test, a novel technology for exploration wastewater remediation," in *International Conference on Environmental Systems*, no. JSC-CN-35746, 2016.

[73] D. J. Barta, R. Wheeler, W. Jackson, K. Pickering, C. Meyer, S. Pensinger, L. Vega, and M. Flynn, "An alternative water processor for long duration space missions," *40th COSPAR Scientific Assembly*, vol. 40, pp. F4–2, 2014.

[74] F. Volpin, U. Badeti, C. Wang, J. Jiang, J. Vogel, S. Freguia, D. Fam, J. Cho, S. Phuntsho, and H. K. Shon, "Urine treatment on the international space station: current practice and novel approaches," *Membranes*, vol. 10, no. 11, p. 327, 2020.

[75] D. L. Carter, "Status of the regenerative eclss water recovery system," *SAE Technical Papers*, Jul 2009.

[76] D. Saha, N. Bazmohammadi, A. Lashab, J. C. Vasquez, and J. M. Guerrero, "Power and energy management system of a lunar microgrid - part ii: Optimal sizing and operation of isru," *IEEE Transactions on Aerospace and Electronic Systems*, 2023, (Submitted).

Part II

Papers

Paper A

Space Microgrids for Future Manned Lunar Bases: A Review

Diptish Saha, *Student Member, IEEE*, Najmeh Bazmohammadi, *Member, IEEE*, José Maurilio Raya-Armenta, *Student Member, IEEE*, Angelina D. Bintoudi, *Student Member, IEEE*, Abderezak Lashab, *Member, IEEE*, Juan C. Vasquez, *Senior Member, IEEE*, and Josep M. Guerrero, *Fellow, IEEE*

The paper has been published in the
IEEE Open Access Journal of Power and Energy Vol. 8, pp. 570–583, 2021.

The layout has been revised.

Paper B

Multiple Microgrids: A Review of Architectures and Operation and Control Strategies

Diptish Saha, Najmeh Bazmohammadi, Juan C. Vasquez, and Josep M. Guerrero

The paper has been published in the
Energies Vol. 16, no. 2, p. 600, Jan. 2023.

The layout has been revised.

Paper C

Optimal Sizing and Siting of PV and Battery based Space Microgrids near the Moon's Shackleton Crater

Diptish Saha, *Student Member, IEEE*, Najmeh Bazmohammadi, *Member, IEEE*, José Maurilio Raya-Armenta, Angelina D. Bintoudi, *Member, IEEE*, Abderezak Lashab, *Senior Member, IEEE*, Juan C. Vasquez, *Senior Member, IEEE*, and Josep M. Guerrero, *Fellow, IEEE*

The paper has been published in the
IEEE Access Vol. 11, no. 2, pp. 8701–8717, Jan. 2023.

The layout has been revised.

Paper D

Lunar Habitat Wastewater Subsystem Power and Water Management

Diptish Saha, Najmeh Bazmohammadi, Abderezak Lashab, Juan C. Vasquez, and Josep M. Guerrero

The paper has been published in the
2023 International Conference on Power, Instrumentation, Energy and Control (PIECON), Aligarh, India, pp. 1–6, Feb. 2023.

The layout has been revised.

Paper E

Power and Energy Management System of a Lunar Microgrid - Part I: Optimal Power Demand of ISRU

Diptish Saha, *Student Member, IEEE*, Najmeh Bazmohammadi, *Senior Member, IEEE*, Abderezak Lashab, *Senior Member, IEEE*, Juan C. Vasquez, *Senior Member, IEEE*, and Josep M. Guerrero, *Fellow, IEEE*

The paper has been submitted for publication in the *IEEE Transactions on Aerospace and Electronic Systems* Vol. XX(X), pp. XXX–XXX, 202X. *(Under review)*

The layout has been revised.

Paper F

Power and Energy Management System of a Lunar Microgrid - Part II: Optimal Sizing and Operation of ISRU

Diptish Saha, *Student Member, IEEE*, Najmeh Bazmohammadi, *Senior Member, IEEE*, Abderezak Lashab, *Senior Member, IEEE*, Juan C. Vasquez, *Senior Member, IEEE*, and Josep M. Guerrero, *Fellow, IEEE*

The paper has been submitted for publication in the *IEEE Transactions on Aerospace and Electronic Systems* Vol. XX(X), pp. XXX–XXX, 202X. *(Under review)*

The layout has been revised.

Paper G

Optimal PV and Battery Sizing for a Space Microgrid Near the Lunar South Pole Considering ISRU, Habitat and Water Subsystem Power Demand

Diptish Saha, Najmeh Bazmohammadi, Juan C. Vasquez, and Josep M. Guerrero

The paper has been accepted for publication in the
52nd International Conference on Environmental Systems (ICES) Vol. XX(X), pp. XXX–XXX, 2023. *(Accepted)*

The layout has been revised.

ISSN (online): 2446-1636
ISBN (online): 978-87-7573-698-0

AALBORG UNIVERSITY PRESS